Università degli Studi di Brescia
Universidad de Almería

MODELING AND CONTROL OF THE MICROALGAE BIOMASS PRODUCTION PROCESS IN RACEWAY REACTORS

Dipartimento di Ingegneria Meccanica e Industriale
Departamento de Informática

Ph.D. Candidate	Supervisor	Supervisor
Enrique[1] Rodríguez Miranda	**Antonio[1] Visioli**	**José Luis[1] Guzmán Sánchez**

[1]digitally signed pursuant to Article 24 of Legislative Decree 82/05.

Università degli Studi di Brescia

DIPARTIMENTO DI INGEGNERIA MECCANICA E INDUSTRIALE

CICLO XXXIII

DOTTORATO DI RICERCA IN INGEGNERIA MECCANICA E INDUSTRIALE

SSD: ING-INF/04

UNIVERSITÀ DEGLI STUDI DI BRESCIA

MODELING AND CONTROL OF THE MICROALGAE BIOMASS PRODUCTION PROCESS IN RACEWAY REACTORS

Ph.D. Candidate
Enrique Rodríguez Miranda

Supervisors: Prof. **Antonio Visioli** and Prof. **José Luis Guzmán Sánchez**

Tutor: Prof. **Manuel Berenguel Soria**

Coordinators: Prof. **Laura Depero** and Prof. **Luis Fernando Iribarne Martínez**

Universidad de Almería

**UNIVERSIDAD
DE ALMERÍA**

MODELING AND CONTROL OF THE MICROALGAE BIOMASS PRODUCTION PROCESS IN RACEWAY REACTORS

Ph.D. Candidate
Enrique Rodríguez Miranda

Supervisors: Prof. **Antonio Visioli** and Prof. **José Luis Guzmán Sánchez**

Tutor: Prof. **Manuel Berenguel Soria**

Coordinators: Prof. **Laura Depero** and Prof. **Luis Fernando Iribarne Martínez**

Acknowledgement

To perform this PhD has been a really new experience in my life, where I have met a multitude of people and colleagues who have helped me to overcome the various challenges that have arisen. Everything I have accomplished on this journey would not have been possible without their help and support.

First of all, I want to greatly thank my supervisors Antonio Visioli and José Luis Guzmán for all the constant support and encouragement they gave me. I have been able to witness first-hand their passion and hardwork for research, and thanks to them I have been able to enter into this world of discovery. In them I have seen both determination and understanding to set me on the right track and achieve my goals. I am very grateful for the opportunity that they have offered me to carry out this stage of my life. Without their guidance and constant feedback, this PhD would never have seen the light.

I would like to thank the department of Mechanical and Industrial Engineering at the University of Brescia for the scholarship they have awarded me. Thanks to that, I will be able to continue carrying out my research work with microalgae. Working in this field has aroused my curiosity for the study of the processes involved in the production of microalgae biomass, and thanks to this grant I can continue to increase my knowledge and experience.

I also want to thank my tutor, Manolo Berenguel, for his unconditional support in the follow-up of my research work. His great interest has allowed me to solve problems that otherwise would not have been possible. In addition, I want to thank Claudio Carnevale, Manuel Beschi and Gabriel Acién for all the help they have given me to carry out the contributions described in this thesis. Much of what I have learned I owe to them and their wisdom on the matter.

I really appreciate the support that I have received from my colleagues, whom I consider my friends. I want to thank all my colleagues from Brescia, for receiving me with open arms and accepting me as one of the group. With them I have felt loved and valued. I have been able to learn many things by working with them. I also want to

thank my colleagues from Almería, both those I already knew and those I have known in this time. I have worked with them very hard side by side to solve all the problems that arose, and they have always been there to help me in everything what I have needed. Thanks to all of them, the slopes that I have had to face during this period have been like a walk.

As cannot be otherwise, I want to warmly thank my family and friends. They are the ones who have seen my dedication and work in first hand, supporting me and clearing my mind in the most necessary moments. They have filled me with love and encouragement to continue without rest until the last moment.

And finally to Elena, who has stayed by my side both in good times and in the most difficult ones. Thanks to her love that I have felt capable of doing anything, in addition to comforting me when I could not solve a problem. She has been like a light to guide me along the path of this journey that I have embarked on. Thank you.

List of parameters and variables

Parameter	Description	Units
a	Absorptivity	−
A	Total surface area of the reactor	m^2
A_{conv}	Calibrated convection experimental coefficient	−
A_{evap}	Calibrated evaporation experimental coefficient	−
α_s	Solar distributed factor that represents the shadow projection on the perpendicular axis of the reactor walls	−
A_{soil}	Surface of the reactor in contact with the ground	m^2
B_1	Pre-exponential factor for pH influence on photosynthesis rate	−
B_2	Pre-exponential factor for pH influence on photosynthesis rate	−
B_{evap}	Calibrated evaporation experimental coefficient	−
B_{conv}	Calibrated convection experimental coefficient	−
C_1	Activation energy factor of the Arrhenius model	−
C_2	Activation energy factor of the Arrhenius model	−
C_b	Biomass concentration	$g\ m^{-3}$
C_p	Specific heat capacity of the culture	$J\ kg^{-1}\ °C^{-1}$
Δ	Symmetric Send On Delta amplitude tolerance for the error deadband	−
Δh_{max}	Maximum culture depth increment	cm
DO	Dissolved oxygen	%
$DO_{2,max,alg}$	Microalgae maximum dissolved oxygen growth value	%
$DO_{2,w}$	Dissolved oxygen culture value	%
e	Water emissivity	−
E_p	Evaporation rate	$m\ s^{-1}$

$E_{y-daytime}$	Number of events for event-based control during daytime period	$-$
$E_{y-nighttime}$	Number of events for event-based control during night-time period	$-$
Gas	Carbon dioxide consumption performance index	m^3
$Gas_{daytime}$	Carbon dioxide consumption during daytime period	m^3
$Gas_{nighttime}$	Carbon dioxide consumption during night-time period	m^3
h	culture depth	m
H^+	Hydrogen ions concentration	g m^{-3}
h_{conv}	Convection transfer coefficient	W m^{-2} $°C^{-1}$
h_{evap}	Evaporation exchange coefficient	m s^{-1} Pa^{-1}
h_{fg}	Latent heat of vaporization	J kg^{-1}
h_{max}	Maximum culture depth	cm
h_{min}	Minimum culture depth	cm
h_{soil}	Heat transfer coefficient for the polyethylene layer under the reactor	W m^{-2} $°C^{-1}$
I_0	Solar irradiance on an horizontal surface	μE m^{-2} s^{-1}
IAE	Integral Absolute Error	$-$
$IAE_{daytime}$	Integral Absolute Error during daytime period	$-$
$IAE_{nighttime}$	Integral Absolute Error during night-time period	$-$
I_{av}	Light availability	μE m^{-2} s^{-1}
I_g	Global (direct+diffuse) solar irradiance	W m^{-2}
I_k	Minimum light needed by microalgae to achieve maximum photosynthesis	μE m^{-2} s^{-1}
$I_{k_{resp}}$	Maximum light needed by the microalgae to stop photosynthesis and start the respiration	μE m^{-2} s^{-1}
IT	Injection time performance index	min
$IT_{daytime}$	Injection time performance index during daytime period	min
$IT_{nighttime}$	Injection time performance index during night-time period	min

K_a	Microalgae extinction coefficient	$m^2 \ g^{-1}$
$K_{I,C,alg}$	Microalgae inhibition constant for carbon	$g \ m^{-3}$
$K_{I,DO_2,alg}$	Microalgae inhibition constant for dissolved oxygen	$g \ m^{-3}$
$K_{I,DO_2,nit}$	Nitrifying bacteria inhibition constant for dissolved oxygen	$g \ m^{-3}$
$K_{I,NH_4,alg}$	Microalgae inhibition constant on ammonium	$g \ m^{-3}$
$K_{I,NO_3,alg}$	Microalgae inhibition constant on nitrate	$g \ m^{-3}$
$K_{S,BSOM,het}$	Heterotrophic bacteria half-saturation constant for biodegradable soluble organic matter	$g \ m^{-3}$
$K_{S,C,alg}$	Microalgae half-saturation constant for carbon	$g \ m^{-3}$
$K_{S,C,nit}$	Nitrifying bacteria half-saturation constant for carbon	$g \ m^{-3}$
$K_{S,DO_2,het}$	Heterotrophic bacteria half-saturation constant for dissolved oxygen	$g \ m^{-3}$
$K_{S,DO_2,nit}$	Nitrifying bacteria half-saturation constant for dissolved oxygen	$g \ m^{-3}$
$K_{S,NH_4,alg}$	Microalgae half-saturation constant on ammonium	$g \ m^{-3}$
$K_{S,NH_4,het}$	Heterotrophic bacteria half-saturation constant for ammonium	$g \ m^{-3}$
$K_{S,NH_4,nit}$	Nitrifying bacteria half-saturation constant for ammonium	$g \ m^{-3}$
$K_{S,NO_3,alg}$	Microalgae half-saturation constant on nitrate	$g \ m^{-3}$
K_{soil}	Calibration parameter of conduction transfer coefficient for the polyethylene layer	$W \ m^{-1} \ ^\circ C^{-1}$
$K_{S,PO_4,alg}$	Microalgae half-saturation constant on phosphate	$g \ m^{-3}$
$K_{S,PO_4,het}$	Heterotrophic bacteria half-saturation constant for phosphate	$g \ m^{-3}$
$K_{S,PO_4,nit}$	Nitrifying bacteria half-saturation constant for phosphate	$g \ m^{-3}$
lb	Lower depth limit	cm

m	Endogenous respiration	day^{-1}
m_{DO}	Form parameter	$-$
$m_{max,alg}$	Microalgae maximum respiration rate	day^{-1}
$m_{min,alg}$	Microalgae minimum respiration rate	day^{-1}
m_I	Form factors for the exponential function of average irradiance	$-$
μ_{alg}	Microalgae specific growth rate	day^{-1}
$\mu_{alg,max}$	Microalgae maximum specific growth rate	day^{-1}
$\overline{\mu_{alg}}(CO_2)$	Microalgae carbon dioxide limitation growth model	$-$
$\overline{\mu_{alg}}(DO)$	Microalgae dissolved oxygen limitation growth model or microalgae dissolved oxygen index	$-$
$\mu_{alg}(I_{av})$	Microalgae light limitation growth model	day^{-1}
$\overline{\mu_{alg}}(NH_4)$	Microalgae ammonium limitation growth model	$-$
$\overline{\mu_{alg}}(NO_3)$	Microalgae nitrate limitation growth model	$-$
$\overline{\mu_{alg}}(pH)$	Microalgae pH limitation growth model or microalgae pH index	$-$
$\overline{\mu_{alg}}(PO_4)$	Microalgae phosphate limitation growth model	$-$
$\overline{\mu_{alg}}(T_w)$	Microalgae temperature limitation growth model or microalgae temperature index	$-$
μ_{het}	Heterotrophic bacteria specific growth rate	day^{-1}
$\mu_{het,max}$	Heterotrophic bacteria maximum growth rate	day^{-1}
$\overline{\mu_{het}}(BSOM)$	Heterotrophic bacteria BSOM limitation growth model	$-$
$\overline{\mu_{het}}(DO)$	Heterotrophic bacteria dissolved oxygen limitation growth model or heterotrophic dissolved oxygen index	$-$
$\overline{\mu_{het}}(NH_4)$	Heterotrophic bacteria ammonium limitation growth model	$-$
$\overline{\mu_{het}}(pH)$	Heterotrophic bacteria pH limitation growth model or heterotrophic pH index	$-$
$\overline{\mu_{het}}(PO_4)$	Heterotrophic bacteria phosphate limitation growth model	$-$

$\overline{\mu_{het}}(T_w)$	Heterotrophic bacteria temperature limitation growth model or heterotrophic temperature index	–
μ_{nit}	Nitrifying bacteria specific growth rate	day^{-1}
$\mu_{nit,max}$	Nitrifying bacteria maximum growth rate	day^{-1}
$\overline{\mu_{nit}}(CO_2)$	Nitrifying bacteria carbon dioxide limitation growth model	–
$\overline{\mu_{nit}}(DO)$	Nitrifying bacteria dissolved oxygen limitation growth model or nitrifying dissolved oxygen index	–
$\overline{\mu_{nit}}(NH_4)$	Nitrifying bacteria ammonium limitation growth model	–
$\overline{\mu_{nit}}(pH)$	Nitrifying bacteria pH limitation growth model or nitrifying pH index	–
$\overline{\mu_{nit}}(PO_4)$	Nitrifying bacteria phosphate limitation growth model	–
$\overline{\mu_{nit}}(T_w)$	Nitrifying bacteria temperature limitation growth model or nitrifying temperature index	–
n	Form parameter	–
$n_{CO_2,alg}$	Microalgae form parameter for carbon	–
$n_{NH_4,alg}$	Microalgae form parameter for ammonium	–
$n_{NO_3,alg}$	Microalgae form parameter for nitrate	–
n_{resp}	Respiration form parameter	–
p'_A	Vapor pressure of the air at ambient temperature	Pa
P_b	Biomass productivity	$\text{g m}^{-2} \text{ day}^{-1}$
P_{O_2}	Photosynthesis rate	day^{-1}
$P_{O_2,max}$	Maximum photosynthesis rate	day^{-1}
$pH_{max,alg}$	Microalgae maximum pH growth value	–
$pH_{max,het}$	Heterotrophic bacteria maximum pH growth value	–
$pH_{max,nit}$	Nitrifying bacteria maximum pH growth value	–
$pH_{min,alg}$	Microalgae minimum pH growth value	–

$pH_{min,het}$	Heterotrophic bacteria minimum pH growth value	–
$pH_{min,nit}$	Nitrifying bacteria minimum pH growth value	–
$pH_{opt,alg}$	Microalgae optimum pH growth value	–
$pH_{opt,het}$	Heterotrophic bacteria optimum pH growth value	–
$pH_{opt,nit}$	Nitrifying bacteria optimum pH growth value	–
pH_w	pH culture value	–
Q_d	Inlet flow rate or dilution flow rate	$m^3\ s^{-1}$
Q_h	Outlet flow rate or harvesting flow rate	$m^3\ s^{-1}$
RH	Relative humidity	%
ρ	Density of the culture	$kg\ m^{-3}$
R_{O_2}	Respiration constant phenomenon	day^{-1}
σ	Stefan-Boltzmann constant	$W\ m^{-2}\ K^{-4}$
T_{amb}	Ambient temperature	°C
T_{dew}	Dew point temperature	°C
T_{max}	Maximum optimization temperature	°C
$T_{max,alg}$	Microalgae maximum temperature growth value	°C
$T_{max,het}$	Heterotrophic bacteria maximum temperature growth value	°C
$T_{max,nit}$	Nitrifying bacteria maximum temperature growth value	°C
T_{min}	Minimum optimization temperature	°C
$T_{min,alg}$	Microalgae minimum temperature growth value	°C
$T_{min,het}$	Heterotrophic bacteria minimum temperature growth value	°C
$T_{min,nit}$	Nitrifying bacteria minimum temperature growth value	°C
t_o	Optimization time	sec
$T_{optimum}$	Optimum optimization temperature	°C
$T_{opt,alg}$	Microalgae optimum temperature growth value	°C
$T_{opt,het}$	Heterotrophic bacteria optimum temperature growth value	°C

$T_{opt,nit}$	Nitrifying bacteria optimum temperature growth value	°C
T_{sky}	Equivalent temperature of the sky	K
T_{soil}	Soil temperature	°C
t_{solar}	Number of hours after solar midnight	−
T_w	Culture temperature	°C
TV_u	Total Variation performance index	−
ub	Upper depth limit	cm
W_s	Wind speed	m s^{-1}
$X_{BSOM,in}$	Inlet biodegradable soluble organic matter concentration	g m^{-3}
$X_{BSOM,out}$	Outlet biodegradable soluble organic matter concentration	g m^{-3}
X_{CO_2}	Carbon dioxide concentration	g m^{-3}
X_{HCO_3}	Bicarbonate concentration	g m^{-3}
$X_{het,in}$	Inlet heterotrophic bacteria concentration	g m^{-3}
$X_{het,out}$	Heterotrophic bacteria concentration inside de reactor	g m^{-3}
X_{NH_4}	Ammonium concentration in the reactor	g m^{-3}
$X_{NH_4,in}$	Inlet ammonium concentration	g m^{-3}
$X_{NH_4,out}$	Outlet ammonium concentration	g m^{-3}
$X_{nit,in}$	Inlet nitrifying bacteria concentration	g m^{-3}
$X_{nit,out}$	Outlet nitrifying bacteria concentration	g m^{-3}
X_{NO_3}	Nitrate concentration in the reactor	g m^{-3}
$X_{NO_3,in}$	Inlet nitrate concentration	g m^{-3}
$X_{NO_3,out}$	Outlet nitrate concentration	g m^{-3}
X_{PO_4}	Phosphate concentration in the reactor	g m^{-3}
$X_{PO_4,in}$	Inlet phosphate concentration	g m^{-3}
$X_{PO_4,out}$	Outlet phosphate concentration	g m^{-3}
x_{soil}	Distance between the bottom of the reactor and the buried temperature probe	m
$Y_{con}\left[\frac{BSOM}{het}\right]$	Biodegradable soluble organic matter consumption rate from heterotrophic bacteria	g$_{BSOM}$ g$_{het}{}^{-1}$

$Y_{con}\left[\frac{NH_4}{alg}\right]$	Ammonium consumption rate from microalgae	$g_{NH_4}\ g_{alg}{}^{-1}$
$Y_{con}\left[\frac{NH_4}{het}\right]$	Ammonium consumption rate from heterotrophic bacteria	$g_{NH_4}\ g_{het}{}^{-1}$
$Y_{con}\left[\frac{NH_4}{nit}\right]$	Ammonium consumption rate from nitrifying bacteria	$g_{NH_4}\ g_{nit}{}^{-1}$
$Y_{con}\left[\frac{NO_3}{alg}\right]$	Nitrate consumption rate from microalgae	$g_{NO_3}\ g_{alg}{}^{-1}$
$Y_{con}\left[\frac{PO_4}{alg}\right]$	Phosphate consumption rate from microalgae	$g_{PO_4}\ g_{alg}{}^{-1}$
$Y_{con}\left[\frac{PO_4}{het}\right]$	Phosphate consumption rate from heterotrophic bacteria	$g_{PO_4}\ g_{het}{}^{-1}$
$Y_{con}\left[\frac{PO_4}{nit}\right]$	Phosphate consumption rate from nitrifying bacteria	$g_{PO_4}\ g_{nit}{}^{-1}$
$Y_{gen}\left[\frac{BSOM}{alg}\right]$	Biodegradable soluble organic matter generation rate from microalgae	$g_{BSOM}\ g_{alg}{}^{-1}$
$Y_{gen}\left[\frac{BSOM}{het}\right]$	Biodegradable soluble organic matter generation rate from heterotrophic bacteria	$g_{BSOM}\ g_{het}{}^{-1}$
$Y_{gen}\left[\frac{BSOM}{nit}\right]$	Biodegradable soluble organic matter generation rate from nitrifying bacteria	$g_{BSOM}\ g_{nit}{}^{-1}$
$Y_{gen}\left[\frac{NO_3}{nit}\right]$	Nitrate generation rate from nitrifying bacteria	$g_{NO_3}\ g_{nit}{}^{-1}$

Acronyms and Abbreviations

API	Application Programming Interfaces
ASM	Activated Sludge Models
BSOM	Biodegradable Soluble Organic Matter
CALRESI	Modelado y **C**ontrol del proceso combinado de producción de micro**AL**gas y tratamiento de aguas **RESI**duales con reactores industriales – (Modeling and control of the combined process of microalgae production and wastewater treatment with industrial reactors)
DO	Dissolved Oxygen
FOPDT	First-Order-Plus-Dead-Time
GAOT	Genetic Algorithm Optimization Toolbox
GPC	Generalize Predictive Controller
IFAPA	Instituto Andaluz de Investigación y Formación Agraria, Pesquera, Alimentaria y de la Producción Ecológica
IT	Injection Time
ODE	Ordinary Differential Equation
PAR	Photosynthetic Active Radiation
PDE	Partial Differential Equation
PID	Proportional-Integral-Derivative
PI-SSOD	Proportional-Integral-Symmetric-Send-On-Delta
PLC	Programmable Logic Controller
QFT	Quantitative Feedback Theory
RMSE	Root Mean Square Error
SABANA	Sustainable Algae Biorefinery for Agriculture aNd Aquaculture
SCADA	Supervisory Control and Data Acquisition System
SIMC	Simple-Internal-Model-Control
SOD	Send-On-Delta
SSOD	Symmetric-Send-On-Delta
SSOD-PI	Symmetric-Send-On-Delta-Proportional-Integral

Contents

List of Figures

List of Tables

Abstract

Research on microalgae is gaining importance due, fundamentally, to the advantages of its cultivation and the diversity of applications that biomass has. Among its many uses, microalgae biomass can be used in commercial applications to obtain products of high added value with applications in human nutrition and health, aquaculture, cosmetics and biofertilizers. Furthermore, other promising application that are currently in improving is the use of microalgae biomass for energy purposes, mainly to obtain biofuel. In addition, during their growth, microalgae capture carbon dioxide, contributing to carbon mitigation, and its production can even be combined with wastewater treatment.

To achieve economic viability and environmental sustainability, it is necessary to significantly reduce production costs and environmental impacts, while improving the productivity of the systems. These processes can be combined in such a way that the produced synergies increase the overall sustainability of the production processes.

This thesis presents different approaches, dealing both with modeling and control, related to the microalgae biomass production process. The main objective of the work carried out has been to improve the biomass productivity in the operation of raceway reactors. This improvement focuses on the development of models that serve for the simulation and estimation of characteristic parameters, such as culture temperature and growth rate, as well as temperature and pH control techniques to maintain optimal conditions during cultivation.

Sommario

La ricerca sulle microalghe sta acquisendo importanza grazie, fondamentalmente, ai vantaggi della sua coltivazione e alla diversità di applicazioni che la biomassa ha. Tra i suoi molteplici usi, la biomassa di microalghe può essere utilizzata in applicazioni commerciali per ottenere prodotti ad alto valore aggiunto con applicazioni nella nutrizione e salute umana, acquacoltura, cosmetici e biofertilizzanti. Un'altra promettente applicazione attualmente in fase di miglioramento è l'uso della biomassa di microalghe a fini energetici, principalmente per ottenere biocarburanti. Inoltre, durante la loro crescita, le microalghe catturano l'anidride carbonica, contribuendo alla mitigazione del carbonio, e la sua produzione può anche essere combinata con il trattamento delle acque reflue.

Per raggiungere la redditività economica e la sostenibilità ambientale, è necessario ridurre in modo significativo i costi di produzione e gli impatti ambientali, migliorando nel contempo la produttività dei sistemi. Questi processi possono essere combinati in modo tale da produrre sinergie che aumentano la sostenibilità complessiva dei processi produttivi.

Questa tesi presenta diversi approcci, sia modellistici che di controllo, relativi al processo di produzione della biomassa di microalghe. L'obiettivo principale del lavoro svolto è stato quello di migliorare la produttività della biomassa nel funzionamento dei reattori a canalizzazione aperta. Questo miglioramento si concentra sullo sviluppo di modelli che servono per la simulazione e la stima di parametri caratteristici, come la temperatura di coltura e il tasso di crescita, nonché le tecniche di controllo della temperatura e del pH per mantenere condizioni ottimali durante la coltivazione.

Resumen

La investigación con microalgas está ganando importancia debido, fundamentalmente, a las ventajas de su cultivo y la diversidad de aplicaciones que tiene la biomasa obtenida. Entre sus múltiples usos, la biomasa de microalgas puede utilizarse en aplicaciones comerciales para obtener productos de alto valor añadido con aplicaciones en nutrición y salud humana, acuicultura, cosmética y biofertilizantes. Además, otra aplicación prometedora que se está mejorando actualmente es el uso de biomasa de microalgas con fines energéticos, principalmente para la obtención de biocombustible. Por otro lado, durante su crecimiento, las microalgas capturan dióxido de carbono, contribuyendo a la mitigación del carbono, y su producción puede incluso combinarse con el tratamiento de aguas residuales.

Para lograr la viabilidad económica y la sostenibilidad ambiental, es necesario reducir significativamente los costes de producción y los impactos ambientales, al tiempo que se mejora la productividad de los sistemas. Estos procesos pueden combinarse de tal manera que las sinergias producidas aumenten la sostenibilidad global de los procesos de producción.

Esta tesis presenta diferentes enfoques, tanto de modelado como de control, relacionados con el proceso de producción de biomasa de microalgas. El principal objetivo del trabajo realizado ha sido mejorar la productividad de la biomasa en la operación de reactores de canalización. Esta mejora se centra en el desarrollo de modelos que sirvan para la simulación y estimación de parámetros característicos, como temperatura de cultivo y tasa de crecimiento, así como técnicas de control de temperatura y pH para mantener condiciones óptimas durante el cultivo.

Preface

Microalgae are microscopic organisms that live in aqueous environments and have the ability to perform photosynthesis. Through this process, the microalgae consume carbon dioxide and nutrients contained in the culture medium to produce oxygen and grow. The objective of microalgae cultivation is the production of biomass in photobioreactors for its subsequent treatment and use in different applications. Depending on the type of strain and its composition, it is possible to use microalgae biomass for human consumption or as animal feed, and even obtain high value products for the chemical or pharmaceutical industries.

Moreover, environmental sustainability has motivated a large effort in the development of renewable energy systems like those based on wind, sunlight, etc. In this field, microalgae have recently become very popular because of their great potential to be used for biofuel production. Certain strains of microalgae contain high amount of lipids, so their biomass can be treated in order to obtain biofuel. The cultivation of microalgae in open reactors does not need fertile soil and its maintenance is relatively simple. This is an interesting alternative to the methods commonly used for the production of biofuel, such as energy crops, which require a large area of fertile land and increase thus the price in the market. However, it is recognized that the cost of production, separation, purification and conversion to fuel is a rather expensive and energy intensive process suggesting that significant advances are needed before the technology can be considered for fuel production

Recently, the use of wastewater as medium is allowing the development of new combined applications such as water treatment and purification together with the production of biomass in a single reactor. As a result of this process, it is possible to obtain clean water for discharge or used in agriculture, while generating microalgae biomass and reducing the costs of these processes compared to the case of their individual implementation.

For the cultivation of microalgae in photobioreactors, it is necessary to keep certain variables at optimal values. The most important are the pH

and dissolved oxygen, which are controlled by injecting carbon dioxide and air into the reactor, respectively. The contribution of carbon dioxide can come even from industrial flue gases, which contributes to environmental carbon mitigation, further motivating the implantation of photobioreactors at industrial level.

Under this approach, the results discussed in this thesis have been achieved within the framework of the CALRESI project, whose purpose is the study and application of modeling and control strategies for the optimization of the microalgae biomass production process, combined with the wastewater treatment process, in large-scale industrial photobioreactors.

Hence, this thesis aims to address challenges related to improve the efficiency, productivity, design and optimization of large-scale raceway microalgae production processes cultivated in outdoor conditions by means of using adequate modeling and control strategies. Thus, the three main objectives of the research project are:

- Development and proposal of strategies for modeling, estimation and identification for the biomass production process on raceway photobioreactors. The resulting models will be used for reactor design and control design purposes.

- Development and proposal of different control strategies for the efficient biomass production in raceway photobioreactors looking for reducing costs and mitigation of environmental pollution.

- Implementation and validation of the developed modeling and control approaches in different experimental plants with clear industrial relevance.

The issues that are specifically addressed in this thesis are the modeling and control related with the microalgae biomass production process, in terms of maximizing the productivity. The proposed developments are focused on the design of applications and new operation techniques for raceway reactors, which serve to reduce costs and increase profits.

As an introduction, Chapter 1 presents the motivation for the development of this thesis and the state of the art related to the

modeling and control techniques related to these processes. Likewise, this chapter describes the microalgae growth rate model, which is the basis for estimating biomass production in a photobioreactor and the biomass production process. Chapter 2 describes the CALRESI project and the facilities where the experimental tests have been carried out, and more specifically, the raceway reactors used for experimentation purposes.

The models used and developed that are related to microalgae processes are presented in Chapter 3. This chapter presents a consortia model for the biomass production process combined with wastewater treatment, where bacteria are also present in the reactor. In addition, a model has been developed to estimate the temperature of the culture inside the reactor, which directly affects its growth and productivity. Therefore, it serves as a design tool and to carry out feasibility studies when cultivating different types of strains.

Open raceway reactors are exposed to disturbances caused by solar radiation and ambient temperature. The control of these conditions requires the incorporation of elements that can suppose a considerable extra cost in the production of microalgae biomass, becoming unviable. Chapter 4 presents a study on the influence of temperature and liquid depth on the growth of microalgae, based on the temperature model developed in the previous chapter. In addition, a simple method for temperature regulation is presented, based on the optimization of the volume in the reactor, without the need to incorporate any additional element in to the operation.

The pH control carried out in the raceway reactor is discussed in Chapter 5, where the different control approaches that have been developed are compared with respect to the classical operation of the reactor. The different control architectures are based on the use of PI controllers and event-based control to keep the culture pH at optimal values. In this way, biomass productivity and resource consumption are improved.

The developed modeling and control architectures have been experimentally tested in industrial-scale raceway reactors, located at the IFAPA research center, in Almería (Spain).

CHAPTER 1

Introduction

Although the biomass production from microalgae started some time ago, it is a research field that is constantly developing and expanding. There are many products and benefits that can be obtained from their cultivation, without counting the positive impact it generates on the environment, due to carbon dioxide (CO_2) mitigation and its low maintenance cost.

This introductory chapter is structured as follows: First, the motivation behind the development of this thesis is presented in Section 1.1, while an introduction on microalgae growth kinetics is presented in Section 1.2. Section 1.3 describes the microalgae biomass production process, the state of the art regarding the modeling and control of these processes is described in Section 1.4 and finally, the contributions that have been made from the results obtained in the development of the research activity are presented in Section 1.5.

1.1 Motivation

The advantages in the cultivation of microalgae have allowed the increment of their use in the last years, being a very innovative research field with a multitude of application branches. The biomass production in photobioreactors is carried out in a sustainable way with the environment. Their operation contributes to CO_2 mitigation (which can come from industrial flue gases) and through high value products that can be obtained from microalgae biomass. Furthermore, the combination of this process with others, such as wastewater treatment or biofuel production, allows for the expansion of new market niches and reduction of production costs, while generating new research opportunities.

Because the system is made up of living organisms, the dynamics and operating conditions are highly changeable. This nonlinear behaviour in the process raises a series of modeling and control challenges that must be adequately addressed to achieve the proposed objectives.

The development of the activities presented in this work has required a deep understanding of the functioning and operation of the microalgae reactors, as well as the process of microalgae growth and biomass production. The knowledge acquired on the processes related to microalgae allows a greater understanding in the aspects related to their control and modeling, with many expectations in the development of future applications.

1.2 Microalgae growth kinetics

Microalgae (and in general unicellular phototops) are fast-growing microorganisms, or more precisely, fast-duplicating organisms with great potential to generate biomass at a much higher rate compared to other types of pluricelular photosynthetic organisms, such as macroalgae (see Figure 1.1). This is due to the simplicity of microalgae to reproduce, being the most important characteristic of these organisms, the high growth rate. They are naturally present in a range of aquatic habitats, including lakes, pounds, rivers, oceans, and even wastewater. The culture is identified as the population of cultivated microalgae, while the medium represents the liquid without microalgae that is added as a habitat for its growth.

The growth of microalgae can be expressed mathematically from the relationship between biomass concentration and time. The biomass concentration of the culture describes de amount of microalgae biomass per unit of culture volume in the reactor. Figure 1.2 represents the high exponential growth on microalgae biomass compared to other macroalgae species.

Although microalgae growth rate is very fast, there is a point where the growth stops and the culture becomes nutrient-limited. A microalgae culture evolves through a series of phases [45], which can be seen in Figure
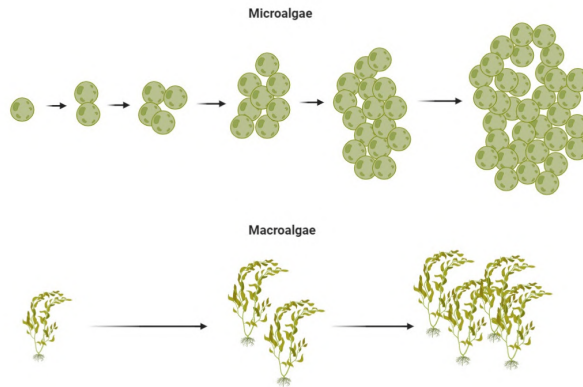
Figure 1.1: Microalgae and macroalgae duplication examples.
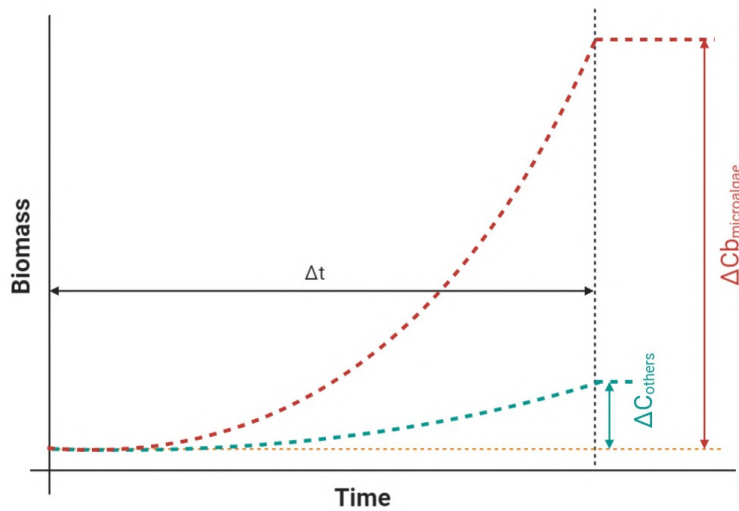
Figure 1.2: Microalgae biomass growth over time compared to other macroalgae species.

1.3 and are detailed below:

- The lag phase is typically observed when a culture has just been

started   and   the   microoganisms   are   adapting   to   the   new
environmental conditions.

- The exponential phase is characterized by unlimited rapid growth
  and frequent cell division.

- Declining relative growth phase normally occurs in cultures when
  either a specific requirement for cell division is limiting or something
  else is inhibiting reproduction.

- During the stationary phase, the cell division slows due to the lack
  of resources necessary for growth.

- Finally, in the death phase,the environment degradates and the death
  rate increases equal to the growth rate and even becomes larger.
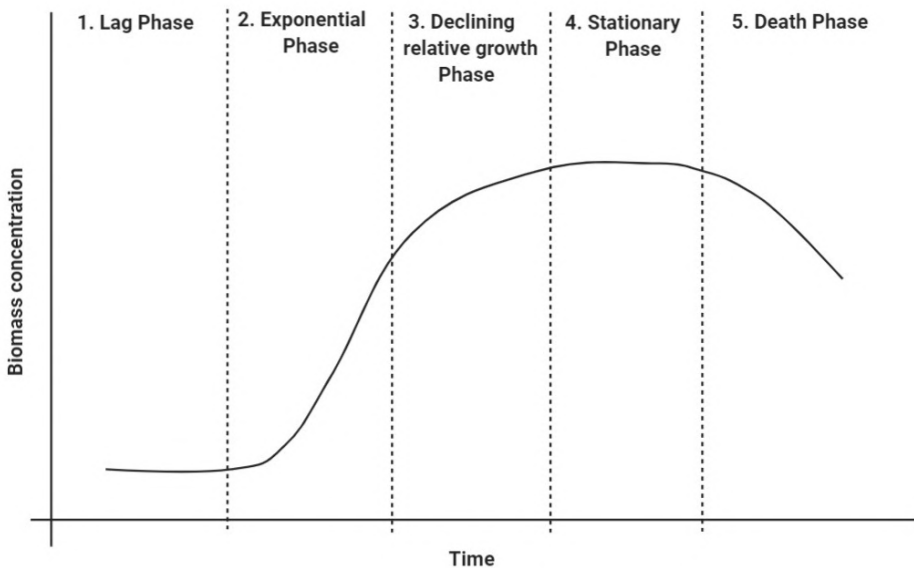
Figure 1.3: Microalgae growth phases.

The microalgae specific growth rate model has been used extensively
in literature [8, 17] and its formulation depends on the different nutrient
limitation influencing the growth, as can be seen in [85].

The most common used model states that the microalgae growth rate, μ_{alg}, is made up of four factors that depend on photosynthetically active radiation and light availability inside the culture (I_{av}), culture temperature (T_w), the pH, and the dissolved oxygen (DO) in the reactor. The specific growth model is described by the following equation:

$$\mu_{alg} = \mu_{alg}(I_{av}) \cdot \overline{\mu_{alg}}(T_w) \cdot \overline{\mu_{alg}}(pH) \cdot \overline{\mu_{alg}}(DO) - m \qquad (1.1)$$

The specific growth rate μ_{alg} is mainly a function of light availability inside the reactor summarized by the average irradiance inside the culture I_{av} [52] and modified by the influence of temperature, pH and dissolved oxygen on culture growth. Moreover, the endogenous respiration m represents the autoxidation of microalgae, where they metabolize their own cellular material.

The main limiting nutrient that is characteristic of microalgae is light limitation. The equations relating the microalgae growth rate μ_{alg} and the solar irradiance I are called light limitation growth models. This influence has been characterized by various authors in the literature to describe the different profiles that microalgae strains can acquire [5, 17, 50, 51, 53, 87, 92].

In general, the incidence of solar irradiance on the culture does not occur in a homogeneous way, but some layers of the culture receive more light than others. To unify this phenomenon, the light availability I_{av} is used to analyze the light-limited growth of microalgae throughout the microalgae culture.

Taking the model described by Molina *et al.* in [51], the light limitation growth model can be expressed as follows:

$$\mu_{alg}(I_{av}) = \left(\mu_{alg,max} \cdot \left(\frac{I_{av}^{\ n}}{I_k^{\ n} + I_{av}^{\ n}} \right) \right) \qquad (1.2)$$

where $\mu_{alg,max}$ [day^{-1}] is the maximum growth rate, I_{av} [μE m^{-2} s^{-1}] is the light availability inside the reactor summarized by the average irradiance inside the culture, I_k [μE m^{-2} s^{-1}] is the minimum light

needed by the microalgae to achieve maximum photosynthesis and n [-] is
a form parameter.

The endogenous respiration term can be expressed as follows:

$$m = \left(m_{min,alg} - \left(m_{max,alg} \cdot \left(\frac{I_{av}{}^{n_{resp}}}{I_{k_{resp}}{}^{n_{resp}} + I_{av}{}^{n_{resp}}} \right) \right) \right) \qquad (1.3)$$

where $m_{min,alg}$ and $m_{max,alg}$ [day^{-1}] represent the minimum and maximum
respiration rates, $I_{k_{resp}}$ [μE m^{-2} s^{-1}] is the maximum light needed by the
microalgae to stop photosynthesis and start the respiration process and
n_{resp} [-] is the form parameter for respiration.

For a specific geometry, the average irradiance I_{av} is a function of the
light path inside the culture, the biomass concentration and the extinction
coefficient of the biomass. The specific growth rate hyperbolically increases
with the average irradiance up to achieve the maximum specific growth
rate $\mu_{alg,max}$ for the selected strain. Whatever the microalgae strains, a
fix specific growth rate is achieved for any operational conditions, being
higher or lower according to the optimal value of other cultures parameters
such as temperature, pH and dissolved oxygen among others. The average
irradiance is expressed as follows:

$$I_{av} = \frac{I_0}{K_a \cdot C_b \cdot h} \left(1 - e^{-K_a \cdot C_b \cdot h} \right) \qquad (1.4)$$

where I_0 [μE m^{-2} s^{-1}] is the solar irradiance on a horizontal surface,
K_a [m^2 g^{-1}] is the microalgae extinction coefficient, C_b [g m^{-3}] is the
microalgae biomass concentration and h [m] is the culture depth in the
reactor.

The influence of temperature, pH and dissolved oxygen affecting
microalgae growth in (1.1) are normalized factors which values vary
between 0 and 1. Therefore, when these three terms ($\overline{\mu_{alg}}(T_w)$, $\overline{\mu_{alg}}(pH)$
and $\overline{\mu_{alg}}(DO)$) are optimal and have a value of 1, the specific growth rate
only depends on solar radiation and would have the maximum possible
value. However, if any of these terms is not optimal, it would have a
direct negative impact on the growth rate. As for light limitation, the

influence of these factors on microalgae growth is expressed by various authors [15, 64] and represent the microalgae limitation growth models for temperature, pH and dissolved oxygen.

The temperature index $\overline{\mu_{alg}}(T_w)$, expressed by Bernard *et al.* in [15], is a term that represents the influence of temperature on microalgae growth, directly related to biomass growth, where 1 means the maximum yield due to an optimal temperature of the culture. The biomass growth performance can be diminished by the effect of the temperature, therefore a temperature above or below the characteristic limits of the microalgae would result in null growth. For example, a strain that does not exceed a temperature index of 0.5 in a location means that at most, it is not capable of reaching half its maximum growth rate. So, it would be limited to a great extent due to temperature conditions. The temperature index can be expressed as follows:

$$\overline{\mu_{alg}}(T_w) = \frac{N_{alg,T}}{D_{alg,T}}$$

where

$$\boldsymbol{N_{alg,T}} = (T_w - T_{max,alg}) \cdot (T_w - T_{min,alg})^2$$
$$\boldsymbol{D_{alg,T}} = (T_{opt,alg} - T_{min,alg}) \cdot ((T_{opt,alg} - T_{min,alg}) \cdot (T_w - T_{opt,alg}) -$$
$$- (T_{opt,alg} - T_{max,alg}) \cdot (T_{opt,alg} + T_{min,alg} - 2 \cdot T_w))$$

$$(1.5)$$

As for the temperature index, the pH index $\overline{\mu_{alg}}(pH_w)$ is a term that represents the influence of pH on the microalgae culture. This factor has limit values (minimum and maximum) in which growth decreases until it stops, even becoming harmful for microalgae. Furthermore, the optimal value represents the pH that maximizes biomass production, being a key value for the control of this variable. It can be expressed as follows:

$$\overline{\mu_{alg}}(pH_w) = \frac{N_{alg,pH}}{D_{alg,pH}}$$

where

$$\boldsymbol{N_{alg,pH}} = (pH_w - pH_{max,alg}) \cdot (pH_w - pH_{min,alg})^2$$
$$\boldsymbol{D_{alg,pH}} = (pH_{opt,alg} - pH_{min,alg}) \cdot ((pH_{opt,alg} - pH_{min,alg}) \cdot (pH_w - pH_{opt,alg})-$$
$$-(pH_{opt,alg} - pH_{max,alg}) \cdot (pH_{opt,alg} + pH_{min,alg} - 2 \cdot pH_w)$$
$$\text{(1.6)}$$

The dissolved oxygen index $\overline{\mu_{alg}}(DO)$ depends on a maximum value, determined by the strain, which represents the amount of oxygen that can be accumulated in the culture without being detrimental to microalgae growth. The dissolved oxygen index is expressed as the following equation [20]:

$$\overline{\mu_{alg}}(DO) = 1 - \left(\frac{DO_{2,w}}{DO_{2,max,alg}} \right)^{m_{DO}} \qquad \text{(1.7)}$$

where m_{DO} [–] is a form parameter.

These indexes depend on the maximum ($T_{max,alg}$, $pH_{max,alg}$, $DO_{2,max,alg}$), minimum ($T_{min,alg}$, $pH_{min,alg}$) and optimum ($T_{opt,alg}$, $pH_{opt,alg}$) values of the microalgae strain, in addition to the temperature of the culture (T_w [°C]), the pH of the culture (pH [-]) and the dissolved oxygen of the culture (DO [%]), respectively.

The biomass productivity P_b has been one of the indicators on microalgae growth more used in literature [10, 11, 25, 35]. This term reflects the amount of biomass generated in the unit time and per unit of culture volume, but it can be also expressed as the biomass generated per unit area and time. It can be used to analyze the differences in growth for different activities developed, such as control approaches. The biomass productivity is expressed as:

$$P_b = \mu_{alg} \cdot C_b \cdot h \qquad \text{(1.8)}$$

where P_b [g m^{-2} day^{-1}] is the biomass productivity, C_b is the biomass concentration and h is the culture depth.

1.3   Biomass production process

Biomass production is the process by which organic matter is obtained from microalgae and is processed for its subsequent use. There are multitude of products that can be obtained from microalgae biomass with diverse applications in industrial sectors such as agriculture, aquaculture, and food production, among others [27, 44]. Depending on the type of strain and its properties, the purpose of the product may vary, such as strains that contain proteins or Omega-3, which serve as food for human consumption or as animal feed. On the other hand, strains that contain a high amount of lipids can be used to produce biofuel [82, 95], as an alternative to energy crops to be used as clean energy. Furthermore, the combination with other processes such as wastewater treatment allows reducing costs and opens the door to new fields of research and innovation [4]. Microalgae large-scale production is still limited by the specific requirements for each microalgae strain, and a multitude of considerations must be taken into account, such as the adequate design of the photobioreactors, the maintenance and control of the cultivation conditions and the optimal supply of nutrients. [1]

There are mainly two types of photobioreactors [58, 65] (or commonly named, reactors): closed reactors and open reactors, as can be seen in Figure 1.4. On the one hand, closed reactors (left) allow precise control of operating conditions and are focused on high-value microalgae that are susceptible to contamination. From this type, tubular reactors are the most commonly used, where quality is more important than production volume. On the other hand, open reactors (right) are characterized by higher biomass production volumes and are oriented to resistant microalgae strains, since it is not possible to control all the variables that affect the microalgae growth. The most extended and widespread open reactors are the raceway reactors, which are more economical and simpler to maintain than closed reactors. Another type of open reactor that is

a) Closed tubular reactor [19].

b) Open raceway reactor.

Figure 1.4: Microalgae photobioreactor types.

currently generating a lot of interest are thin layer reactors, which are characterized by operating at a shallow culture depth to maximize the effect of photosynthesis. However, the production volume is small. In order to carry out the experimental tests designed from the strategies developed in this thesis, two open raceway-type reactors have been used, described later in Section 2.2.

The raceway reactors are mainly composed of three parts, which can be seen in Figure 1.5. Point 1 represents the channel through which the culture flows, which has bands to improve hydrodynamic circulation. It is the area where the phenomenon of photosynthesis and cell growth of microalgae occurs. Point 2 represents the paddlewheel that drives the culture. It must always be in motion, to prevent the water from stagnating and the microalgae from precipitating to the bottom. The speed at which the paddlewheel is operated is usually constant and its movement allows the culture to be mixed to improve cell distribution on the surface and microalgae rotation to perform photosynthesis. Point 3 represents the pit or sump, a deep and unlit area where air (or oxygen) and CO_2 are bubbled in to control dissolved oxygen and pH levels in the culture, respectively.

From the photosynthesis process, microalgae consume CO_2 from the
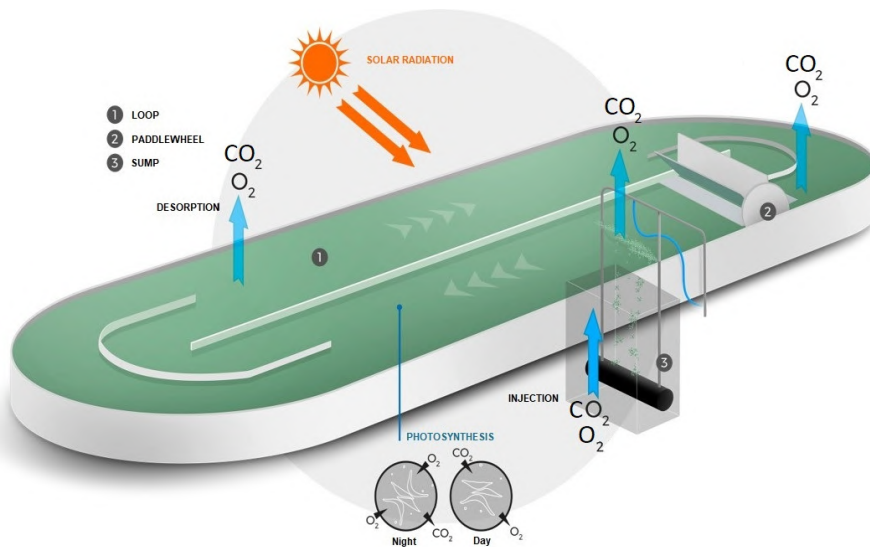
Figure 1.5: Schematic of a raceway reactor [6].

culture and generate oxygen (O_2). This process acidifies the liquid culture in the reactor and changes the carbonate-bicarbonate equilibrium, increasing the pH value. If this parameter reaches a limit value for a long period of time, it can be detrimental to the state of the microalgae and limit their growth. Each microalgae strain has an optimal pH value that maximizes growth, as well as lower and upper limits, where growth stops, or can even negatively affect microalgae health. To reduce it, CO_2 is bubbled in the sump, taking into account that the pH cannot fall below a certain lower limit. Due to this behavior, the pH in the culture maintains an oscillating dynamics, which requires adequate control to keep this parameter close to an optimal value. Injections of CO_2 in the culture regulate the balance between ions and anions, lowering the pH value.

In parallel, the oxygen generated during the daytime by the photosynthesis process accumulates inside the reactor and can reach high values. This parameter does not pose any risk for the growth of microalgae, except if it exceeds an upper limit value, in which the biomass productivity declines and there is risk of cell damage. To avoid

this situation, air is bubbled through the sump, which breaks up the oxygen molecules and releases them out of the liquid contained in the reactor.

During normal operation of the reactor, dissolved oxygen and pH control are usually performed in industry with an On/Off control applied to a valve, where CO_2 or air is bubbled into the sump when the pH or dissolved oxygen levels exceed a certain value. This control is normally carried out automatically during the daytime period and is deactivated at night due to the inactivity of the microalgae, so it is a process that does not require frequent maintenance. On the other hand, the dilution and harvesting processes are those that are responsible for extracting the microalgae biomass from the reactor, and are usually carried out manually. Harvesting is the process by which culture is removed from the reactor through a pipe, for further treatment and processing. On the other hand, dilution is the process by which fresh water with fertilizers or another type of culture medium (such as wastewater or salt water) is added. During the dilution process with fresh water, the necessary nutrients are added to allow the growth of microalgae. These nutrients have a lower pH than the culture pH of the reactor, which causes disturbances during dilution.

Generally, temperature control is not carried out in open reactors at industrial level, due to their high energy and investment related costs. However, the volume variation in the reactor through the harvesting and dilution processes affects the dynamic evolution of the culture temperature. Through the use of optimal control of these processes is possible to regulate the temperature of the culture in order to improve the productivity of the microalgae.

Each day, the biomass in the reactor is harvested by removing a certain percentage of liquid in the reactor. The volume amount removed from the reactor is determined depending on the month, taking into account that the concentration of microalgae biomass at the end of the day must be the same as at the beginning of the same day, that is, the decrease that occurs in the biomass concentration can be compensated. The growth varies depending on the month, therefore, the amount harvested will also change depending on the month. As the harvest flow rate is fixed, the

duration of this process is variable, between 1 and 2 hours. Afterwards, new medium is added to restore the volume in the reactor to its initial depth level. Likewise for harvesting, the dilution flow rate is fixed, so this process also lasts between 1 and 2 hours. As a result of the harvesting process, wet biomass is obtained. The wet biomass is collected and stored to be subsequently centrifuged at high speed, which removes much of the water and becomes a thick paste. Once the compact biomass is obtained, it is heated in an oven for hours to completely remove residual moisture. As a result, a block of microalgae is obtained, which is subsequently pulverized until obtaining a fine powder, thus ending the process. This pulverized microalgae biomass is the final result of the whole process and can be used for all the applications mentioned above, such as the elaboration of food for human consumption or animal feed.

1.4   State of art

Biotechnology and bioprocesses are considered as one of the emerging areas in the automatic control community. The complexity of these processes and the challenging modeling and control problems open a huge number of research topics in this field. Among them, wastewater treatment, food engineering, and biomass production are current research lines with special attention.

Biological microalgae models can help to estimate and maximize biomass productivity [11], as well as characteristic parameters that can be used in control systems to maximize biomass production [20, 26, 61]. It is possible to find in the literature multiple models that represent the behavior of microalgae. For example, in [29] a descriptive model of the production of microalgae biomass in tubular reactors is presented, which was later adapted to raceway reactors in [31]. However, although there exist some studies combining the microalgae productivity and culture temperature [15, 42], most existing biological models do not take the culture temperature into account, that is a limiting factor in the analysis of the microalgae productivity results [39, 43, 67, 81]. Béchet *et al.* presented a universal temperature model for open reactors [9], which

makes use of dimensionless parameters for heat transfer and evaporation phenomena. The evaporation phenomenon is a complex process and difficult to estimate. In [13] a comparison of different evaporation models is presented. On the other hand, in [46], a dynamic model for the cultivation of microalgae is developed where an empirical temperature model based on thermal energy balances suggested in [83] is included. These studies demonstrated the importance of temperature on microalgae growth and the complexity of accurately estimate its value. The combination of a temperature model with the current microalgae growth models would allow a greater improvement in the representation of the microalgae behaviour. Due to this combination, better control architectures for biomass production and associated applications could be developed.

The influence of temperature in a microalgae-based process is a crucial aspect, not only in biomass production but also in the choice of production areas, since it can negatively affect the crop when temperature exceeds certain limits [67]. Therefore, multiple results and studies can be found about the effect of temperature on growth rate and biomass production for algae and cyanobacteria [81]. In [56], a study of the effect of temperature, ranging from $9°C$ to $32°C$, on growth rate and biomass production in a composition of 26 algae species from 5 different functional groups is presented. On the other hand, the effect of temperature on the microalgae *Tetraselmis sp.* is analyzed in [21], where the effect of light is considered independent of temperature. The effect of high temperatures has been shown to be more detrimental to biomass production, as described in [12], where the impact of high temperatures on algae activity and viability is modeled. On the other hand, low temperatures reduce growth until it stops, but without negatively affecting its health. That is why high temperatures are more critical.

It is possible to find multiple examples of models in the literature where both the incident light in the reactor and its temperature are taken into account. One of these cases can be found in [10], where a review of the state of the art in this topic is carried out, exposing which are the most promising or viable models. In [8], the variations in culture conditions in an open thin-layer were studied, both in terms of position inside the

reactor and time of the daylight cycle. A comprehensive model developed for microalgae growth in outdoor ponds under fluctuating light intensity and temperature conditions is presented in [39]. In [15], a simple model for the influence of light and temperature on the growth of algae is developed, estimating their production outdoors, based on the growth model presented in [17]. A new alternative for modeling the effect of temperature on growth has been recently presented in [64]. These models have been widely used to develop new biomass growth models [85]. All these different models can be used as design tools coupled with productions models, which allow the estimation of the process behaviour based on environmental conditions. Moreover, these models can be used to determine the suitability of a certain area for the production of microalgae biomass.

Despite the fact that the influence of temperature on the outdoor production of biomass is widely analyzed and studied in the literature, temperature control techniques are scarce [34]. It is possible to find some studies of temperature control in closed photobioreactors, as in [91], since it is possible to install heat exchangers in the bubble column. In [93], a particular design of the reactor is proposed to minimize the diurnal and seasonal temperature fluctuations, but based on an unconventional design and adapted to a specific area of Arizona. On the other hand, recently, in [40], a heat exchanger based on wasted heat from flue gases is proposed to heat the reactor volume up for temperature regulation purposes. However, although this solution is available from a technical point of view, it requires a complex and expensive installation. Moreover, the proposed system does not allow cooling of the reactor, being a critical aspect for the cultivation of microalgae in warm areas. One of the most interesting techniques is presented in [23], where an optimization strategy is used based on a microalgae productivity prediction model together with weather forecasts. In this study, the fresh medium injection and culture removal rates are controlled to maintain the biomass concentration and pond temperature at their optimal values at two locations in France. Later, this strategy was used in [24] to analyze the improvement in productivity in the operation of the reactor. This optimization has recently been improved in [25], together with a study of the influence of weather variables on the growth of microalgae and the

inaccuracy of weather forecast.

On the other hand, the combined biomass production process coupled with wastewater treatment and bacteria groups a series of processes that must be evaluated and characterized. In the literature, it is possible to find different models and approaches that describe the processes related to the growth of the species. In [76] the variations and the impact of environmental conditions in the cultivation of microalgae and bacteria in a thin layer reactor are analyzed, for the treatment of wastewater. On the other hand, in [18], a new model (ALBA) describing the algae-bacteria ecosystem evolution in an outdoor raceway for wastewater treatment is presented by Bernard *et al.*. In addition, innovative techniques such as neural networks and fuzzy logic control are being used to characterize processes related to wastewater treatment, as presented in [55]. Moreover, a dynamic model considering the main environmental variables (light intensity, temperature, pH, and dissolved oxygen) which influence on microalgae and bacteria growth is presented by Sánchez Zurano *et al.* in [78]. This model is based on the equation stated in the BIO_ALGAE model described by Solimeno in [86], where an integral mechanistic model describing the complex interactions in mixed algal-bacterial systems is presented. In addition, in [77], a new photo-respirometry method for determining the rates of the main metabolic processes of microalgae-bacteria consortia in microalgae-based wastewater treatment processes has been developed and tested. These combined processes present changing dynamics depending on the type of medium and its composition. So, it is difficult to have models that faithfully adjust to its evolution. The need for models that allow adjusting to the changing characteristics of the culture or calibration methods of certain parameters belonging to the process whose value is known in a certain range is evident.

Related to pH and dissolved oxygen control, some approach examples using Proportional-Integral-Derivative (PID) controllers have been proposed in the literature, as they are widely used in industry with satisfactory results and can be used for this type of processes. An example of a linear Proportional-Integral (PI) controller with feedforward compensation for pH control in tubular photobioreactors can be found in

[29]. In [37], a robust PID controller for pH in raceway reactors based on Quantitative Feedback Theory (QFT) is used. Recently, a PI for pH control in raceway reactor based on Wiener models is presented in [63]. On the other hand, event-based control is gaining a great interest for this kind of processes. Concerning this type of control, in [59], a controller with a sensor deadband achieves a considerable reduction of CO_2 losses in a microalgae tubular photobioreactor. Another example can be seen in [60], where an event-based Generalize Predictive Controller (GPC) with a disturbance compensation approach is used for the effective use of CO_2 in a raceway reactor. Subsequently, this GPC scheme was improved in [61] and combined with a selective control for dissolved oxygen. A simulation study using Proportional-Integral (PI) and GPC controllers plus a feedforward compensator in raceway reactors is presented in [62]. More recently, in [38], a predictive linear control law for pH in a raceway reactor is used to design a GPC based on a simplified First-Order-Plus-Dead-Time (FOPDT) model of the reactor. It should be noted that event-based pH control has great potential due to the low computational cost and characteristics of the process, in addition to considerably reducing CO_2 injection due to the fact that it is not carried out continuously. Furthermore, most of the control approaches proposed in the literature are carried out exclusively during the daytime period, so there are no references of control architectures during the whole day. An approach that encompasses both daytime and night-time control would be really interesting, since it could control the pH fluctuations that occur during the night due to variations in the carbonate-bicarbonate equilibrium.

1.5 Contributions

The results discussed in this thesis have been presented in the following scientific publications:

Journals

1. E. Rodríguez, A. Sánchez, F.G. Acién and J.L. Guzmán. Feasibility seasonal study for culture depth influence on temperature for different microalgae strains. *Biotechnology and Bioengineering, 2021. (Submitted)*

2. A. Sánchez, E. Rodríguez, J.L. Guzmán, F.G. Acién, J.M. Fernández and E. Molina. ABACO: A New Model of Microalgae-Bacteria Consortia for Biological Treatment of Wastewaters. *Applied Sciences, 11(3):998 – 1022, 2021.* doi:10.3390/app11030998.

3. E. Rodríguez, F.G. Acién, J.L. Guzmán, M. Berenguel and A. Visioli. Indirect regulation of temperature in raceway reactors by optimal management of culture depth. *Biotechnology and Bioengineering, 1– 13, 2020.* doi:10.1002/bit.27642.

4. E. Rodríguez, F.G. Acién, J.L. Guzmán, M. Berenguel and A. Visioli. A new model to analyze the temperature effect on the microalgae performance at large scale raceway reactors. *Biotechnology and Bioengineering, 118:877 – 889, 2020.* doi:10.1002/bit.27617.

5. E. Rodríguez, J.L. Guzmán, M. Berenguel, F.G. Acién and A. Visioli. Diurnal and nocturnal pH control in microalgae raceway reactors by combining classical and event based control approaches. *Water Science and Technology, 82(6):1155 – 1165, 2020.* doi:10.2166/wst.2020.260.

6. E. Rodríguez, M. Beschi, J.L. Guzmán, M. Berenguel and A. Visioli. Daytime/nighttime Event based PI control for the PH of microalgae raceway reactor. *Processes, 7(5):247 – 263, 2019.* doi:10.3390/pr7050247.

Conferences

1. E. Rodríguez, F.G. Acién, J.L. Guzmán, M. Berenguel and A. Visioli. Modelo de temperatura para reactores abiertos de microalgas. *In XL Jornadas de Automática, Ferrol, Spain, 582 – 588, 2019.* doi:10.17979/spudc.9788497497169.582.

2. E. Rodríguez, J.L. Guzmán, M. Berenguel, F.G. Acién and A. Visioli. Diurnal and nocturnal pH control in microalgae raceway reactors. *In the 2nd IWA Conference on Algal Technologies for Wastewater Treatment and Resource Recovery, Valladolid, Spain, 1 – 2, 2019.*

3. E. Rodríguez, M. Beschi, J.L. Guzmán, M. Berenguel and A. Visioli. Application of a Symmetric-Send-On-Delta Event-based controller for a microalgal raceway reactor. *In the 18th European Control Conference, ECC 2019, Naples, Italy, 1 – 6, 2019.* doi:10.23919/ECC.2019.8795912.

Framework and facilities

This chapter is structured as follows: Section 2.1 introduces the research project where this thesis was carried out and Section 2.2 describes the research center and the raceway reactors used for the experimental tests.

2.1 The CALRESI project

The project CALRESI (Modelado y **C**ontrol del proceso combinado de producción de micro**AL**gas y tratamiento de aguas **RESI**duales con reactores industriales – Modeling and control of the combined process of microalgae production and wastewater treatment with industrial reactors) deals with the analysis, study and application of modeling and control strategies for the optimization of the process of wastewater treatment and biomass production of microalgae in large scale industrial photobioreactors. This project aims to achieve optimal working conditions that allow an efficient synergy of the combined process of optimal microalgae growth and wastewater treatment, trying to achieve an appropriate balance between the energy required for such a process, the injection of CO_2 for the maximization of microalgae production, and cost recovery through the derived products. Microalgae use nutrients from wastewater (carbon, nitrogen and phosphorus), thus avoiding the use of chemical fertilizers. The appropriate combination of microalgae with wastewater will allow the achievement of an energy balance for this type of processes and, at the same time, contributing to carbon mitigation of emissions to the environment.

It is relevant to stress that the presence of microalgae, bacteria and organic matter makes such systems to have highly complex and nonlinear

dynamics. As a result, there are different modeling and control tasks to be achieved along this project:

- Development and proposal of strategies of modeling, estimation and identification for the combined process of the production of microalgae and treatment of wastewater in raceway reactors.

- Development and proposal of different control strategies for the efficient production of biomass and wastewater in order to contribute to the reduction of costs and environmental impact.

- Implementation and validation of modeling and control strategies developed in two industrial large scale raceway photobioreactors.

The focus of this project will address issues that are related to improve the efficiency, productivity, design and optimization of large-scale raceway combined wastewater treatment and microalgae production processes cultivated in outdoor conditions by means of using adequate modeling and control strategies. The implementation of these strategies will contribute in better reproducible conditions with competitive market costs by analysing/simulating new photobioreactor designs, compensating for the permanent non-stationary behaviour of the processes, the presence of disturbances, taking advantage of nutrients provided by wastewater to the culture (mainly carbon, nitrogen, oxygen and phosphorous), removing any toxic metabolic products (e.g. CO_2 mitigation), and controlling important internal cellular parameters (e.g. temperature, pH), in order to optimize the biomass production.

2.2   IFAPA research center

The research activities carried out during the period of the doctoral program have been carried out in facilities located in the IFAPA research center, near the University of Almería, in Spain.

The Andalusian Institute for Agricultural, Fisheries, Food and Ecological Production Research and Training (IFAPA) bases its creation

to respond to the demands of the Andalusian agricultural, fishing, aquaculture and food sectors.

IFAPA aims to be an agile and efficient instrument in its operation, realistic and pragmatic in its action programs, and focused on promoting research, technological innovation and training in the field of agriculture, fisheries and the food industries.

This center has many facilities for the cultivation and production of microalgae biomass, with multiple photobioreactors both closed tubular and raceway of different sizes. In addition, it has laboratories and equipments to analyze the status of microalgae culture and other parameters related to their growth.

2.2.1   Raceway reactors

For the development of the models and approaches presented in this thesis, two identical raceway reactors located at the IFAPA center have been used. These reactors are found in Figure 2.1 and their main objective is the biomass production establishing comparisons between both reactors, such as tests with different control architectures or different culture medium. The reactors have a total surface of 80 m^2 and are composed of two 40 m long channels, connected by a 1 m wide U-shaped bends. The channel walls are made of low density polyethylene of 3 mm thickness while the curves and sump walls are made of high density polyethylene of 3 mm thickness. The mixing of the culture inside the reactors is made by a paddlewheel of aluminum blades with a diameter of 1.5 m, driven by an electric motor (W12 35 kW, 1500 rpm, Ebarba, Barcelona, Spain), with gear reduction (WEB Ibérica S.A., Barcelona, Spain). The control of the paddlewheel is performed with a frequency inverter (CFW 08 WEB Ibérica, S.A., Barcelona, Spain) at a constant velocity of 0.2 m/s. Carbonation is performed inside a sump located 1.8 m downstream of the paddlewheel, which dimensions are 1.0 m depth, 0.65 m length and 1.0 m width. In this sump, CO_2 gas or air can be injected through three plate membrane diffusers at the bottom of the sump (AFD 270, EcoTec, Spain).

The measurements of the climatic conditions are obtained from a meteorological station, while the reactors have different probes for pH,

dissolved oxygen and temperature. Table 2.1 shows the sensors used to take measurements of all the variables related to the developed control architectures. The sampling period for all the measurements is one second.

Figure 2.1: Raceway reactors located at IFAPA research center.

Measure	*Sensors*
Wind speed	Anemometer Thies Clima 4.3400.30.000
Global solar irradiance	Pyranometer Kipp & Zonen CM 6B
Ambient temperature and relative humidity	Delta Ohm HD 9008TRR
Culture temperature	Pt100 transducer
Culture pH	Crison 5330
Dissolved oxygen	Mettler Toledo InPro 6050
Culture depth	Ultrasonic Wenglor UMD402U035

Table 2.1: Description for the raceway sensors.

2.2.2 Laboratory scale photobioreactors

Experiments concerning biomass production with wastewater treatment were performed at laboratory scale in four stirred-tank reactors presented in Figure 2.2. They are made with polymethylmethacrylate (0.08 m in diameter, 0.2 m in height and with a 1 L capacity) operated in the laboratory but simulating outdoor raceway reactors.
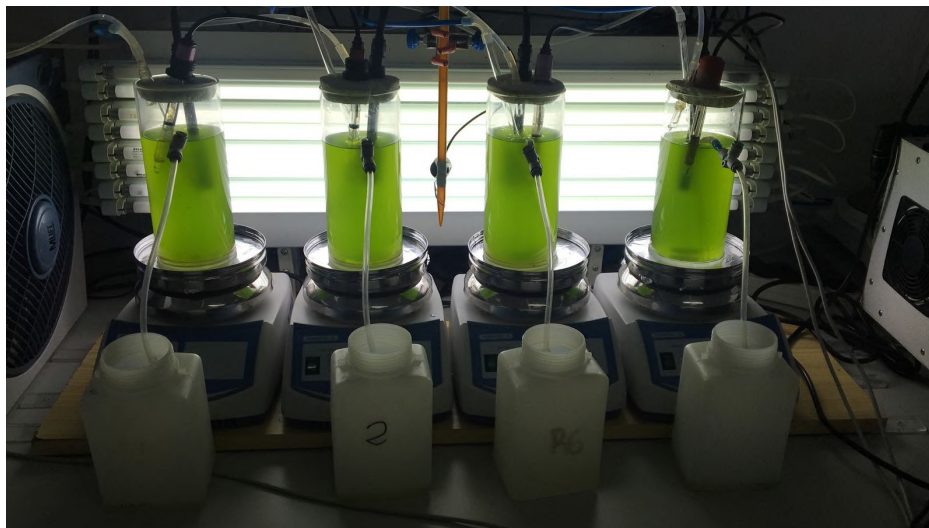
Figure 2.2: Laboratory scale photobioreactors.

These reactors were filled with sewage taken directly after primary treatment from the wastewater treatment plant in Roquetas de Mar (Almería) and 20% of *Scenedesmus almeriensis* inoculum. First, they were operated in batch mode for 6 days to achieve a high biomass concentration, next they being operated in continuous mode by replacing 20% of the culture volume with fresh wastewater daily, until the steady state is reached, after 10 days. To prevent the adverse effect of excessive dissolved oxygen accumulation, the dissolved oxygen was controlled below 200% of saturation by supplying air on demand; CO_2 was also injected on demand to control the pH at a value of 8. Concerning illumination, the reactors were artificially illuminated using eight 28 W

fluorescent tubes (Philips Daylight T5) on a simulated solar cycle. The maximum photosynthetic active radiation (PAR) inside the reactors in the absence of cells was 1000 μE m^{-2} s^{-1}, measured using an SQS-100 spherical quantum sensor (Walz GmbH, Effeltrich, Germany). The culture temperature was kept at 25°C by controlling the temperature of the culture chamber in which the reactors were located. Regarding pH and dissolved oxygen control, it is carried out through an On/Off control, injecting carbon dioxide or air when the established setpoints are exceeded, respectively.

2.2.3   Microalgae strain

Despite the fact that the characteristic parameters of different strains have been used during the development of the activities presented in this thesis, the microalgae strain that has been cultivated in the physical reactor corresponds to *Scenedesmus almeriensis* (CCAP 276/24) species. This strain can be used for animal and / or human consumption, and produces high amounts of carotenoids, especially lutein and beta-carotene. It is especially suitable for the production of carotenoids for application in the treatment of ocular macular disorders. It has been chosen for its cultivation because it is an autochthonous strain of the research location and its cultivation conditions are adequate. A detailed study about its characteristic parameters and conditions related to pH, dissolved oxygen and temperature can be found in [8]. The pH value ranges from 3 up to 10, but the net photosynthesis rate is close to the maximal value around 8. Regarding the temperature, the value ranges from 12 to 46 °C, but the optimum range is around 30 °C. The culture medium used in the growth of the microalgae has been freshwater and Mann & Myers medium prepared using fertilizers (0.14 g L^{-1} K(PO$_4$)$_2$, 0.18 g L^{-1} Mg(SO$_4$)$_2$, 0.9 g L^{-1} NaNO$_3$, 0.02 mL L^{-1} Welgro, and 0.02 g L^{-1} Kalentol) as described in [30].

2.2.4   Supervisory Control and Data Acquisition System

Both reactors have pH control, dissolved oxygen control, harvest and dilution control, and culture depth control. These control algorithms are

implemented in a Supervisory Control and Data Acquisition System (SCADA) tool, where it is possible to monitor all the measurable variables associated with the control of the reactors. Figure 2.3 shows the main screen of the SCADA tool, which contains the control and displays windows.
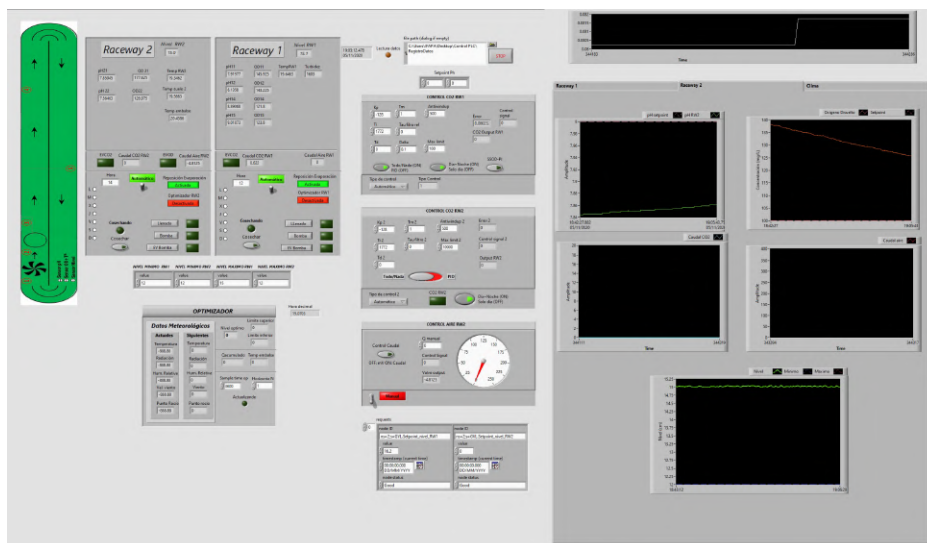
Figure 2.3: SCADA tool to control raceway reactors.

Data collection is done through a Schneider brand Programmable Logic Controller (PLC), model M241 TM241CE24T. Communication between the PLC and the SCADA tool is carried out through the OPC protocol using the UaExpert software tool.

On the other hand, the SCADA tool is designed using the LabVIEW software, developed by National Instruments. From its main screen, it is possible to view the measured variables of the reactors, as well as to activate the different actuators, such as CO_2, air or harvesting and dilution injection valves. In addition, all data are saved daily in a file for further processing.

The IFAPA research center, in addition to the raceway reactors presented above, has more facilities for the cultivation of microalgae. The

monitoring and control of these facilities is carried out through another SCADA tool belonging to the SABANA project (Sustainable Algae Biorefinery for Agriculture aNd Aquaculture). Figure 2.4 shows the main screen of this tool, designed in DAQfactory by Azeotech.

This tool allows the control and monitoring of the harvesting and dilution processes of all the facilities, in addition to recording the data measured from two weather stations, one outside and the other inside a greenhouse. Among the controlled facilities are: bubble columns with the inoculums of the microalgae strains, a greenhouse with three tubular photobioreactors and three raceway reactors, two external thin-layer reactors and a large raceway reactor (500 m^3).
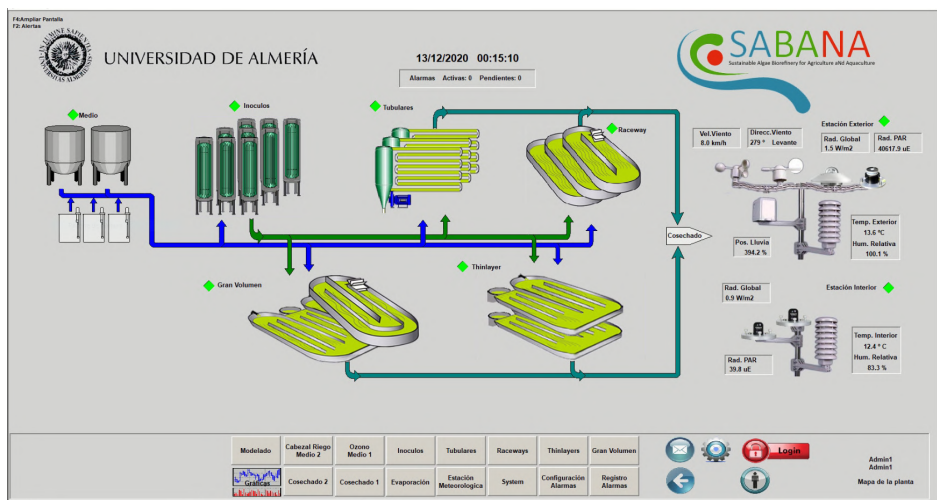
Figure 2.4: SABANA project SCADA tool.

Modeling approaches

The modeling of the processes related to microalgae biomass production is a fundamental aspect to understand the operation of these systems and analyze their behavior. Because they are living organisms, their dynamics are nonlinear and changing. So, it is necessary to develop models that faithfully describe these dynamics.

This chapter is structured as follows: Section 3.1 details the developed temperature model for raceway reactors. The combined model of microalgae growth and wastewater treatment is presented in Section 3.2. The changes made to a descriptive model for raceway reactors is showed in Section 3.3. Finally, conclusions are stated in Section 3.4.

3.1 Temperature modeling

In this section, a new simple temperature model is presented [68, 74], based on a review of the empirical relationships defined by Béchet *et al.* and Slegers *et al.* in [9, 83], and adapted to a raceway reactor. The culture temperature is calculated from a thermal balance in the reactor, taking into account all available environmental variables. This model allows the estimation of the culture temperature in the reactor for certain environmental conditions. In this way, the model could estimate parameters of interest, such as the time for harvesting or anticipate risk temperatures that can negatively affect the culture. In addition, the model may be used to analyse the temperature impact on biomass production for different locations. Therefore, design tools could be developed to study the viability of the microalgae production zones to determine the most suitable cultivation strains. Moreover, the temperature model can be used to improve existing microalgae

estimation models or biomass growth models, such as those presented in
[30] and [34]. Also, the temperature model can be used when there is a
lack of temperature measurements in the reactor, being useful as a
temperature estimator. Furthermore, the model can be used for optimal
control purposes, where knowledge of the evolution of the controlled
variables is essential to develop control approaches.

3.1.1   Thermal balance

The thermal balance described in this section is based on first principles
and empirical equations defined for the transfer of energy due to solar
irradiance, long wave radiation, evaporation, convection, and conduction.

Based on the models described in [9, 83], the energy balances that
affect the culture have been analized and established, and a new thermal
balance has been developed to estimate the culture temperature in the
reactor from measurable variables. The solar irradiance input comes from
data measured by the global (direct + diffuse) irradiance sensor
mentioned in Table 2.1. Long-wave radiation losses are calculated by the
Stefan-Boltzmann Law [28]. There are different methodologies in the
literature to obtain the evaporation flow [9]. In this case, the energy
balance by evaporation is calculated from the evaporation rate obtained
from an experimental evaporation exchange coefficient. Convection is
expressed by Newton's Law of cooling, and finally, conduction is
expressed as the heat transfer between the mass of the culture in the
reactor and the polyethylene layer that insulates the reactor from the
ground. The dilution and harvesting processes affect the temperature of
the culture due to the removal of volume or the injection of medium at
different temperatures. As a result of the introduced energy balances, the
thermal balance is expressed by the following equation (Q_i in W):

$$Q_{accumulated} = Q_{irradiance} + Q_{radiation} + Q_{evaporation} +$$
$$+ Q_{convection} + Q_{conduction} + Q_{harvesting} + Q_{dilution} \tag{3.1}$$

where $Q_{accumulated}$ is the heat accumulated in the reactor, $Q_{irradiance}$
represents the heat flow from sunlight, $Q_{radiation}$ is the long-wave

radiation heat flow, $Q_{evaporation}$ accounts for the heat flow produced by the evaporation process, $Q_{convection}$ is the heat flow caused by convection, $Q_{conduction}$ represents the heat flow between the reactor and the polyethylene layer under it through a conduction process, $Q_{harvesting}$ represents the heat flow due to volume loss by harvesting, and $Q_{dilution}$ describes the heat flow by the difference of new medium added into the reactor.

Accumulated heat flow

The heat accumulated in the reactor represents the sum of all energy terms that affect the reactor, and it is expressed as:

$$Q_{accumulated} = h \cdot A \cdot C_p \cdot \rho \cdot \frac{dT_w}{dt} \tag{3.2}$$

where h [m] is the culture depth, A [m^2] is the surface of the reactor, C_p [J kg^{-1} °C^{-1}] is the specific heat capacity of the culture, ρ [kg m^{-3}] is the density of the culture, and T_w [°C] is the culture temperature in the reactor.

Heat flow due to the effect of solar irradiance

The heat flow due to incident solar irradiance on the reactor surface represents the main heat input into the reactor. It is expressed as:

$$Q_{irradiance} = I_g \cdot a \cdot A \tag{3.3}$$

where I_g [W m^{-2}] is the global (direct + diffuse) solar irradiance, a [-] is the absorptivity, and A [m^2] represents the total area of the reactor.

Radiation heat losses

The reactor emits thermal energy as long-wave radiation. The flow of radiated energy between the reactor and the sky is calculated as:

$$Q_{radiation} = \sigma \cdot A \cdot e \cdot \left(T_{sky}{}^4 - (T_w + 273.15)^4 \right) \tag{3.4}$$

where σ [W m^{-2} K^{-4}] is the Stefan-Boltzmann constant, e [-] is the water emissivity and T_{sky} [K] is the equivalent temperature of the sky, expressed as [28]:

$$T_{sky} = (273.15 + T_{amb})(0.711 + 0.0056 \cdot T_{dew} \cdot 0.000073 \cdot T_{dew}^2 + 0.13 \cdot \cos{(15 \cdot t_{solar})})^{0.25} \tag{3.5}$$

where T_{amb} [°C] is the ambient temperature, T_{dew} [°C] the dew point temperature, and t_{solar} [-] represents the number of hours after midnight.

Evaporation heat flow

The evaporation process represents the main source of heat loss in the reactor and depends on the shape of the reactor, the evaporation rate and the latent heat of vaporization, as presented in [66]. The evaporation heat flow is determined as:

$$Q_{evaporation} = A \cdot E_p \cdot \rho \cdot h_{fg} \tag{3.6}$$

where E_p [m s^{-1}] is the evaporation rate and h_{fg} [J kg^{-1}] is the latent heat of vaporization, expressed as follows:

$$h_{fg} = (2494 - 2.2 \cdot T_w) \cdot 1000 \tag{3.7}$$

The evaporation rate can be calculated as an empirical equation which depends on the difference in vapour pressures between the ambient air and the reactor culture mass [66, 80], in addition to an evaporation exchange coefficient which depends on wind speed W_s:

$$E_p = \left(\frac{RH \cdot p'_A}{100} - p'_A \right) \cdot h_{evap} \tag{3.8}$$

where RH [%] is the relative humidity, p'_A [Pa] is the vapor pressure of the air at ambient temperature and h_{evap} [m s^{-1} Pa^{-1}] is an evaporation exchange coefficient, obtained experimentally from the following equation:

$$h_{evap} = A_{evap} + B_{evap} \cdot W_s \tag{3.9}$$

where W_s [m s^{-1}] is the wind speed and A_{evap} [-] and B_{evap} [-] are evaporation experimental coefficients that must be calibrated (with adequate units).

For the calculation of the vapour pressure of the environment at ambient temperature p'_A [Pa], the Tetens equation [54, 89] has been used:

$$p'_A = 0.61078 \cdot exp\left(\frac{17.27 \cdot T_{amb}}{T_{amb} + 237.3}\right) \cdot 1000 \tag{3.10}$$

Convection heat flow

The phenomenon of convection occurs between the mass of water in the reactor and the air in the environment, resulting in a positive or negative balance depending on the moment of the day and the ambient temperature. The convection balance is represented as:

$$Q_{convection} = h_{conv} \cdot A \cdot (T_{amb} - T_w) \tag{3.11}$$

where h_{conv} [W m^{-2} °C^{-1}] is the convection transfer coefficient, obtained experimentally as previously done for the evaporation:

$$h_{conv} = A_{conv} + B_{conv} \cdot W_s \tag{3.12}$$

with A_{conv} [-] and B_{conv} [-] experimental coefficients that must be calibrated.

Heat flow by conduction

The thermal conduction balance represents the thermal exchange between the reactor and the surface under it. Notice that polyethylene was the material used for the construction of the bottom of the reactor. So, the following equation represents the conduction balance:

$$Q_{conduction} = h_{soil} \cdot A_{soil} \cdot (T_{soil} - T_w) \tag{3.13}$$

where h_{soil} [W m^{-2} °C^{-1}] is the heat transfer coefficient for the polyethylene layer under the reactor, A_{soil} [m^2] is the surface of the reactor in contact with the ground and T_{soil} [°C] represents the temperature under the polyethylene layer of the reactor. The transfer coefficient h_{soil} can be expressed as:

$$h_{soil} = \frac{K_{soil}}{x_{soil}} \tag{3.14}$$

where K_{soil} [W m^{-1} °C^{-1}] is the conduction transfer coefficient for the polyethylene layer (calibration parameter) and x_{soil} [m] represents the distance between the bottom of the reactor and the buried temperature probe.

Harvesting heat flow

The harvesting process removes a certain amount of volume from the reactor, decreasing the total net heat and modifying the volume of the reactor. This flow depends on the harvesting flow rate determined by the pump and the temperature of the culture T_w. The balance is described as:

$$Q_{harvesting} = -Q_h \cdot \rho \cdot C_p \cdot T_w \tag{3.15}$$

where Q_h [m^3 s^{-1}] is the harvesting pump flow rate.

Dilution heat flow

The dilution process introduces medium into the reactor, increasing its volume. In addition, the medium is at a different temperature, so it influences the culture temperature. This balance depends on the dilution flow rate and the temperature of the dilution medium. It is expressed as:

$$Q_{dilution} = Q_d \cdot \rho \cdot C_p \cdot T_m \tag{3.16}$$

where Q_d [m^3 s^{-1}] is the dilution pump flow rate and T_m [°C] is the temperature of the dilution medium.

3.1.2 Temperature model

The model depends on a series of environmental input variables that are solar irradiance, ambient temperature, relative humidity and wind speed. Other input variables are culture depth, harvesting and dilution rates, soil temperature and dilution medium temperature, which can be easily estimated or approximated, instead of measured. Specifically, the culture depth can be set to its common value, the harvesting and dilution rate usually are constant values, and the temperature of the soil under the reactor and the dilution medium can be estimated or set to constant values, based on approximations with ambient temperature or historical data. In this way, only the measurements of the environmental variables would be needed to run the model and use it as a temperature estimator.

The dynamic evolution of culture temperature is obtained from (3.1), based on the thermal balances described and reformulated as:

$$\frac{dT_w}{dt} = \frac{Q_{total}}{h \cdot A \cdot C_p \cdot \rho}$$

where

$$\boldsymbol{Q_{total}} = Q_{irradiance} + Q_{radiation} + Q_{evaporation} + Q_{convection} +$$
$$+ Q_{conduction} + Q_{harvesting} + Q_{dilution}$$

$$\tag{3.17}$$

Table 3.1 contains the description and the values of all the parameters used in the thermal balance of the temperature model, separated in constant and variable parameters.

Parameter	Description	Value	Unit
Parameters			
A	Surface of the reactor	80	m^2
C_p	Specific heat capacity of the culture	4184	$J\,kg^{-1}\,°C^{-1}$
ρ	Density of the culture	1000	$kg\,m^{-3}$
a	Absorptivity	0.7	-
σ	Stefan–Boltzmann constant	$5.6697 \cdot 10^{-8}$	$W\,m^{-2}\,K^{-4}$
e	Water emissivity	0.9	-
A_{evap}	Evaporation experimental coefficient A	$1.20 \cdot 10^{-11}$	-
B_{evap}	Evaporation experimental coefficient B	$4.67 \cdot 10^{-12}$	-
A_{conv}	Convection experimental coefficient A	4.78	-
B_{conv}	Convection experimental coefficient B	6.83	-
K_{soil}	Conduction transfer coefficient for the polyethylene layer	0.43	$W\,m^{-1}\,°C^{-1}$
x_{soil}	Thickness of the polyethylene layer of the reactor	0.02	m
A_{soil}	Surface of the reactor in contact with the ground	80	m^2
Q_h	Harvesting pump flow rate	$0.66 \cdot 10^{-3}$	$m^3\,s^{-1}$
Q_m	Dilution pump flow rate	$0.82 \cdot 10^{-3}$	$m^3\,s^{-1}$
Variables			
h	Medium depth	–	m
T_w	Temperature of the culture	–	°C
I_g	Global solar irradiance	–	$W\,m^{-2}$
T_{sky}	Temperature of the sky	–	°C
T_{amb}	Ambient temperature	–	°C
T_{dew}	Dew point temperature	–	°C
t_{solar}	Number of hours after midnight	–	-
h_{fg}	Latent heat of vaporization	–	$J\,kg^{-1}$
E_p	Evaporation rate	–	$m\,s^{-1}$
RH	Relative humidity	–	%
p'_A	Vapor pressure of the air at ambient temperature	–	Pa
h_{evap}	Evaporation exchange coefficient	–	$m\,s^{-1}\,Pa^{-1}$
W_s	Wind speed	–	$m\,s^{-1}$
h_{conv}	Convection transfer coefficient	–	$W\,m^{-2}\,°C^{-1}$
T_{soil}	Soil temperature	–	°C
T_m	Dilution medium temperature	–	°C

Table 3.1: Temperature model parameters description.

3.1.3 Results and discussion

The results are presented in two parts: first, the calibration process is shown, and second, the results for the validation stage are presented.

Calibration

The temperature model equation makes use of a series of parameters whose exact values are unknown, or the values are known in a defined range. The uncertainty of these parameters shows the need for a calibration process, which has been carried out through genetic algorithms. Calibration using genetic algorithms results in an useful and reliable method in the estimation of uncertain parameters, since it allows optimizing a certain cost function that measures the deviation of the output of the model from that of the real system by modifying the parameter values between the established limits. The range of the estimated parameters has been obtained from the cited literature, as well as from the experience in the design of the installation.

The calibration process using genetic algorithms has been implemented in Matlab using the Genetic Algorithm Optimization Toolbox (GAOT), based on [36], with an initial population of 50 phenotypes (solutions) and a termination condition of 50 generations. This method starts with an initial set of calibration parameters and runs the model to obtain the error. The cost function is computed as the Root Mean Square Error (RMSE) between the simulated temperature and the real culture temperature, expressed as the following equation:

$$J = \sqrt{\sum_{i=1}^{N} \frac{(T_{sim}(i) - T_w(i))^2}{N}} \qquad (3.18)$$

where T_{sim} [°C] is the estimated temperature, T_w [°C] is the real culture temperature in the reactor and N represents the size of the data vector.

The method modifies the calibration parameters in each iteration of the genetic algorithm in the simulation as new population generations, within established limits, until the error cost function is minimized.

Three consecutive days from every month from August to December 2019 (15 days in total) have been used by the genetic algorithm to estimate the values of the calibration parameters trying to capture the different season dynamics. The measured data used for calibration purposes, which represent the input variables for the model (solar irradiance, ambient temperature, soil temperature, wind speed, the relative humidity and the culture depth), are shown in Figure 3.1 and separated by colours for each different month. As can be seen, there exist a large variability in the climatic data. Notice that the temperature of the dilution medium is not represented. This is due to the lack of measurement sensors in the reservoir used as fresh medium, so the mean value of ambient temperature will be used as the temperature of the dilution medium.

Table 3.2 presents the values of the calibration parameters obtained using the calibration data set. The evaporation (A_{evap} and B_{evap}) and convection (A_{conv} and B_{conv}) calibration parameters are related to evaporation and convection transfer coefficients, respectively. The conduction coefficient (K_{soil} [$W\ m^{-1}\ °C^{-1}$]) ranges from 0.33 to 0.50 due to the polyethylene thermal conduction coefficient.

Symbol	Parameter	Value	Unit
A_{evap}	Evaporation coefficient parameter A	$1.20 \cdot 10^{-11}$	–
B_{evap}	Evaporation coefficient parameter B	$4.67 \cdot 10^{-12}$	–
A_{conv}	Convection coefficient parameter A	4.78	–
B_{conv}	Convection coefficient parameter B	6.83	–
K_{soil}	Conduction coefficient	0.43	W m^{-1} °C^{-1}

Table 3.2: Calibration parameters for the temperature model.

The calibration results are shown in Figure 3.2, where the results of each month are individually plotted in different colors for better visualization. The differences between the temperature from one month to another are clearly visible, and the model is able to capture the temperature dynamics during the whole day, in addition to adjust to the
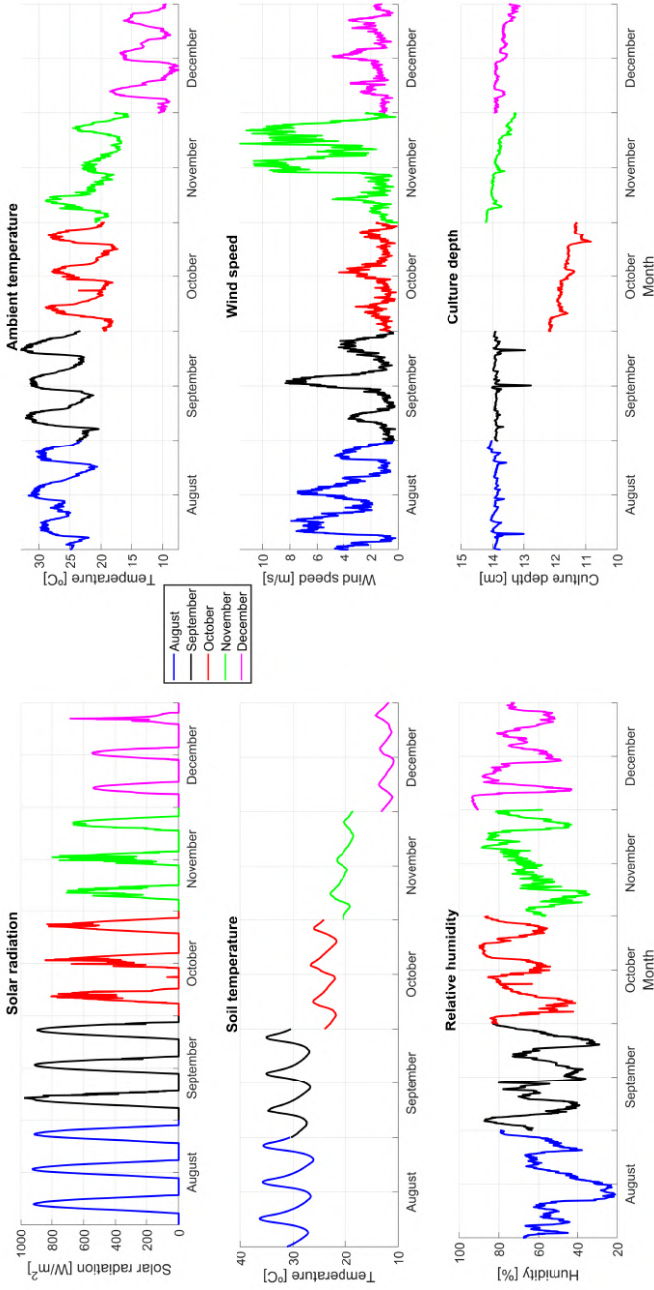
Figure 3.1: Environmental input variables for calibration. Every color represents three consecutive days of the month from August to December.
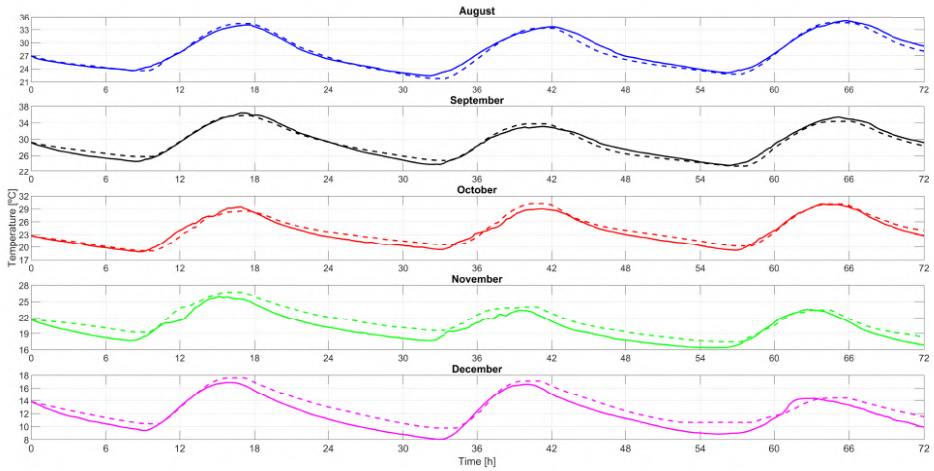
Figure 3.2: Temperature calibration results. Each individual color plot represents three consecutive days for the selected months from August to December. Dashed lines represent real reactor temperature while solid lines represent estimated temperature.

ranges of each month. The RMSE value obtained is 0.97 °C, while the mean temperature error is 0.85 °C, which is a satisfactory result. A maximum temperature error of 2.36 °C occurs during night-time periods on November.

When the results of each month are analyzed, it can be seen that the dynamics of the model resembles the real temperature in the raceway reactor during all months. Although the dynamics and the maximum and minimum temperatures of each month vary, the model fits the real evolution in all cases, estimating the temperature properly. For the months of August, September and October, the model correctly estimates the culture temperature in the reactor, with an average error of 0.6 °C. However, for the cold months of November and December, the model presents slightly larger errors, especially at night, with an average error of 1.1 °C for those months. Anyway, the relevant dynamics of the temperature variable is captured and the errors are small for the model purposes.

Validation

For the validation of the model, a set of 50 days has been used, belonging to the months from August to December 2019. This data set, presented in Figure 3.3, shows the entire range of temperatures that can occur in the year, from the high values of August to the low ones on December. Due to the scarcity of data and the fact that the temperature maintains a similar evolution for each day (corresponding to the solar radiation bell), it has been decided to use a data set for validation that is greater than the calibration data set. The input data is grouped in 5 months with 10 consecutive days each, presented in different colors for a better visualization. The temperature differences are perfect to check the adaptability of the temperature model and verify that it faithfully represents the dynamics of the system, regardless of the month. Figure 3.4 shows the validation results for the temperature model, where each month is represented individually following the same than for the calibration results. The model follows the dynamics of the culture temperature in the reactor, with a maximum error of 3.9 °C and an average error of 0.86 °C. For the entire data set, an RMSE value of 1.03 °C has been obtained.

As in the calibration results shown in Figure 3.2, the estimated temperature for the months of August and September adequately resembles the real temperature of the reactor, with a mean error of 0.5 °C. The results for the month of October during the daytime period are very satisfactory. However, during the night-time there are certain discrepancies, increasing the mean error to 0.95 °C. These errors, as the last plotted day of October, may be due to errors in the measurements of the input variables or isolated punctual phenomena that affect the temperature of the reactor. On the other hand, the months of November and December have a greater error (mean error of 1.15 °C) in the estimation, although the dynamics resembles the real temperature and the results are adequate.
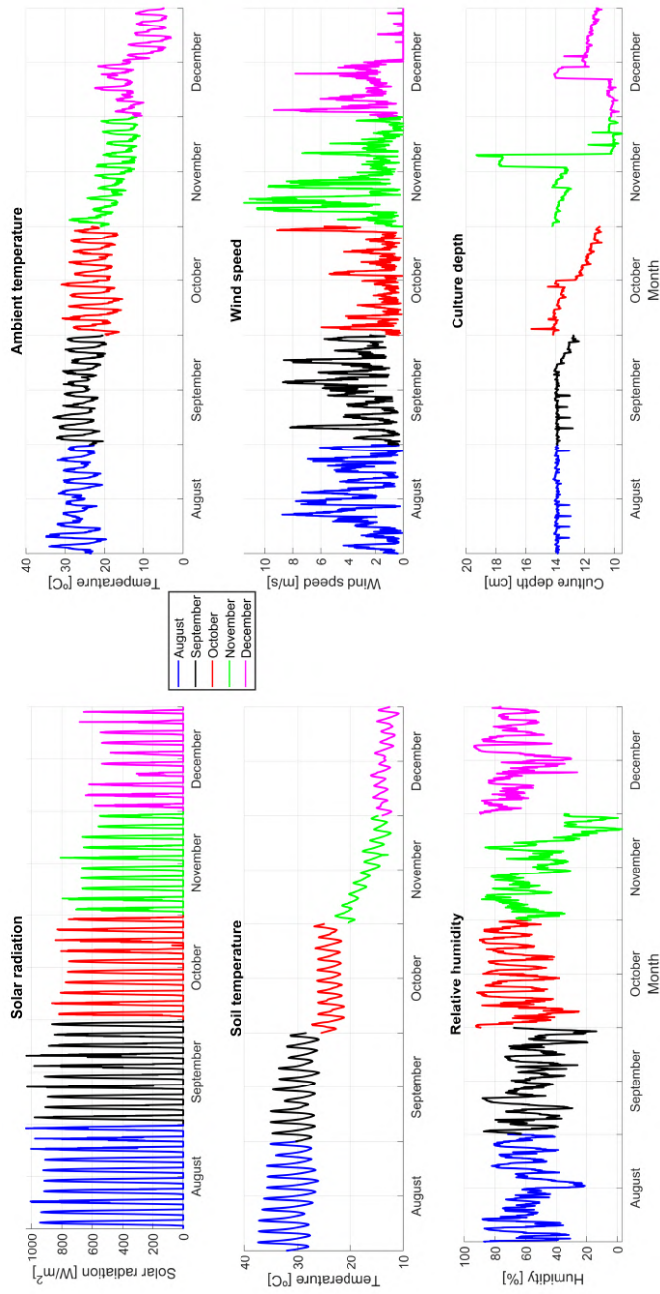
Figure 3.3: Environmental input variables for validation. Each month (from August to December) is represented by different colors and it is made up of 10 consecutive days each.
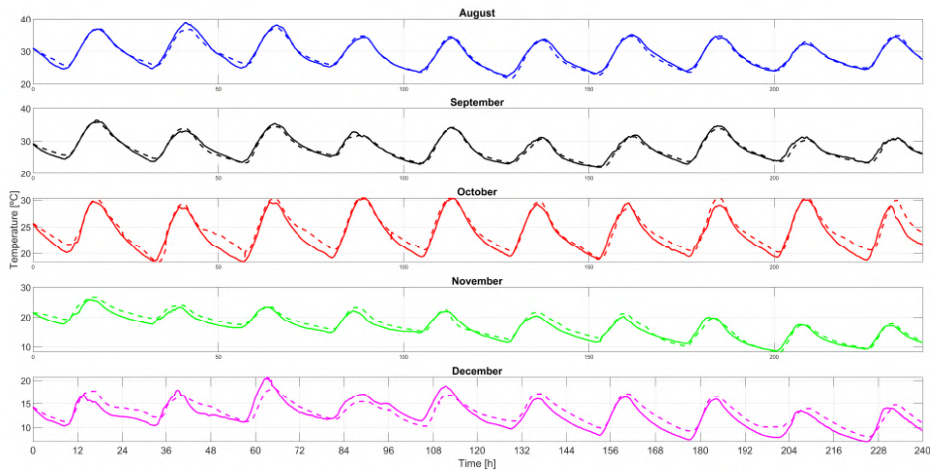
Figure 3.4: Temperature validation results. Every individual color plot represents ten consecutive days for the selected months from August to December. Solid line represents estimated temperature while dashed line represents real reactor temperature.

Discussion

The error obtained in Figures 3.2 and 3.4 denotes a promising accuracy in the model obtained from thermal balances. From the biological point of view, the error related to the estimated and the actual temperature would not be a problem according to the global process dynamics. The model is able to accurately represent the temperature during the whole day. However, notice that in some days the error is larger than in others. These mismatches may be due to the existence of non-measurable terms or disturbances that have not been contemplated in the thermal balances, such as punctual errors in the measurements, irregular operations in the reactor or the temperature of dilution medium. On the other hand, the calibration by means of genetic algorithms allows to obtain specific values of parameters used in the equations that are subjected to uncertainty, as they are in lumped-parameters representations of balances that should require distributed parameter representations and, thus, are usually difficult to obtain from tables. In general, the results obtained have been

positive and notable for the use of the model in the development of microalgae growth models where its dynamics and other parameters such as productivity, performance, consumption of CO_2, and evolution of pH are estimated.

The environmental conditions depend on the weather and can be very different from one season to another. This fact has been taken into account in the calibration of the model so that it can adjust to all the environmental conditions of each month, without changing the parameters or increasing the model complexity. On the other hand, being a model designed for all months of the year, there are certain errors due to a generalization of parameters, but a tradeoff between performance and complexity has been found.

The temperature estimation is really useful in the microalgae production process. The temperature model can be combined with existing microalgae biomass production models to add the effect of temperature on growth and thus making more accurate and complete microalgae production models. On the other hand, temperature estimation can be used as a design tool when installing a reactor in a determined location. From the growth productivity model and the environmental conditions, it is possible to estimate the temperature of the culture for a reactor in that area and establish its maximum biomass productivity or the microalgae strain viability. In this way, it is possible to assess the suitability to install a raceway reactor in any specific area or establish different microalgae cultures depending on the season. Moreover, it can also be used to design control algorithms to optimize the reactor temperature.

3.2 Combined microalgae biomass production process and wastewater treatment

The combination of microalgae biomass production processes and wastewater treatment is an innovative goal that poses several challenges. On the one hand, wastewater has a number of components that affect microalgae growth. On the other hand, in addition to microalgae, new

microorganisms are introduced into the reactor, such as nitrifying and heterotrophic bacteria, which compete for the consumption of some common nutrients.

That is why the study and analysis of the behavior of each species in this new process, as well as the control of the nutrients on it, becomes evident. The diversity in the composition of the wastewater and the difficulty in measuring bacterial populations are the main obstacles to overcome [78].

In collaboration with a researcher from the IFAPA center and using a biomass growth and production model for this combined process, a calibration of its characteristic parameters has been carried out [79]. This model represents the influence of the nutrients and compounds present in the wastewater on the growth of microalgae and bacteria. The model is made up of a series of parameters, some of which are known for their value in a certain range. This fact highlights the need for an adequate calibration process to determine the value of these parameters. From experimental data and through genetic algorithm calibration, the value of the model parameters has been determined, making it possible to use it in the estimation of all the compounds that form the combined biomass production and wastewater treatment process.

3.2.1 Photosynthesis process

The combined process of production of microalgae biomass with wastewater treatment introduces the bacteria as new organisms present in the photobioreactor. Bacteria grow independently of microalgae and are related in various processes, especially in the consumption of nutrients present in wastewater. Microalgae and bacteria growth depends on solar irradiance, temperature, pH, dissolved oxygen and nutrients present in the culture medium. Figure 3.5 presents a diagram of the photosynthesis process on a laboratory scale.

During the photosynthesis process, the microalgae grow, fixing inorganic carbon (CO_2 and HCO_3), consuming substrates present in the wastewater (NH_4, NO_3, PO_4 and SO_4) and producing oxygen. On the other hand, from the oxygen produced by the microalgae, the
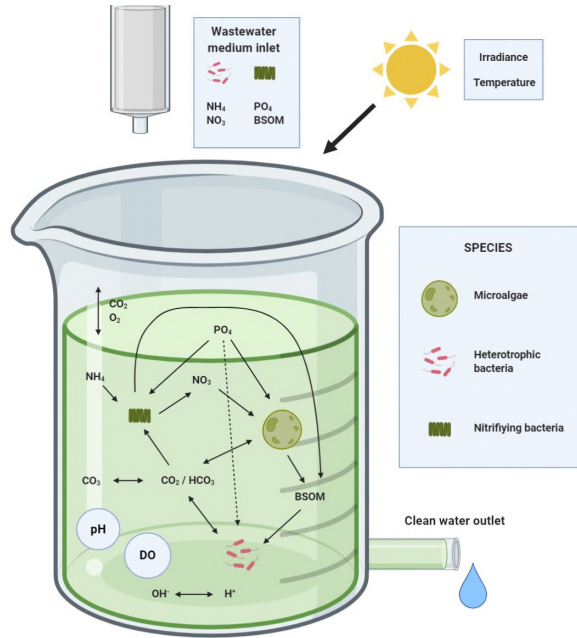
Figure 3.5: Microalgae and bacteria photosynthesis process scheme.

heterotrophic bacteria (X_{HET}) oxidize the biodegradable soluble organic matter (BSOM) and the nitrifying bacteria (X_{NIT}) carry out the nitrification process.

As a result of the activities of the microalgae, the concentration of hydroxide anions (OH^-) and the pH increase. Due to this process, the bicarbonate-carbonate equilibrium shifts, increasing the production of carbonate (CO_3), which causes the volatilization of ammonium (NH_4) and the precipitation of phosphorus.

Moreover, during the oxidation of organic matter, the carbon dioxide (CO_2) produced is used for the photosynthesis and nitrification processes. The nitrification process consists of two phases: first, ammonium oxidizing bacteria convert ammonium to nitrite (NO_2), and then nitrite oxidizing bacteria convert nitrite to nitrate (NO_3). This transformation releases hydrogen ions in the process. Both species are considered as a group of

nitrifying bacteria.

In darkness, both bacteria and microalgae release CO_2 through oxidation of organic matter and endogenic respiration, respectively. This release of CO_2 increases the concentration of hydrogen ions (H^+), which causes a drop in pH and the bicarbonate-carbonate balance shifts in the opposite direction, converting carbonate into bicarbonate (HCO_3).

3.2.2   Combined specific growth rate model

The combined biological model for wastewater treatment has been developed considering the main microalgal and bacterial processes which occur simultaneously in the microalgae-based wastewater treatment.

This model, which is based on the initial dynamic models presented in [78], has been evaluated and validated from two sets of experimental data considering the effects of the different elements on the growth rate and respiration of microalgae-bacteria consortium, distinguishing between the activity of microalgae, the activity of heterotrophic bacteria and the activity of nitrifying bacteria, considering the methodology set out by Sánchez Zurano *et al.* in [77].

This biological model was improved considering the influence of the CO_2 and nutrients (NH_4, NO_3, PO_4 and biodegradable soluble organic matter) in the microalgae and bacteria growth. The influence of these nutrients has been analyzed in collaboration with a researcher from the IFAPA center. The combined specific growth model adds new normalized terms to the specific growth rate model described in Section 1.2.

The parameters of the model related with the microalgae processes have been determined experimentally [77], while the bacterial parameters were obtained from the Activated Sludge Models (ASM). Figure 3.6 shows the inputs and outputs of the simulation model developed to estimate the concentration of the different elements involved in the reactor.

The nutrients present in the culture medium affect the growth of the different species in the reactor. Therefore, the growth rate model for the two species of bacteria treated in the reactor is presented.
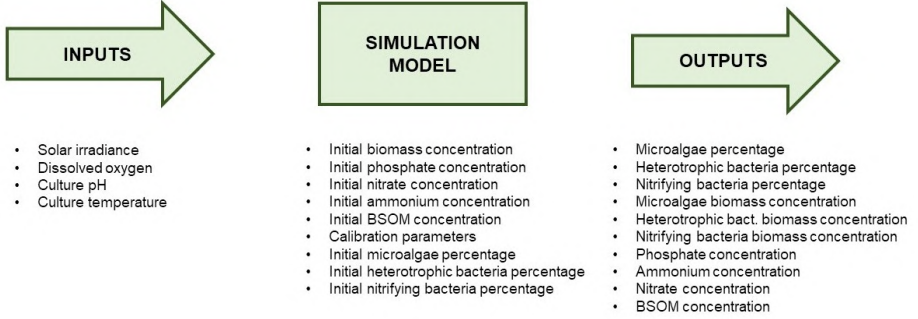
Figure 3.6: Inputs and outputs of the model.

Microalgae

The microalgae specific growth rate described in Section 1.2 depends on pH ($\overline{\mu_{alg}}(pH)$), dissolved oxygen ($\overline{\mu_{alg}}(DO)$) and temperature ($\overline{\mu_{alg}}(T_w)$). With fresh water and fertilizers as a culture medium, nutrients are always in excess, so they do not limit growth. However, when using wastewater as the culture medium, the nutrient concentrations change depending on the type of wastewater and the growth of microalgae and bacteria in the reactor. That is why it is necessary to include the influence of nutrients as a limiting factor on microalgae growth. Specifically, the influence of CO_2 ($\overline{\mu_{alg}}(CO_2)$), ammonium ($\overline{\mu_{alg}}(NH_4)$), nitrate ($\overline{\mu_{alg}}(NO_3)$) and phosphate ($\overline{\mu_{alg}}(PO_4)$). The complete growth rate of microalgae is described as:

$$\mu_{alg} = \mu_{alg}(I_{av}) \cdot \overline{\mu_{alg}}(T_w) \cdot \overline{\mu_{alg}}(pH) \cdot \overline{\mu_{alg}}(DO) \cdot \overline{\mu_{alg}}(CO_2) \cdot \overline{\mu_{alg}}(NH_4) \cdot$$
$$\cdot \overline{\mu_{alg}}(PO_4)$$

$$(3.19)$$

If ammonium is present in the medium, the microalgae will consume the nitrogen from the ammonium first. When there is no ammonium present in the medium, the microalgae consume the nitrogen from the nitrate, so the specific growth rate would be represented as:

$$\mu_{alg} = \mu_{alg}(I_{av}) \cdot \overline{\mu_{alg}}(T_w) \cdot \overline{\mu_{alg}}(pH) \cdot \overline{\mu_{alg}}(DO) \cdot \overline{\mu_{alg}}(CO_2) \cdot \overline{\mu_{alg}}(NO_3) \cdot$$
$$\cdot \overline{\mu_{alg}}(PO_4)$$

$$(3.20)$$

The new factors introduced to the specific growth rate equation are normalized terms whose value is between 0 and 1. Each term represents the influence of the element on the microalgae growth. The influence of carbon dioxide (CO_2) is described as:

$$\overline{\mu_{alg}}(CO_2) = \frac{X_{CO_2} + X_{HCO_3}}{K_{S,C,alg} + X_{CO_2} + X_{HCO_3} + \frac{X_{CO_2}^{n_{CO_2,alg}}}{K_{I,C,alg}}} \qquad (3.21)$$

where X_{CO_2} [g m^{-3}] is the carbon dioxide concentration in the reactor, X_{HCO_3} [g m^{-3}] is the bicarbonate concentration in the reactor, $K_{S,C,alg}$ [g m^{-3}] is the microalgae half-saturation constant for carbon, $K_{I,C,alg}$ [g m^{-3}] is the microalgae inhibition constant for carbon, and $n_{CO_2,alg}$ is the microalgae form parameter for carbon.

The influence of ammonium (NH_4) is represented as:

$$\overline{\mu_{alg}}(NH_4) = \frac{X_{NH_4}}{X_{NH_4} + K_{S,NH_4,alg} + \frac{X_{NH_4}^{n_{NH_4,alg}}}{K_{I,NH_4,alg}}} \qquad (3.22)$$

where X_{NH_4} [g m^{-3}] is the ammonium concentration in the reactor, $K_{S,NH_4,alg}$ [g m^{-3}] is the microalgae half-saturation constant on ammonium, $K_{I,NH_4,alg}$ [g m^{-3}] is the microalgae inhibition constant on ammonium, and $n_{NH_4,alg}$ is the microalgae form parameter for ammonium.

The influence of nitrate (NO_3) is represented as:

$$\overline{\mu_{alg}}(NO_3) = \frac{X_{NO_3}}{X_{NO_3} + K_{S,NO_3,alg} + \frac{X_{NO_3}^{n_{NO_3,alg}}}{K_{I,NO_3,alg}}} \qquad (3.23)$$

where X_{NO_3} [g m^{-3}] is the nitrate concentration in the reactor, $K_{S,NO_3,alg}$ [g m^{-3}] is the microalgae half-saturation constant on nitrate, $K_{I,NO_3,alg}$ [g m^{-3}] is the microalgae inhibition constant on nitrate, and $n_{NO_3,alg}$ represents the microalgae form parameter for nitrate.

The influence of phosphate (PO$_4$) is represented as:

$$\overline{\mu_{alg}}(PO_4) = \frac{X_{PO_4}}{X_{PO_4} + K_{S,PO_4,alg}} \tag{3.24}$$

where X_{PO_4} [g m^{-3}] is the phosphate concentration in the reactor and $K_{S,PO_4,alg}$ [g m^{-3}] is the microalgae half-saturation constant on phosphate.

Heterotrophic bacteria

The specific growth rate for heterotrophic bacteria μ_{het} has the same structure as for microalgae, with the difference that it starts from a maximum base value ($\mu_{het,max}$), that is modified by a series of terms that represent the influence of the nutrients present in the culture medium on the growth of heterotrophic bacteria. Specifically, the elements that affect the growth of hetrotrophic bacteria are temperature ($\overline{\mu_{het}}(T_w)$), pH ($\overline{\mu_{het}}(pH)$), dissolved oxygen ($\overline{\mu_{het}}(DO)$), ammonium ($\overline{\mu_{het}}(NH_4)$), phosphate ($\overline{\mu_{het}}(PO_4)$) and biodegradable soluble organic matter ($\overline{\mu_{het}}(BSOM)$). The specific growth rate for heterotrophic bacteria is expressed as:

$$\begin{aligned} \mu_{het} = \mu_{het,max} \cdot \overline{\mu_{het}}(T_w) \cdot \overline{\mu_{het}}(pH) \cdot \overline{\mu_{het}}(DO) \cdot \overline{\mu_{het}}(NH_4) \cdot \\ \cdot \overline{\mu_{het}}(PO_4) \cdot \overline{\mu_{het}}(BSOM) \end{aligned}$$

$$\tag{3.25}$$

where $\mu_{het,max}$ [day^{-1}] is the maximum specific growth rate for heterotrophic bacteria.

The temperature and pH factors are based on a cardinal model, so they are identical to those expressed for microalgae in (1.5) and (1.6). These factors depend on the maximum ($T_{max,het}$ and $pH_{max,het}$),

minimum ($T_{min,het}$ and $pH_{min,het}$) and optimal ($T_{opt,het}$ and $pH_{opt,het}$) values of temperature and pH for heterotrophic bacteria:

$$\overline{\mu_{het}}(T_w) = \frac{N_{het,T}}{D_{het,T}}$$

where

$$\boldsymbol{N_{het,T}} = (T_w - T_{max,het}) \cdot (T_w - T_{min,het})^2$$
$$\boldsymbol{D_{het,T}} = (T_{opt,het} - T_{min,het}) \cdot ((T_{opt,het} - T_{min,het}) \cdot (T_w - T_{opt,het})-$$
$$-(T_{opt,het} - T_{max,het}) \cdot (T_{opt,het} + T_{min,het} - 2 \cdot T_w))$$

$$(3.26)$$

and

$$\overline{\mu_{het}}(pH) = \frac{N_{het,pH}}{D_{het,pH}}$$

where

$$\boldsymbol{N_{het,pH}} = (pH - pH_{max,het}) \cdot (pH - pH_{min,het})^2$$
$$\boldsymbol{D_{het,pH}} = (pH_{opt,het} - pH_{min,het}) \cdot ((pH_{opt,het} - pH_{min,het}) \cdot (pH - pH_{opt,het})-$$
$$-(pH_{opt,het} - pH_{max,het}) \cdot (pH_{opt,het} + pH_{min,het} - 2 \cdot pH))$$

$$(3.27)$$

The influence of dissolved oxygen (DO_2) is expressed as:

$$\overline{\mu_{het}}(DO) = \frac{DO_2}{K_{S,DO_2,het} + DO_2} \tag{3.28}$$

where $K_{S,DO_2,het}$ [g m^{-3}] is the heterotrophic bacteria half-saturation constant for dissolved oxygen.

The influence of ammonium (NH_4) is represented as:

$$\overline{\mu_{het}}(NH_4) = \frac{X_{NH_4}}{X_{NH_4} + K_{S,NH_4,het}} \tag{3.29}$$

where $K_{S,NH_4,het}$ [g m^{-3}] is the heterotrophic bacteria half-saturation constant for ammonium.

The influence of phosphate (PO_4) is represented as:

$$\overline{\mu_{het}}(PO_4) = \frac{X_{PO_4}}{X_{PO_4} + K_{S,PO_4,het}} \qquad (3.30)$$

where $K_{S,PO_4,het}$ [g m^{-3}] is the heterotrophic bacteria half-saturation constant for phosphate.

The influence of biodegradable soluble organic matter (BSOM) is represented as:

$$\overline{\mu_{het}}(BSOM) = \frac{X_{BSOM}}{X_{BSOM} + K_{S,BSOM,het}} \qquad (3.31)$$

where $K_{S,BSOM,het}$ [g m^{-3}] is the heterotrophic bacteria half-saturation constant for the biodegradable soluble organic matter.

Nitrifying bacteria

The specific growth rate of nitrifying bacteria μ_{nit}, as heterotrophic bacteria, depends on a maximum growth rate value ($\mu_{nit,max}$), which is modified by different factors. These terms represent the influence of the elements on the growth of nitrifying bacteria, which are temperature ($\overline{\mu_{nit}}(T_w)$), pH ($\overline{\mu_{nit}}(pH)$), dissolved oxygen ($\overline{\mu_{nit}}(DO)$), carbon dioxide ($\overline{\mu_{nit}}(CO_2)$), ammonium ($\overline{\mu_{nit}}(NH_4)$) and phosphate ($\overline{\mu_{nit}}(PO_4)$). The following equation represents the nitrifying specific growth rate:

$$\begin{aligned} \mu_{nit} = {}& \mu_{nit,max} \cdot \overline{\mu_{nit}}(T_w) \cdot \overline{\mu_{nit}}(pH) \cdot \overline{\mu_{nit}}(DO) \cdot \overline{\mu_{nit}}(CO_2) \cdot \\ & \cdot \overline{\mu_{nit}}(NH_4) \cdot \overline{\mu_{nit}}(PO_4) \end{aligned}$$

$$(3.32)$$

where $\mu_{nit,max}$ [day^{-1}] is the maximum specific growth rate for nitrifying bacteria.

The influence of temperature and pH is the same as for microalgae and
heterotrophic bacteria. These factors depend on the maximum ($T_{max,nit}$
and $pH_{max,nit}$), minimum ($T_{min,nit}$ and $pH_{min,nit}$) and optimal ($T_{opt,nit}$
and $pH_{opt,nit}$) values of temperature and pH for nitrifying bacteria. They
can be expressed as:

$$\overline{\mu_{het}}(T_w) = \frac{N_{nit,T}}{D_{nit,T}}$$

where

$$\boldsymbol{N_{nit,T}} = (T_w - T_{max,nit}) \cdot (T_w - T_{min,nit})^2$$
$$\boldsymbol{D_{nit,T}} = (T_{opt,nit} - T_{min,nit}) \cdot ((T_{opt,nit} - T_{min,nit}) \cdot (T_w - T_{opt,nit}) -$$
$$-(T_{opt,nit} - T_{max,nit}) \cdot (T_{opt,nit} + T_{min,nit} - 2 \cdot T_w))$$

$$(3.33)$$

and

$$\overline{\mu_{het}}(pH) = \frac{N_{nit,pH}}{D_{nit,pH}}$$

where

$$\boldsymbol{N_{nit,pH}} = (pH - pH_{max,nit}) \cdot (pH - pH_{min,nit})^2$$
$$\boldsymbol{D_{nit,pH}} = (pH_{opt,nit} - pH_{min,nit}) \cdot ((pH_{opt,nit} - pH_{min,nit}) \cdot (pH - pH_{opt,nit}) -$$
$$-(pH_{opt,nit} - pH_{max,nit}) \cdot (pH_{opt,nit} + pH_{min,nit} - 2 \cdot pH))$$

$$(3.34)$$

On the other side, the influence of dissolved oxygen (DO_2) is
represented as:

$$\overline{\mu_{nit}}(DO) = \frac{DO_2}{(DO_2 + K_{S,DO_2,nit}) \cdot (1 + \frac{DO_2}{K_{I,DO_2,nit}})} \qquad (3.35)$$

where $K_{S,DO_2,nit}$ [g m^{-3}] is the nitrifying bacteria half-saturation
constant for dissolved oxygen and $K_{I,DO_2,nit}$ [g m^{-3}] is the nitrifying
bacteria inhibition constant for dissolved oxygen.

The influence of carbon dioxide (CO_2) is expressed as:

$$\overline{\mu_{nit}}(CO_2) = \frac{X_{CO_2} + X_{HCO_3}}{K_{S,C,nit} + X_{CO_2} + X_{HCO_3}} \tag{3.36}$$

where $K_{S,C,nit}$ [g m^{-3}] is the nitrifying bacteria half-saturation constant for carbon.

The influence of ammonium (NH_4) is represented as:

$$\overline{\mu_{nit}}(NH_4) = \frac{X_{NH_4}}{X_{NH_4} + K_{S,NH_4,nit}} \tag{3.37}$$

where $K_{S,NH_4,nit}$ [g m^{-3}] is the nitrifying bacteria half-saturation constant for ammonium.

The influence of phosphate (PO_4) is represented as:

$$\overline{\mu_{nit}}(PO_4) = \frac{X_{PO_4}}{X_{PO_4} + K_{S,PO_4,nit}} \tag{3.38}$$

where $K_{S,PO_4,nit}$ [g m^{-3}] is the nitrifying bacteria half-saturation constant for phosphate.

Table of parameters

Tables 3.3, 3.4 and 3.5 list all the parameters described for the growth rates developed above. The values of these parameters have been obtained experimentally and from the literature [84, 86].

3.2.3 Biomass production process mass balances

All the mass balances involved in the reactor during the biomass production process are described below, using wastewater as culture medium. These balances have been used as a model to estimate the concentrations of each element present in the reactor.

Parameter	Description	Value	Unit
Microalgae			
$\mu_{alg,max}$	Maximum specific growth rate	1.591	day^{-1}
Ik	Minimum light needed by the microalgae to achieve maximum photosynthesis	168	μE m^{-2} s^{-1}
n	Form parameter	1.640	$-$
$T_{max,alg}$	Maximum microalgae temperature	48.960	°C
$T_{min,alg}$	Minimum microalgae temperature	3.370	°C
$T_{opt,alg}$	Optimum microalgae temperature	25	°C
$pH_{max,alg}$	Maximum microalgae pH	12.900	$-$
$pH_{min,alg}$	Minimum microalgae pH	1.800	$-$
$pH_{opt,alg}$	Optimum microalgae pH	8.500	$-$
$DO_{2,max,alg}$	Maximum dissolved oxygen	356	%
m	Dissolved oxygen form parameter	4.150	$-$
K_a	Dissolved oxygen form parameter	0.100	m^2 g^{-1}
$m_{max,alg}$	Maximum microalgae respiration rate	0.276	day^{-1}
$m_{min,alg}$	Minimum microalgae respiration rate	0.010	day^{-1}
Ik_{res}	Maximum light needed by the microalgae to achieve maximum photosynthesis during respiration	134	μE m^{-2} s^{-1}
n_{res}	Form respiration parameter	1.390	$-$
$K_{S,C,alg}$	Microalgae half-saturation constant for carbon	0.004	g m^{-3}
$K_{I,C,alg}$	Microalgae inhibition constant for carbon	120	g m^{-3}
$n_{C,alg}$	Microalgae form parameter for carbon	2	g m^{-3}
$K_{S,NH_4,alg}$	Microalgae half-saturation constant for ammonium	1.540	g m^{-3}
$K_{I,NH_4,alg}$	Microalgae inhibition constant for ammonium	571	g m^{-3}
$n_{NH_4,alg}$	Microalgae form parameter for ammonium	2	g m^{-3}
$K_{S,NO_3,alg}$	Microalgae half-saturation constant for nitrate	2.770	g m^{-3}
$K_{I,NO_3,alg}$	Microalgae inhibition constant for nitrate	386.600	g m^{-3}
$n_{NO_3,alg}$	Microalgae form parameter for nitrate	2	g m^{-3}
$K_{S,PO_4,alg}$	Microalgae half-saturation constant for phosphate	0.430	g m^{-3}

Table 3.3: Specific growth rate nutrients model parameters for microalgae.

Parameter	Description	Value	Unit
Heterotrophic bacteria			
$\mu_{het,max}$	Maximum heterotrophic bacteria specific growth rate	1.235	day^{-1}
$T_{max,het}$	Maximum heterotrophic bacteria temperature	47	°C
$T_{min,het}$	Minimum heterotrophic bacteria temperature	9	°C
$T_{opt,het}$	Optimum heterotrophic bacteria temperature	36	°C
$pH_{max,het}$	Maximum heterotrophic bacteria pH	12	–
$pH_{min,het}$	Minimum heterotrophic bacteria pH	6	–
$pH_{opt,het}$	Optimum heterotrophic bacteria pH	9	–
$K_{S,DO_2,het}$	Heterotrophic bacteria half-saturation constant for dissolved oxygen	1.980	g m^{-3}
$K_{S,NH_4,het}$	Heterotrophic bacteria half-saturation constant for ammonium	0.050	g m^{-3}
$K_{S,PO_4,het}$	Heterotrophic bacteria half-saturation constant for phosphate	0.010	g m^{-3}
$K_{S,BSOM-het}$	Heterotrophic bacteria half-saturation constant for biodegradable soluble organic matter	20	g m^{-3}

Table 3.4:   Specific growth rate nutrients model parameters for heterotrophic bacteria.

Parameter	Description	Value	Unit
Nitrifying bacteria			
$\mu_{nit,max}$	Maximum nitrifying bacteria specific growth rate	0.730	day^{-1}
$T_{max,nit}$	Maximum nitrifying bacteria temperature	49	°C
$T_{min,nit}$	Minimum nitrifying bacteria temperature	0	°C
$T_{opt,nit}$	Optimum nitrifying bacteria temperature	33.600	°C
$pH_{max,nit}$	Maximum nitrifying bacteria pH	13.500	–
$pH_{min,nit}$	Minimum nitrifying bacteria pH	2	–
$pH_{opt,nit}$	Optimum nitrifying bacteria pH	9.700	–
$K_{S,DO_2,nit}$	Nitrifying bacteria half-saturation constant for dissolved oxygen	1.080	g m^{-3}
$K_{I,DO_2,nit}$	Nitrifying bacteria inhibition constant for dissolved oxygen	104.900	g m^{-3}
$K_{S,C,nit}$	Nitrifying bacteria half-saturation constant for carbon	0.500	g m^{-3}
$K_{S,NH_4,nit}$	Nitrifying bacteria half-saturation constant for ammonium	1	g m^{-3}
$K_{S,PO_4,nit}$	Nitrifying bacteria half-saturation constant for phosphate	0.010	g m^{-3}

Table 3.5:   Specific growth rate nutrients model parameters for heterotrophic bacteria.

Microalgae

Microalgae biomass grows inside the reactor and it is not present in the inlet wastewater medium. The evolution of the microalgae biomass concentration within the reactor is described as:

$$V \cdot C_b \cdot \mu_{alg} = Q_h \cdot C_b + V \cdot \frac{dC_b}{dt} \tag{3.39}$$

where V [m^3] is the volume in the reactor, C_b [g m^{-3}] is the microalgae biomass, μ_{alg} [day^{-1}] is the specific growth rate for microalgae and Q_h [m^3 s^{-1}] is the outlet flow rate or harvesting flow rate.

Heterotrophic bacteria

Heterotrophic bacteria consume organic matter and are present both in the reactor and in the inlet wastewater medium. Its evolution is expressed as:

$$Q_d \cdot X_{het,in} + V \cdot X_{het,out} \cdot \mu_{het} = Q_h \cdot X_{het,out} + V \cdot \frac{dX_{het,out}}{dt} \tag{3.40}$$

where Q_d [m^3 s^{-1}] is the inlet medium flow rate or dilution flow rate, Q_h [m^3 s^{-1}] represents the outlet flow rate or harvesting flow rate, $X_{het,in}$ [g m^{-3}] is the inlet heterotrophic bacteria concentration, $X_{het,out}$ [g m^{-3}] is the outlet heterotrophic bacteria concentration and μ_{het} [day^{-1}] is the specific growth rate for heterotrophic bacteria.

Nitrifying bacteria

Nitrifying bacteria are responsible for nitrification, that is the conversion of ammonium to nitrate. These microorganisms are composed of ammonium oxidizing bacteria and nitrate oxidizing bacteria. They are produced by aerobic growth and are present both in the reactor and in the inlet wastewater medium. The evolution of the nitrifying biomass is described as:

$$Q_d \cdot X_{nit,in} + V \cdot X_{nit,out} \cdot \mu_{nit} = Q_h \cdot X_{nit,out} + V \cdot \frac{dX_{nit,out}}{dt} \qquad (3.41)$$

where $X_{nit,in}$ [g m^{-3}] is the inlet nitrifying bacteria concentration, $X_{nit,out}$ [g m^{-3}] is the outlet nitrifying bacteria concentration and μ_{nit} [day^{-1}] is the specific growth rate for nitrifying bacteria.

Ammonium nitrogen

The ammonium nitrogen (NH$_4$) enters with the wastewater inlet medium and is consumed by the nitrifying bacteria. Also, it is assimilated during the growth of microalgae and heterotrophic bacteria. The evolution of ammonium within the reactor is expressed as:

$$Q_d \cdot X_{NH_4,in} = Q_h \cdot X_{NH_4,out} + V \cdot \left(C_b \cdot \mu_{alg} \cdot Y_{con} \left[\frac{NH_4}{alg} \right] + \right.$$
$$\left. + X_{het,out} \cdot \mu_{het} \cdot Y_{con} \left[\frac{NH_4}{het} \right] + X_{nit,out} \cdot \mu_{nit} \cdot Y_{con} \left[\frac{NH_4}{nit} \right] \right) + V \cdot \frac{dX_{NH_4,out}}{dt}$$
$$(3.42)$$

where $X_{NH_4,in}$ [g m^{-3}] is the inlet ammonium concentration, $X_{NH_4,out}$ [g m^{-3}] is the outlet ammonium concentration, $Y_{con} \left[\frac{NH_4}{alg} \right]$ [g$_{NH_4}$ g$_{alg}$$^{-1}$] is the ammonium consumption rate from microalgae, $Y_{con} \left[\frac{NH_4}{het} \right]$ [g$_{NH_4}$ g$_{het}$$^{-1}$] is the ammonium consumption rate from heterotrophic bacteria, and $Y_{con} \left[\frac{NH_4}{nit} \right]$ [g$_{NH_4}$ g$_{nit}$$^{-1}$] is the ammonium consumption rate from nitrifying bacteria.

Nitrate nitrogen

Nitrate nitrogen (NO$_3$) is produced by nitrifying bacteria during nitrification, and is assimilated by microalgae in the absence of ammonium. It can enter the reactor from inlet wastewater medium, but in small concentrations. The evolution is described as:

$$Q_d \cdot X_{NO_3,in} + V \cdot X_{NO_3,out} \cdot \mu_{nit} \cdot Y_{gen} \left[\frac{NO_3}{nit}\right] = Q_h \cdot X_{NO_3,out} +$$

$$+ V \cdot \left(C_b \cdot \mu_{algae} \cdot Y_{con} \left[\frac{NO_3}{alg}\right]\right) + V \cdot \frac{dX_{NO_3,out}}{dt}$$

$$(3.43)$$

where $X_{NO_3,in}$ [g m^{-3}] is the inlet nitrate concentration, $X_{NO_3,out}$ [g m^{-3}] is the outlet nitrate concentration, $Y_{gen} \left[\frac{NO_3}{nit}\right]$ [g$_{NO_3}$ g$_{nit}$$^{-1}$] is the nitrate generation rate from nitrifying bacteria, and $Y_{con} \left[\frac{NO_3}{alg}\right]$ [g$_{NO_3}$ g$_{alg}$$^{-1}$] is the nitrate consumption rate from microalgae.

Phosphate

Phosphate phosphorus (PO_4) enters into the reactor from inlet wastewater medium and is assimilated during growth of microalgae, heterotrophic bacteria and nitrifying bacteria. The evolution of phosphate can be expressed as:

$$Q_d \cdot X_{PO_4,in} = Q_h \cdot X_{PO_4,out} + V \cdot \left(C_b \cdot \mu_{alg} \cdot Y_{con} \left[\frac{PO_4}{alg}\right] + \right.$$

$$\left. + X_{het,out} \cdot \mu_{het} \cdot Y_{con} \left[\frac{PO_4}{het}\right] + X_{nit,out} \cdot \mu_{nit} \cdot Y_{con} \left[\frac{PO_4}{nit}\right]\right) + V \cdot \frac{dX_{PO_4,out}}{dt}$$

$$(3.44)$$

where $X_{PO_4,in}$ [g m^{-3}] is the inlet phosphate concentration, $X_{PO_4,out}$ [g m^{-3}] is the outlet phosphate concentration, $Y_{con} \left[\frac{PO_4}{alg}\right]$ [g$_{PO_4}$ g$_{alg}$$^{-1}$] is the phosphate consumption rate from microalgae, $Y_{con} \left[\frac{PO_4}{het}\right]$ [g$_{PO_4}$ g$_{het}$$^{-1}$] is the phosphate consumption rate from heterotrophic bacteria, and $Y_{con} \left[\frac{PO_4}{nit}\right]$ [g$_{PO_4}$ g$_{nit}$$^{-1}$] is the phosphate consumption rate from nitrifying bacteria.

Biodegradable soluble organic matter

The biodegradable soluble organic matter (BSOM) is the fraction of the soluble organic matter directly available for biodegradation by the

heterotrophic bacteria. It is generated by the death of microorganisms in the culture and from the inlet wastewater medium. Its evolution can be described as:

$$
\begin{aligned}
Q_d \cdot X_{BSOM,in} + V \cdot \left(C_b \cdot \mu_{alg} \cdot Y_{gen} \left[\frac{BSOM}{alg} \right] + \right. \\
+ X_{het,out} \cdot \mu_{het} \cdot Y_{gen} \left[\frac{BSOM}{het} \right] + X_{nit,out} \cdot \mu_{nit} \cdot Y_{gen} \left[\frac{BSOM}{nit} \right] \Bigg) = \\
= Q_h \cdot X_{BSOM,out} + V \cdot \left(X_{het,out} \cdot \mu_{het} \cdot Y_{con} \left[\frac{BSOM}{het} \right] \right) + V \cdot \frac{dX_{BSOM,out}}{dt}
\end{aligned}
$$

$$(3.45)$$

where $X_{BSOM,in}$ [g m^{-3}] is the inlet BSOM concentration, $Y_{gen} \left[\frac{BSOM}{alg} \right]$ [g$_{BSOM}$ g$_{alg}$$^{-1}$] is the BSOM generation rate from microalgae, $Y_{gen} \left[\frac{BSOM}{het} \right]$ [g$_{BSOM}$ g$_{het}$$^{-1}$] is the BSOM generation rate from heterotrophic bacteria, $Y_{gen} \left[\frac{BSOM}{nit} \right]$ [g$_{BSOM}$ g$_{nit}$$^{-1}$] is the BSOM generation rate from nitrifying bacteria, $X_{BSOM,out}$ [g m^{-3}] is the outlet BSOM concentration, and $Y_{con} \left[\frac{BSOM}{het} \right]$ [g$_{BSOM}$ g$_{het}$$^{-1}$] is the BSOM consumption rate from heterotrophic bacteria.

Carbon dioxide and bicarbonate

Carbon dioxide and bicarbonate are in equilibrium in the reactor. Carbon dioxide is generated by respiration of microalgae, in addition to being injected into the reactor to control the pH and exchanged with the atmosphere. It is consumed by microalgae and nitrifying bacteria. The following equilibrium constants between carbon dioxide, carbonate and bicarbonate are defined as:

$$
K_1 = \frac{[X_{HCO_3}][H^+]}{[X_{CO_2}]} = 10^{-6.381} \tag{3.46}
$$

$$
K_2 = \frac{[X_{CO_3}][H^+]}{[X_{HCO_3}]} = 10^{-6.381} \tag{3.47}
$$

where H^+ [g m^{-3}] is the concentration of hydrogen ions, which can be obtained from the pH in the reactor by means of the following formula:

$$H^+ = 10^{-pH} \tag{3.48}$$

Assuming a total inorganic carbon concentration (X_{C_T}) of 100 [g m^{-3}] in the reactor, the concentration of bicarbonate and carbon dioxide can be obtained from the following equations:

$$X_{HCO_3} = \frac{(H^+ \cdot X_{C_T})}{(K_2 + H^+ + H^{+2})}$$
$$X_{CO_2} = \frac{(X_{HCO_3} \cdot H^+)}{K_1} \tag{3.49}$$

3.2.4 Calibration and validation results

Although the equations of the growth rate model for all organisms are well defined, the consumption and generation parameters of nutrients associated with each species present some uncertainty. The cultivation of microalgae using wastewater as a medium presents diverse variability in the model parameters. Depending on the type of wastewater and its components, the generation and consumption parameters associated with microalgae and bacteria may vary. This fact raises the need for a model that allows adapting its parameters for each situation. Therefore, a calibration method is presented using genetic algorithms that is capable of estimating the characteristic parameters of the model from experimental data measured in the reactor.

Calibration

As for the temperature model described in Section 3.17, the genetic algorithms implemented in Matlab have been used to calibrate the model parameters. The initial population has been of 50 phenotypes, with a condition of completion of 50 generations. The cost function is computed as the Root Mean Square Error (RMSE) between the simulated organism

and nutrients (total biomass, ammonium, nitrate, phosphate and BSOM) and the real measured values, expressed as the following equation:

$$J = \left(\sqrt{\sum_{i=1}^{N} \frac{(Cb_{total_{est}}(i) - Cb_{total_{real}}(i))^2}{N}} \right) + \left(\sqrt{\sum_{i=1}^{N} \frac{(X_{NH_4,est}(i) - X_{NH_4,real}(i))^2}{N}} \right) +$$

$$+ \left(\sqrt{\sum_{i=1}^{N} \frac{(X_{NO_3,est}(i) - X_{NO_3,real}(i))^2}{N}} \right) + \left(\sqrt{\sum_{i=1}^{N} \frac{(X_{PO_4,est}(i) - X_{PO_4,real}(i))^2}{N}} \right) +$$

$$+ \left(\sqrt{\sum_{i=1}^{N} \frac{(X_{BSOM_{est}}(i) - X_{BSOM_{real}}(i))^2}{N}} \right)$$

(3.50)

where $Cb_{total_{est}}$ [g m^{-3}] is the estimated total biomass concentration (microalgae + heterotrophic bacteria + nitrifying bacteria), $Cb_{total_{real}}$ [g m^{-3}] is the experimental total biomass concentration measured. The other parameters also describe the difference between the estimated concentration and the experimentally measured one for each element. N represents the size of the data vector.

The estimated calibration parameters are related to the maximum growth rates for each microorganism and the coefficients of generation and nutrient consumption. Table 3.6 lists the description of all the calibration parameters, as well as the values obtained as a result of the calibration process.

In addition to the parameters described in the table, through this calibration process, it is possible to estimate the percentages of each species in the reactor. The experimental measurement of the concentration for the species of bacteria is something complex to carry out and highlights the need for a simple way of being able to estimate the percentages of each species within the reactor. Therefore, for both the calibration and validation data, the genetic algorithm method will be used to determine the initial percentages of each species. In this way, the calibration process acts as a tool to estimate the percentages of microalgae and bacteria involved in the reactor from the measurements of total biomass and nutrients in it.

The data used during the calibration process correspond to the

experimental measurements taken for a 0.7 L laboratory scale reactor for
14 consecutive days. The reactor operating conditions are equivalent to
the operation of a raceway reactor, with light and dark cycles
representing day and night. In addition, pH and dissolved oxygen are
controlled by injecting CO_2 and air. Figure 3.7 represents the
experimental data measured, which correspond to measurements of
irradiance, pH, dissolved oxygen and temperature. Moreover,
measurements of total biomass dry weight (microalgae, heterotrophic
bacteria and nitrifying bacteria) and measurements of nutrients
(ammonium, nitrate, phosphate and BSOM) are represented.

Symbol	Parameter	Value	Unit
$\mu_{alg,max}$	Microalgae maximum growth rate	1.591	day^{-1}
$\mu_{het,max}$	Heterotrophic bacteria maximum growth rate	1.235	day^{-1}
$\mu_{nit,max}$	Nitrifying bacteria maximum growth rate	0.730	day^{-1}
$m_{min,alg}$	Microalgae endogenous respiration minimum rate	0.010	day^{-1}
$m_{max,alg}$	Microalgae endogenous respiration maximum rate	0.276	day^{-1}
$Y_{con}\left[\frac{NH_4}{alg}\right]$	Ammonium consumption rate from microalgae	0.369	$g_{NH_4}\ g_{alg}^{-1}$
$Y_{con}\left[\frac{NO_3}{alg}\right]$	Nitrate consumption rate from microalgae	0.214	$g_{NO_3}\ g_{alg}^{-1}$
$Y_{con}\left[\frac{PO_4}{alg}\right]$	Phosphate consumption rate from microalgae	0.008	$g_{PO_4}\ g_{alg}^{-1}$
$Y_{gen}\left[\frac{BSOM}{alg}\right]$	BSOM generation rate from microalgae	0.148	$g_{BSOM}\ g_{alg}^{-1}$
$Y_{con}\left[\frac{NH_4}{het}\right]$	Ammonium consumption rate from heterotrophic bacteria	0.299	$g_{NH_4}\ g_{het}^{-1}$
$Y_{con}\left[\frac{PO_4}{het}\right]$	Phosphate consumption rate from heterotrophic bacteria	0.017	$g_{PO_4}\ g_{het}^{-1}$
$Y_{gen}\left[\frac{BSOM}{het}\right]$	BSOM generation rate from heterotrophic bacteria	0.153	$g_{BSOM}\ g_{het}^{-1}$
$Y_{con}\left[\frac{BSOM}{het}\right]$	BSOM consumption rate from heterotrophic bacteria	0.478	$g_{BSOM}\ g_{het}^{-1}$
$Y_{con}\left[\frac{NH_4}{nit}\right]$	Ammonium consumption rate from nitrifying bacteria	3.224	$g_{NH_4}\ g_{nit}^{-1}$
$Y_{gen}\left[\frac{NO_3}{nit}\right]$	Nitrate generation rate from nitrifying bacteria	0.355	$g_{NO_3}\ g_{nit}^{-1}$
$Y_{con}\left[\frac{PO_4}{nit}\right]$	Phosphate consumption rate from nitrifying bacteria	0.182	$g_{PO_4}\ g_{nit}^{-1}$
$Y_{gen}\left[\frac{BSOM}{nit}\right]$	BSOM generation rate from nitrifying bacteria	0.149	$g_{BSOM}\ g_{nit}^{-1}$

Table 3.6: Calibration parameters for the combined microalgae and
bacteria model.

Figure 3.8 represents the calibration results obtained in the
estimation of the model variables. This figure is made up of six
independent graphs that represent different variables estimated in the
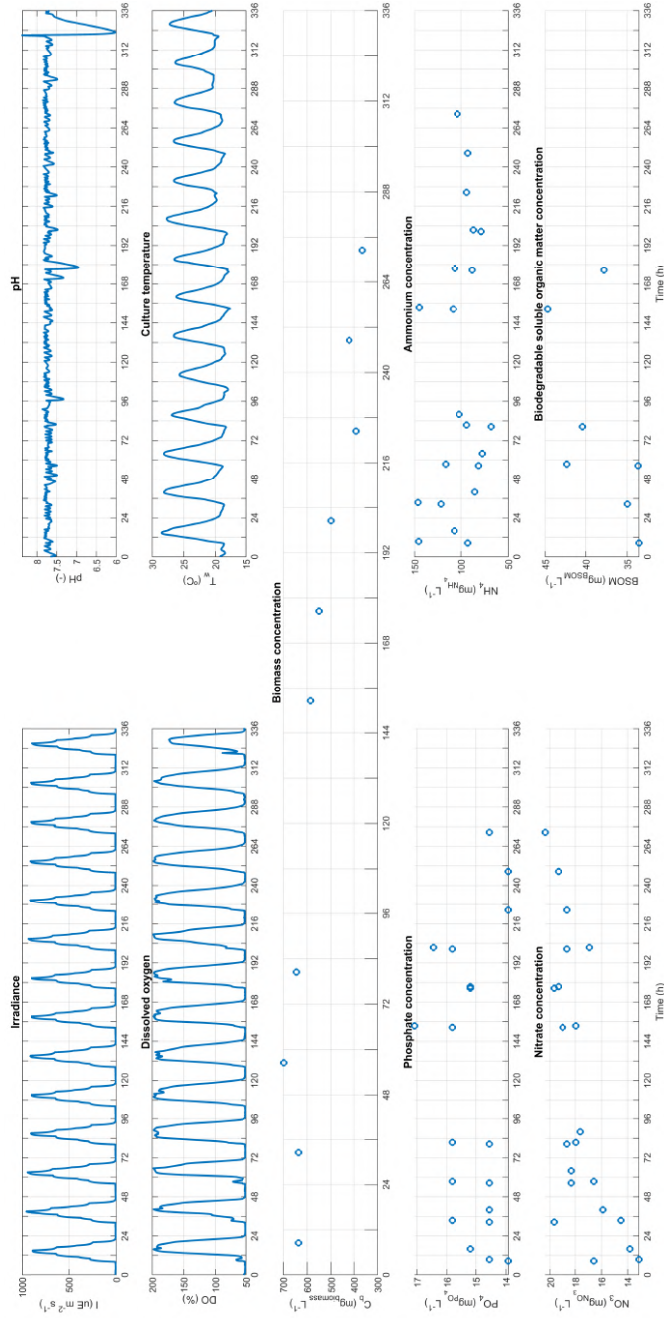
Figure 3.7: Input variables for calibration.

model. Figure 3.8.a shows the percentages of each species of microorganisms within the reactor. Figure 3.8.b represents the biomass concentration for each organism in the reactor (microalgae, heterotrophic bacteria and nitrifying bacteria), in addition to the total biomass concentration, expressed as the sum of the individual concentrations and the representation of the experimental measured points. Figure 3.8.c represents the estimated phosphate concentration and the experimental measured points. Figure 3.8.d shows the estimated ammonium concentration and the experimental measurements points taken. Figure 3.8.e represents the estimated nitrate concentration and the experimental measured points. Finally, Figure 3.8.f represents the estimated biodegradable soluble organic matter concentration, compared with the experimental measurements points taken.

As a result of the calibration, initial percentages of 82.1% for microalgae, 13.2% for heterotrophic bacteria and 4.7% for nitrifying bacteria have been established. Looking at Figures 3.8.a and 3.8.b, it is observed how the concentration of microalgae decreases until reaching a steady state. On the other hand, the concentration of heterotrophic bacteria grows slightly, consuming ammonium and organic matter, while the concentration of nitrifying bacteria remains practically constant. The sum of the concentrations of each species represents the total biomass concentration (dashed line), which properly adjust to the points measured experimentally in the reactors described in Section 2.2.2.

Although the experimental data for nutrients (phosphate, ammonium, nitrate and BSOM) are very scattered, a certain trend is observed for them. The estimated values for each element represented in Figures 3.8.c, 3.8.d, 3.8.e and 3.8.f fit correctly within the range that make up the experimental data.

Validation

The validation data used to verify the value of the parameters obtained during the calibration process come from the experimental measurements of another vessel reactor, operated in parallel with the vessel used for calibration. These data collect the experimental measurements for 14 days,
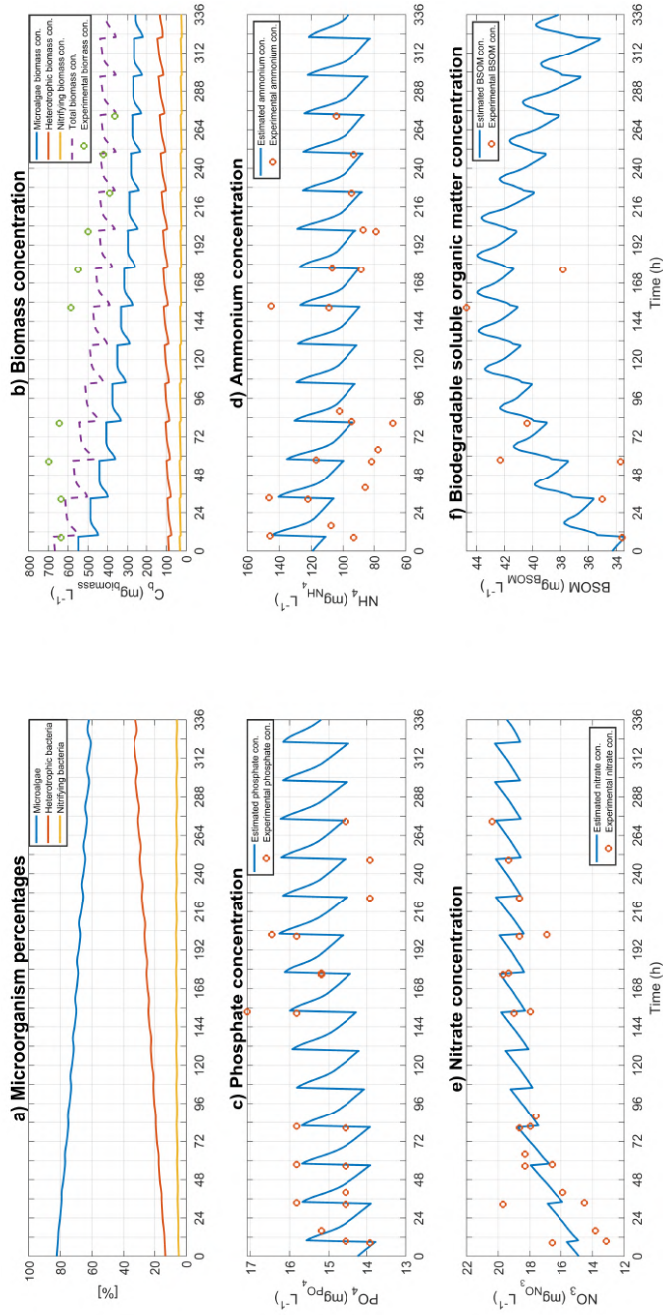
Figure 3.8: Calibration results for the biomass production model with wastewater medium.

represented in Figure 3.9.

For the validation process, calibration using genetic algorithms has
been used to determine the initial percentages of microorganisms in the
reactor. In this way, it is possible to estimate the starting point for the
concentration of microalgae and bacteria. In this case, the initial
percentages obtained were 85% for microalgae, 12.6% for heterotrophic
bacteria and 2.4% for nitrifying bacteria, very similar to the percentages
obtained during the calibration test. From this initial point, the
concentration of all the elements in the reactor has been estimated and
compared with the points measured experimentally, represented in Figure
3.10.

Figures 3.10.a and 3.10.b represent a trend in biomass concentrations
similar to those obtained during calibration. The concentration of
microalgae decreases to steady state, while the heterotrophic bacteria
grow slightly and the nitrifying bacteria remain constant. The total
concentration correctly resembles the trend shown by the measured
experimental points.

The estimation of the phosphate concentration (Figure 3.10.c) shows an
increasing trend, slightly away from the center of the measurement points.
However, the estimation is within the range of the experimental values.
The concentration of ammonium (Figure 3.10.d) maintains a good trend
within the established range, as does the estimated nitrate concentration
(Figure 3.10.e). Finally, the BSOM estimation (Figure 3.10.f) shows a
trend similar to the calibration results, within the experimental points.

Discussion

The results obtained from the comparison between the estimated values
with respect to the measured experimental data have been satisfactory.
The concentrations of the elements are adjusted within the range formed
by the measurement points, despite being scattered data. The percentages
of microalgae and bacteria within the reactor over time show values close
to those obtained in the literature.

The complexity in measuring individual concentrations of each species
highlights the need for a reliable estimation method. Due to the calibration
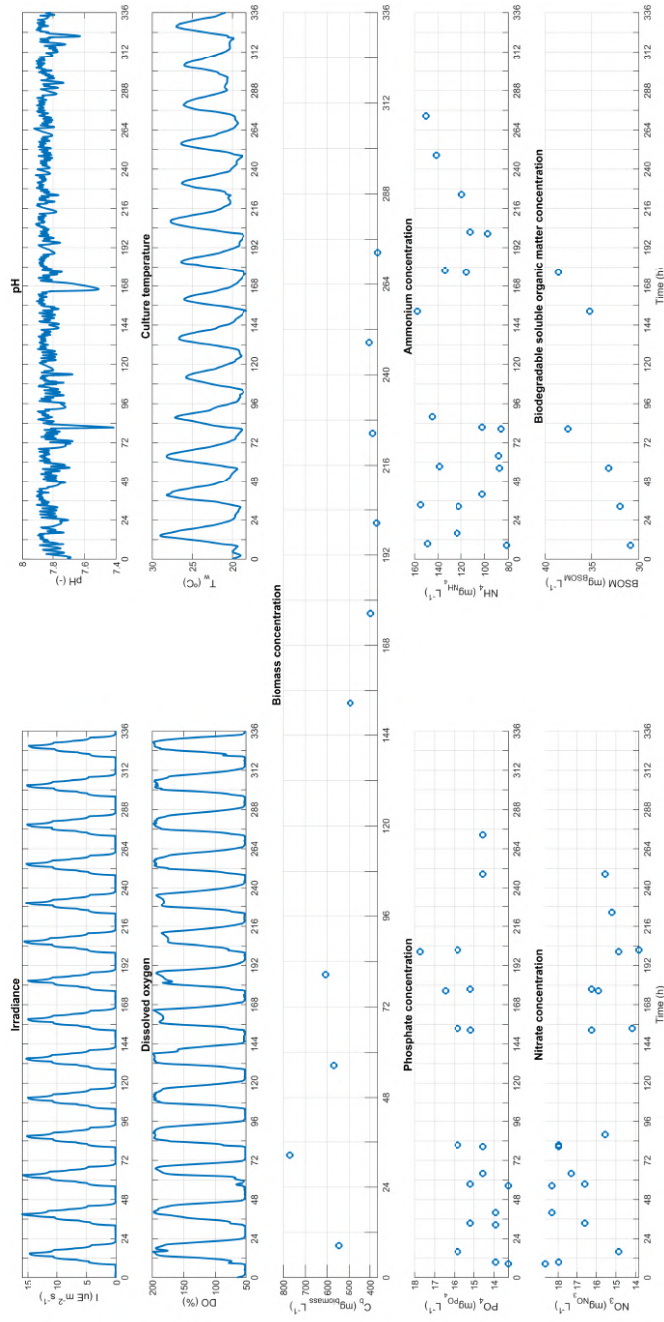
Figure 3.9: Input variables for validation.
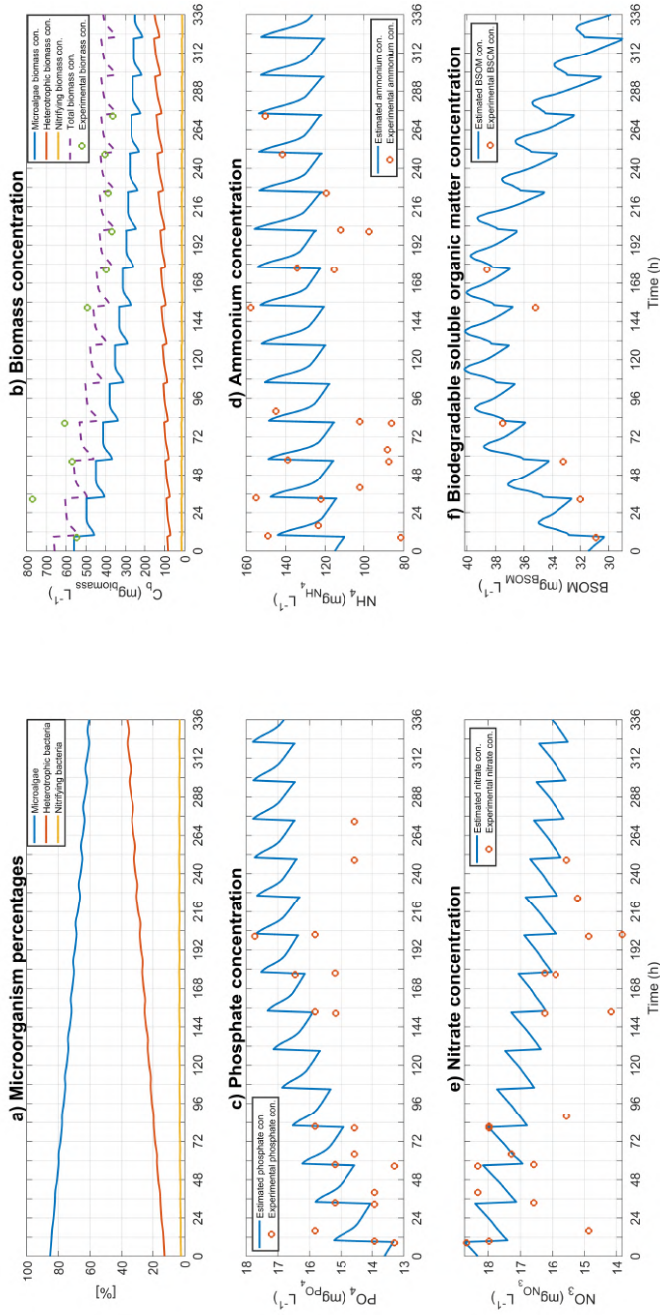
Figure 3.10: Validation results for the biomass production model with wastewater medium.

using genetic algorithms, it is possible to estimate the percentages of each microorganism in the reactor. From experimental data, the model allows the determination of the initial percentages of each element and estimate its evolution over time. In this way, the model can act as a simulator to predict the behavior of organisms based on the concentrations of nutrients present in the reactor medium. This model and the calibration parameters obtained will serve as the basis for the development of simulation models where the production of microalgae biomass is combined with wastewater treatment.

3.3   Raceway reactor model improvement

For the simulation results developed in Chapter 5 (Section 5.5), a dynamic model of microalgae production in raceway reactors has been used. It was originally developed by Fernández *et al.* in [31]. The model is based on fundamental principles instead of empirical equations and takes into account mass balances, thermodynamic relationships and biological phenomena. This model can be used to predict the evolution of the main reactor variables, such as biomass concentration, pH and dissolved oxygen.   It has been calibrated and validated using experimental data from a 100 m^2 pilot-scale raceway reactor.   As an improvement to this model, various changes have been made to the equations and balances it contains. Two main changes stand out:

- Modification of the photosynthesis rate model to reflect the latest contributions presented in the literature [15, 85].

- Implementation of the temperature model described in Section 3.1 to add the effect of temperature on the growth of microalgae.

- Implementation improvements that make the simulation flow 10 times faster.

3.3.1 Photosynthesis rate update

The microalgae culture growth is modelled as a function of the photosynthesis rate, that represents the production of oxygen per unit of biomass. The main parameter that determines the photosynthesis rate is the available light (presented in (1.4)), which is based on different parameters such as solar irradiance, culture characteristic, and reactor design [2]. The photosynthesis rate is modelled with the available light by the following equation [41]:

$$
P_{O_2}(t) = (1 - \alpha_s) \cdot \frac{P_{O_2,max} \cdot I_{av}(t)^n}{I_k e^{(I_{av}(t) \cdot m_I)} + I_{av}(t)^n} \cdot \left(1 - \left(\frac{[DO_2](t)}{K_{I,DO_2,alg}} \right)^{m_{DO}} \right) \cdot \\
\cdot \left(B_1 \cdot e^{\left(\frac{-C_1}{pH(t)} \right)} - B_2 \cdot e^{\left(\frac{-C_2}{pH(t)} \right)} \right) - \alpha_s \cdot R_{O_2}
\tag{3.51}
$$

where P_{O_2} [day^{-1}] is the photosynthesis rate, α_s [–] is a solar distributed factor that represents the shadow projection on the perpendicular axis of the reactor walls, $P_{O_2,max}$ [day^{-1}] is the maximum photosynthesis rate for microalgae under culture conditions, I_{av} [μE m^{-2} s^{-1}] is the light availability inside the reactor, n [–] is the form exponent, I_k [μE m^{-2} s^{-1}] is the minimum light needed by the microalgae to achieve maximum photosynthesis, m_I [–] is a form factor for the exponential function of average irradiance, DO_2 [%] is the percentage of dissolved oxygen in the reactor, $K_{I,DO_2,alg}$ [g m^{-3}] represents an inhibition microalgae constant for dissolved oxygen and m_{DO} [–] is a dissolved oxygen form parameter. Furthermore, B_1 [–] and B_2 [–] are pre-exponential factors for the pH influence on the photosynthesis rate, and C_1 [–] and C_2 [–] are the activation energies of the Arrhenius model. R_{O_2} [day^{-1}] is a respiration constant that represents the respiration phenomenon.

  The initial formulation for the photosynthesis rate was made from calibration and from parameters that represent the influence of pH and oxygen on the growth of microalgae, in addition to a solar distributed factor. New models have emerged to represent the photosynthesis rate, as is the case of the model described by Solimeno *et al.* or Bernard *et al.* in [15, 85]. As an improvement of the biomass production model in raceway reactors, the initial photosynthesis rate has been changed for a more

updated version, represented by the following formula:

$$P_{O_2} = P_{O_2}(I_{av}) \cdot \overline{P_{O_2}}(T_w) \cdot \overline{P_{O_2}}(pH) \cdot \overline{P_{O_2}}(DO) \qquad (3.52)$$

The photosynthesis rate has the same structure as the specific growth rate described in Section 1.2, being equivalent representing the growth of microalgae biomass. The oxygen production rate ($P_{O_2}(I_{av})$) represents the production of oxygen based on solar irradiance. The temperature ($\overline{P_{O_2}}(T_w)$), pH ($\overline{P_{O_2}}(pH)$) and dissolved oxygen ($\overline{P_{O_2}}(DO)$) factor terms are the same as those described in (1.5), (1.6) and (1.7), and are equivalent to $\overline{\mu_{alg}}(T_w)$, $\overline{\mu_{alg}}(pH)$ and $\overline{\mu_{alg}}(DO)$. The photosynthesis rate is directly related to the specific growth rate from a coefficient of relation between the production of oxygen and the biomass, expressed as follows:

$$P_{O_2}(I_{av}) = \mu_{alg} \cdot Y_b \qquad (3.53)$$

where P_{O_2} [day^{-1}] is the photosynthesis rate, μ_{alg} [day^{-1}] is the specific growth rate and $Y_b = 1.33$ [–] is the relation between the production of oxygen per unit of biomass.

The oxygen production rate ($P_{O_2}(I_{av})$) can be expressed as in (1.2), but using the maximum value of the photosynthesis rate ($P_{O_{2,max}}$), instead of the maximum specific growth rate ($\mu_{max,alg}$). This is due to the relationship between oxygen production and growth rate, because biomass growth is expressed by the Monod model [51]:

$$P_{O_2} = P_{O_{2,max}} \cdot \left(\frac{I_{av}{}^n}{I_k{}^n + I_{av}{}^n} \right) \qquad (3.54)$$

In addition to the new photosynthesis rate model, the temperature model for raceway reactors described in Section 3.1 has been implemented, so that the culture temperature can be estimated and applied to the temperature index $\overline{P_{O_2}}(T_w)$.

3.4 Conclusions and contributions

In this chapter, different modeling approaches related to the microalgae growth have been developed, such as a temperature estimation model for raceway reactors and a new growth model where the concentrations of nutrients in the microalgae and bacteria culture are taken into account. The objective of these models is to improve the dynamic models of biomass production so that they faithfully represent the processes carried out within the reactor. In this way, models can be made that act as simulators or estimators of the parameters involved in the process.

The description of the combined model of biomass production and wastewater treatment has been introduced. The calibration carried out by means of genetic algorithms opens the door to a simple method of adjusting the various parameters that make up the model, so that it can be recalibrated from experimental measurements of different medium and culture scenarios, since the concentration of nutrients varies from one type of medium to another.

On the other hand, the results of the dynamic temperature evolution obtained from the temperature model show satisfactory performance that closely resemble the actual temperature values, measured in the reactor. The great impact of temperature on the productivity of microalgae has been demonstrated in the literature and, therefore, this type of models has a fundamental role in the development of new and more complete models of microalgae that allow us to fully understand all the parameters that affect its growth.

The use of industrial scale models that take into account all the variables affecting the microalgae growth is scarce in practice, and thus, this temperature model aims to complement the use of more complete models that allow the development of precise evaluation applications in the field of microalgae, such as optimal reactor control, variable impact studies, performance improvement or parameter estimation.

Indirect regulation of temperature

Temperature and irradiance are the two most relevant factors determining the performance of microalgae cultures in raceway reactors. Moreover, inadequate temperature strongly reduces the biomass productivity in these systems even if enough sunlight is available. Controlling the temperature directly in large raceway reactors is considered unaffordable because of the large amount of required energy. This chapter presents a study of the influence of temperature and culture depth on biomass productivity, in addition to an indirect method for temperature regulation in microalgae raceway reactors by optimizing the culture depth.

The structure of this chapter is as follows: Section 4.1 shows the effect of the liquid depth on the culture temperature inside the reactor. The optimization control problem approach is detailed in Section 4.2, while simulation and experimental results are presented in Sections 4.3 and 4.4. Finally, conclusions are drawn in Section 4.5.

4.1 Temperature and depth studies on microalgae growth

The temperature of the culture in the reactor is a very important factor in the microalgae biomass productivity. It is possible to find in the literature multiple studies and tests regarding the characterization of various microalgae and bacteria strains under different temperature conditions.

This section presents various studies on the influence of temperature on the growth of microalgae and their biomass productivity. In addition, the

variation of the culture temperature is shown as a function of the depth of the culture, which affects the volume of liquid in the reactor. These studies serve as design and evaluation tools to analyze different strains and locations in order to determine the suitability for biomass production.

4.1.1   Culture temperature influence on microalgae growth

Using the temperature model developed in Section 3.1, an analysis on how temperature influences on microalgae growth has been carried out for five different microalgae strains. For this issue, the temperature-effect on growth model presented by Bernard *et al.* in [15] and described in (1.5) has been used together with the temperature model described, establishing a culture depth of 15 cm during the entire analyzed period.

The analysis has been done with representative data of 8 days of each seasonal period over a year at Almería, in Spain, characterized by moderate temperatures in summer and in winter. The climate in Almería is considered a local steppe climate, with little rainfall. During the course of the year, the temperature generally varies from 8°C to 30°C and rarely drops below 6°C or rises above 35°C. The objective has been to verify the influence of temperature on microalgae cultivation for five different species of microalgae throughout an annual period in this location. These microalgae species correspond to *Dunaliella tertiolecta*, *Nannochloropsis oceanica*, *Chlorella pyrenoidosa* and *Spirulina platensis*, being commonly used for biomass production at industrial scale, in addition to *Scenedesmus almeriensis*, the strain used in the raceway reactor studied in this thesis. Table 4.1 presents the characteristic temperature parameters for each microalgae strain, applied to the temperature index model and obtained from the literature [8, 15] and experimental tests in our research group. Despite the fact that the microalgae used in the reactor is *Scenedesmus almeriensis*, the temperature model is independent of the type of strain used, because it is a model to estimate the culture temperature of a mass of water. The characteristic temperature parameters for each strain are necessary in the cardinal model (1.5), which in combination with the temperature model, allows to analyzing its influence for any microalgae strain.
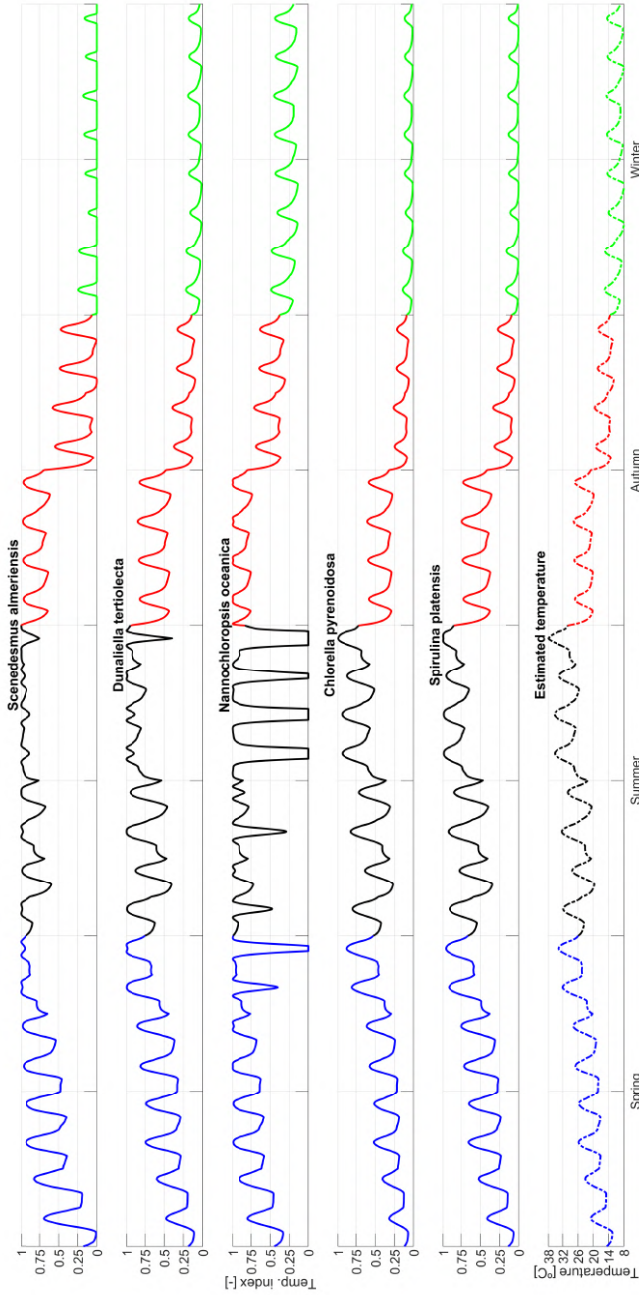
Figure 4.1: Temperature index analysis during seasonal periods. The results for the data set of 8 days are represented individually and divided in four colours representing the different seasons. First graph corresponds to *Scenedesmus almeriensis*. Second graph corresponds to *Dunaliella tertiolecta*. Third graph corresponds to *Nannochloropsis oceanica*. Fourth graph corresponds to *Chlorella pyrenoidosa*, while fifth graph corresponds to *Spirulina platensis*. Sixth graph represents the estimated temperature in the raceway reactor (dashed line).

Microalgae strain	T_{min} [°C]	T_{opt} [°C]	T_{max} [°C]
Scenedesmus almeriensis	12	27	46
Dunaliella tertiolecta	5	32.6	38.9
Nannochloropsis oceanica	-0.2	26.7	33
Chlorella pyrenoidosa	5.2	38.7	45.8
Spirulina platensis	7.7	37	50.6

Table 4.1: Microalgae characteristic temperatures for the feasibility study.

Figure 4.1 represents the analysis carried out for the five types of microalgae during 8 days for each season of the year. The first five graphs represent the temperature indexes for each strain, that affects the microalgae growth. The last graph at the bottom represents the estimated culture temperature in the raceway reactor for the entire data set using the temperature model with a fixed culture depth of 15 cm. From the results obtained in the figure, it is possible to establish different conclusions. The ideal seasons to cultivate the microalgae *Scenedesmus almeriensis*, used in the reactor described in Section 2, are the last half of spring, the summer and the first half of autumn. However, during winter, the temperature index is practically 0, which denotes zero growth. The *Dunaliella tertiolecta* strain is resistant to medium/high temperatures and with a good temperature index late spring, summer and early autumn, while its performance can be diminished by the low temperatures of winter. The microalgae *Nannochloropsis oceanica* would not resist the summer period but it shows good results during the rest of the year, especially in winter, where the temperature index exceeds the other strains analyzed. Both *Chlorella pyrenoidosa* and *Spirulina platensis* strains show a good temperature index during the summer period, together with late spring and the early autumn, as for *Dunaliella tertiolecta*, in contrast to practically no growth in winter due to low temperatures. The results obtained show a clear relationship with the characteristic values of each strain represented in Table 4.1, allowing an estimation of the viability of each strain for the studied location.

The results of the temperature analysis for the cultivation of

microalgae in Almería using the temperature model for raceway reactors have determined that *Scenedesmus almeriensis* and *Dunaliella tertiolecta* microalgae are suitable for production during most part of the year, especially during summer, due to its high temperature index. Both *Chlorella pyrenoidosa* and *Spirulina platensis* strains are also suitable for cultivation during the spring, summer and autumn periods, due to a good temperature index behaviour but less suitable than those described above. On the other hand, the microalgae *Nannochloropsis oceanica* is not capable of withstanding the temperatures reached during late spring and summer periods, being a microalgae difficult to cultivate in these periods, but being the most suitable for cultivation in autumn and winter because it shows the highest temperature index of all the strains for this seasonal period.

4.1.2   Liquid depth effect on culture temperature

From the dynamic evolution of the temperature described in (3.17) (Section 3.1), it follows that it is possible to indirectly modify the culture temperature by varying the depth of the liquid in the raceway reactor. Furthermore, from the specific biomass growth rate model described in (1.1) (Section 1.2), it is assumed that the pH and dissolved oxygen are controlled at their optimal values all the time. This is possible if adequate design and operation of the reactor is performed [7, 22, 47, 48]. Therefore, the growth rate only depends on the solar radiation, which cannot be controlled, and on the culture temperature, which can be modified by varying the volume of the culture in the reactor.

Figures 4.2 and 4.3 show the variations of the culture temperature on the reactor as a result of (3.17), the normalized temperature factor from (1.5), and the biomass productivity from (1.8), for different culture depths and for winter and summer seasons, respectively. The culture depth was varied from 5 cm to 30 cm. These culture depth ranges have been considered due to the physical and operating characteristics of the reactor. Due to the paddlewheel that propels liquid inside the reactor, the liquid depth cannot be less than 5 cm. On the other hand, reactors, in general, are operated between 13 - 30 cm, so it has been chosen to take

30 cm as the maximum depth. As observed, the microalgae growth is highly affected based on the culture depth modifications. In the figures, the maximum biomass productivity considering all cardinal factors in (1.1) for pH, dissolved oxygen and temperature equal to one is represented by the dashed line. On the other hand, the estimated biomass productivity by modifying the temperature factor according to the culture depth variations and keeping the pH and dissolved oxygen factors equal to one is represented by solid lines. Table 4.2 shows the initial biomass concentration used for each culture depth case, where these values represent the optimal biomass concentration to operate a microalgae raceway reactor in continuous mode at different culture depths. The biomass concentration represents the grams of biomass for each liter of medium in the reactor, while the biomass productivity will be used as an indicator to analyze the differences using different cultivation depths.
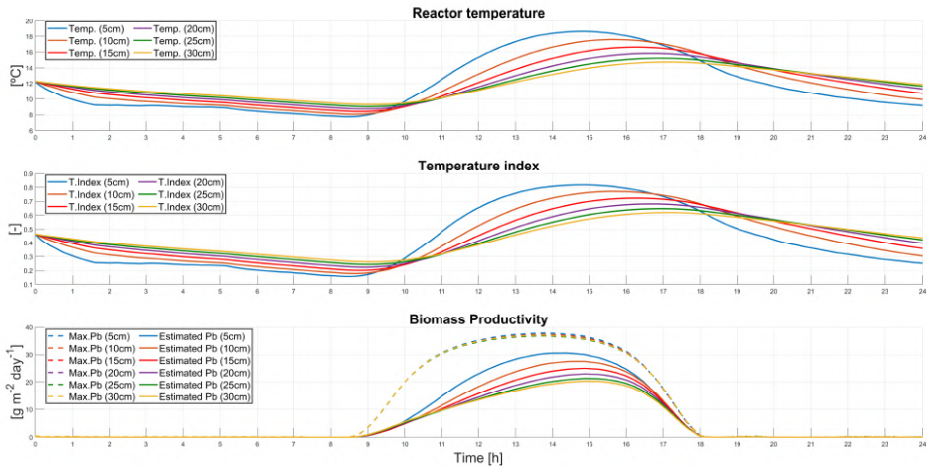
Figure 4.2: Temperature and biomass productivity differences by liquid depth on January. Upper plot corresponds to the culture temperature on the reactor by (3.17). Middle plot represents the temperature index stated by (1.5). Bottom plot refers to the biomass productivity.

Figure 4.2 represents one day of January, as representative of the

winter season. The maximum temperature profile is reached with a culture depth of 5 cm, being the closest to the optimum temperature (27°C such as described in Table 4.1). In this way, with this culture depth, the maximum value is reached during the daytime period for the temperature index and, therefore, the highest value of biomass productivity. On the contrary, a culture depth of 30 cm maintains a temperature profile with less amplitude, reaching the lowest temperature value during the daytime period, decreasing the temperature index and, therefore, the biomass productivity.

Culture [cm] depth	Biomass concentration [g L^{-1}]	
	January	August
5	0.97	2.25
10	0.48	1.12
15	0.32	0.75
20	0.24	0.56
25	0.19	0.45
30	0.16	0.37

Table 4.2: Initial biomass concentration for each culture depth.

Figure 4.3 represents one day of August, as representative of the summer season. Unlike Figure 4.2, in this case, the maximum temperature profile, which occurs also with a culture depth of 5 cm, has a temperature value above the optimal temperature growth value. For this reason, the temperature index in this case is the lowest one, causing a decrease in the biomass productivity. On the other hand, a culture depth of 30 cm keeps a lower temperature profile, with values closer to the optimal value, increasing so the temperature index and the biomass productivity.

These figures demonstrate how the liquid depth affects the culture temperature on the reactor and, consequently, the growth rate and biomass productivity. The maximum and minimum values depend on the season, but they can be modified in a range by changing the culture depth in the reactor. Thus, an interesting approach results in the
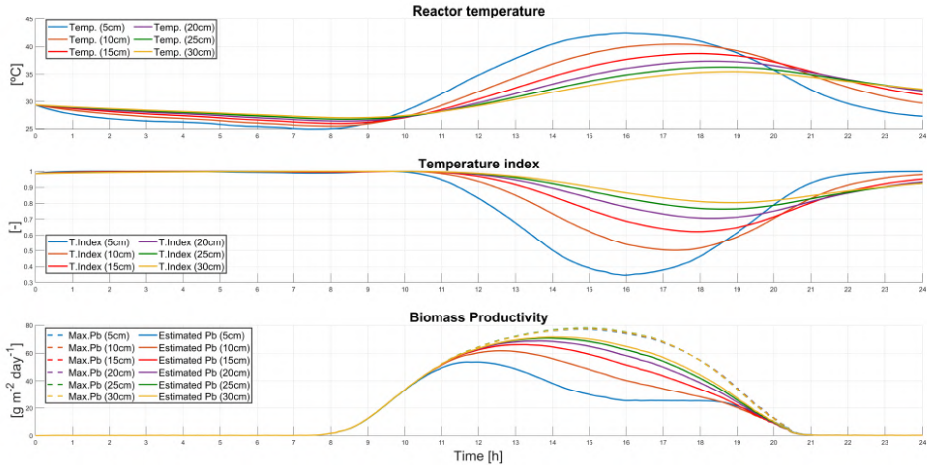
Figure 4.3: Temperature and biomass productivity differences by liquid depth on August. Upper plot corresponds to the culture temperature on the reactor by (3.17). Middle plot represents the temperature index stated by (1.5). Bottom plot refers to the biomass productivity.

modification of the liquid volume in the reactor during the daytime period in order to regulate its temperature and maximize the temperature index in the biomass productivity, through increasing the specific growth rate (see (1.1)).

4.1.3   Feasibility study on biomass productivity

From the temperature model described in Section 3.1 and the characterization of four new strains, an analysis of the influence of the culture depth on biomass productivity has been carried out [75]. This study has focused on four types of microalgae strains that correspond to *Chlorella vulgaris*, *Isochrysis galbana*, *Nannochloropsis gaditana* and *Spirulina platensis*. The characterization of each strain has been carried out at the IFAPA center by the research staff, using specific material for analysis. These strains are commonly grown on an industrial level and are characterized by a high optimum growing temperature. Table 4.3 presents the characteristic parameters obtained experimentally for the

four types of microalgae strains. These parameters describe the characteristic temperatures of each strain (T_{max}, T_{min}, T_{opt}) and the characteristic growth parameters: the maximum productivity $PO_{2,max}$, the form factor n and the minimum irradiance to reach the maximum photosynthesis rate I_k.

Parameter	Chlorella vulgaris	Isochrysis galbana	Nannochloropsis gaditana	Spirulina platensis	Units
T_{max}	49.7	46.1	41.0	50.6	°C
T_{min}	6.6	9.7	4.6	7.7	°C
T_{opt}	33.1	33.0	32.0	37.0	°C
$PO_{2,max}$	301	305	139	218	g m^{-2} day^{-1}
n	2	2	2	2	–
I_k	228	77	151	110	μE m^{-2} s^{-1}

Table 4.3: Characteristic microalgae strain parameters.

A feasibility simulation study has been carried out with environmental data, corresponding to all seasons, for each strain of microalgae presented. The simulation has been based on the dimensions of an 80 m^2 raceway reactor, corresponding to that described in Section 2.2.1. Under this approach, 8 characteristic days of each season have been taken throughout a year, with the aim of analyzing the temperature and biomass productivity under different cultivation depths, ranging from 5 cm to 30 cm. For each value of culture depth, the optimal biomass concentration associated with each season has been used, as shown in Table 4.4.

Chlorella vulgaris

The *Chorella vulgaris* strain is characterized by a high optimum temperature and high productivity. Its main applications are as a dietary supplement due to its antioxidant and probiotic properties. Furthermore, in the industrial field, it shows promising opportunities for biofuel and as a natural food coloring agent. Figures 4.4, 4.5, 4.6 and 4.7 represent the results obtained for this strain during spring, summer, autumn and winter, respectively. All the figures are divided into four graphs: a)

Culture [cm] depth	Biomass concentration [g L^{-1}]			
	Spring	*Summer*	*Autumn*	*Winter*
5	1.92	2.60	1.29	0.97
10	0.96	1.30	0.65	0.48
15	0.64	0.87	0.43	0.32
20	0.48	0.65	0.32	0.24
25	0.38	0.52	0.26	0.19
30	0.32	0.43	0.22	0.16

Table 4.4: Optimum biomass concentration dependent on culture depth.

Culture temperature, where the culture temperature is represented for each depth; b) *Temperature index*, where the temperature index calculated with (1.5) is represented; c) *Oxygen production rate*, which represents radiation-dependent oxygen production (see (3.54)); and d) *Biomass productivity*, which represents the biomass productivity depending on culture depth.

In Figure 4.4, it can be seen that for cold days, such as the first ones in spring, the maximum biomass productivity is reached with shallow depth (5 cm), although it can be detrimental as the temperature increases throughout the season, as can be seen in the last days, where biomass productivity decreases. This effect is very representative looking at the temperature index (Figure 4.4.b). From Figure 4.4.c, it can be seen that all the curves are superimposed one on top of the other. This is because when the optimal concentration associated with the culture depth is used, the oxygen production rate is the same, being independent of the depth at which the reactor is operated.

Summer (see Figure 4.5) is a critical period for the cultivation of microalgae, due to possible overheating in the culture, resulting in their death. In Figure 4.5.a, it can be seen how the culture temperature range oscillates around the optimum temperature value. With depths of 5 cm, high temperatures are reached, which decrease biomass productivity. On the other hand, a cultivation depth of 30 cm keeps the temperature close to optimal, increasing productivity.

Figure 4.4: Culture depth analysis for *Chlorella vulgaris* during spring. Dashed black line represents the optimum growth temperature, while dashed red line represents the maximum growth temperature. Color description is as follows: Blue 5 cm, Orange 10 cm, Yellow 15 cm, Purple 20 cm, Green 25 cm and Cian 30 cm.

Figure 4.5: Culture depth analysis for *Chlorella vulgaris* during summer. Dashed black line represents the optimal temperature, while dashed red line represents the maximum growth temperature. Color description is as follows: Blue 5 cm, Orange 10 cm, Yellow 15 cm, Purple 20 cm, Green 25 cm and Cian 30 cm.

Figure 4.6: Culture depth analysis for *Chlorella vulgaris* during autumn. Dashed black line represents the optimal temperature, while dashed red line represents the maximum growth temperature. Color description is as follows: Blue 5 cm, Orange 10 cm, Yellow 15 cm, Purple 20 cm, Green 25 cm and Cian 30 cm.

In autumn, represented in Figure 4.6, the reactor temperature is not capable of reaching the optimum temperature. So, a 5 cm operation will raise the culture temperature to the maximum possible, increasing biomass productivity.

Winter (see Figure 4.7) is the worst season for the cultivation of microalgae, due to the low temperatures, which reduce the temperature index and the biomass productivity considerably. That is why, as in autumn, a depth of 5 cm increases the temperature, with the subsequent increase in productivity.

Isochrysis galbana

The microalgae strain *Isochrysis galbana* is characterized by a high optimum temperature, with resistance to high temperatures. However, its minimum characteristic temperature is also high, making it difficult to cultivate in cold seasons. Its cultivation is very widespread as feed in the aquaculture industry. Figures 4.8, 4.9, 4.10 and 4.11 represent the results obtained with the depth analysis for the four seasons.

In Figure 4.8, during spring, it can be seen that a culture depth of 5 cm results in high temperatures, close to the optimum temperature. However, as the season approaches summer, the temperature increases, and greater depths increase productivity.

In summer (see Figure 4.9), shallow culture depths raise the temperature above the optimal, reducing biomass productivity. In contrast, high cultivation depths improve productivity.

During autumn, represented in Figure 4.10, shallow depths of culture increase the temperature in the reactor, which does not reach the optimum temperature, but increases productivity.

During winter (see Figure 4.11), as with the rest of the strains, the low temperatures do not favor the proper cultivation of microalgae. Still, a shallow depth of 5 cm maximizes productivity at this season.

Nannochloropsis gaditana

For the microalgae strain *Nannochloropsis gaditana*, despite its high optimum temperature, its maximum temperature is close to the optimal.

Figure 4.7: Culture depth analysis for *Chlorella vulgaris* during winter. Dashed black line represents the optimal temperature, while dashed red line represents the maximum growth temperature. Color description is as follows: Blue 5 cm, Orange 10 cm, Yellow 15 cm, Purple 20 cm, Green 25 cm and Cian 30 cm.
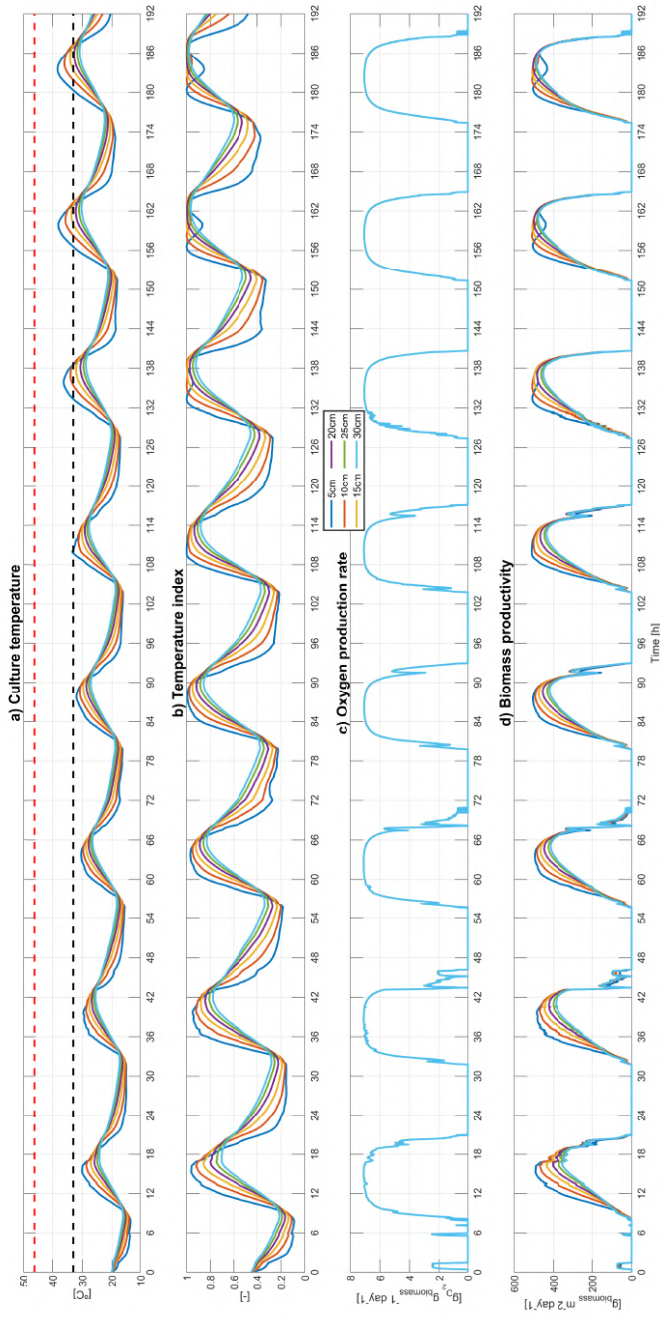
Figure 4.8: Culture depth analysis for *Isochrysis galbana* during spring. Dashed black line represents the optimal temperature, while dashed red line represents the maximum growth temperature. Color description is as follows: Blue 5 cm, Orange 10 cm, Yellow 15 cm, Purple 20 cm, Green 25 cm and Cian 30 cm.
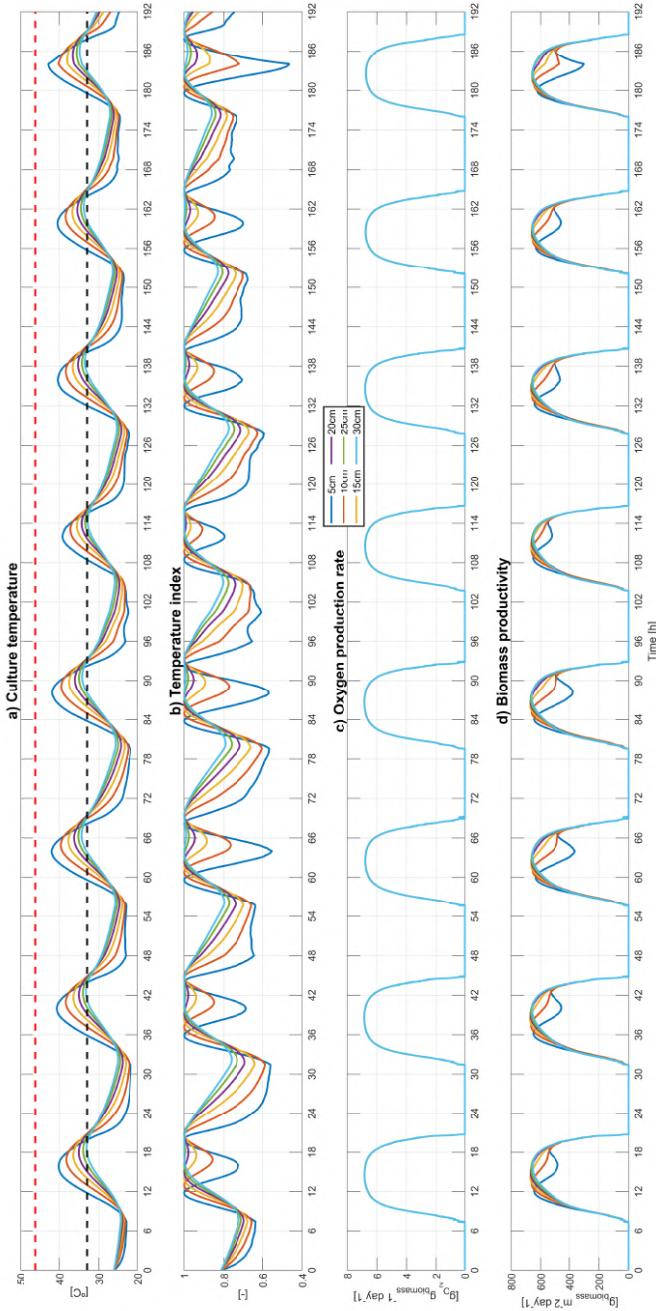
Figure 4.9: Culture depth analysis for *Isochrysis galbana* during summer. Dashed black line represents the optimal temperature, while dashed red line represents the maximum growth temperature. Color description is as follows: Blue 5 cm, Orange 10 cm, Yellow 15 cm, Purple 20 cm, Green 25 cm and Cian 30 cm.
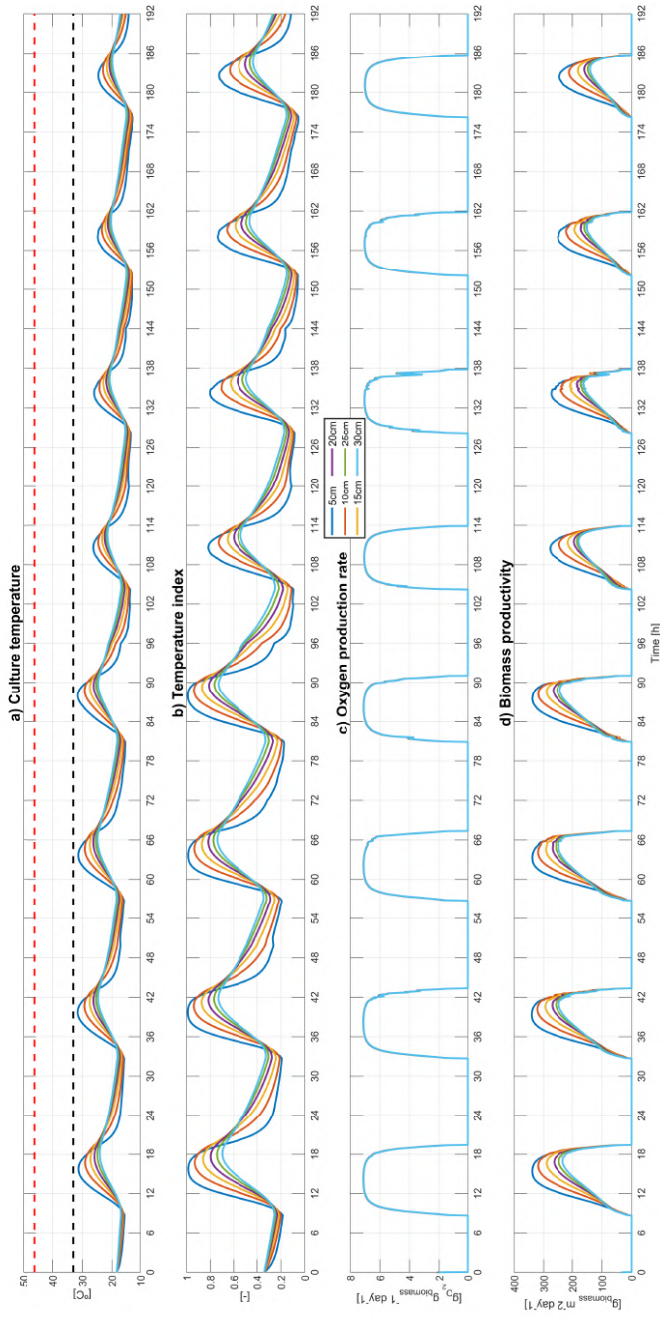
Figure 4.10: Culture depth analysis for *Isochrysis galbana* during autumn. Dashed black line represents the optimal temperature, while dashed red line represents the maximum growth temperature. Color description is as follows: Blue 5 cm, Orange 10 cm, Yellow 15 cm, Purple 20 cm, Green 25 cm and Cian 30 cm.
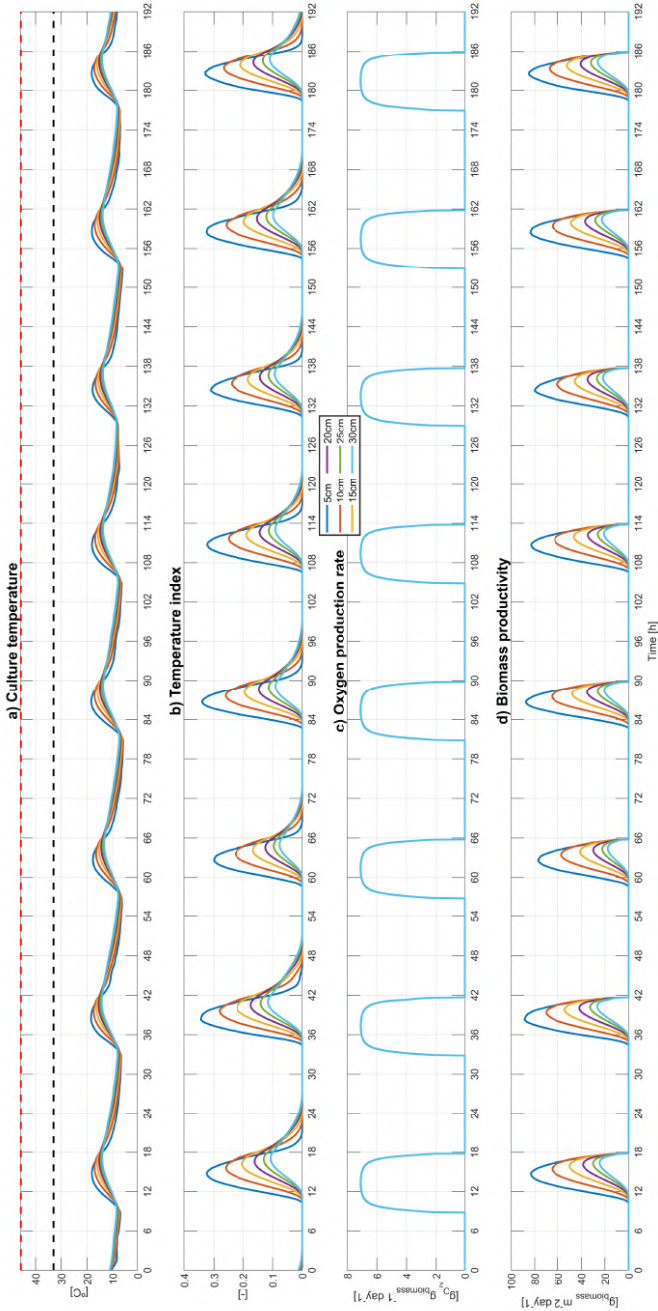
Figure 4.11.: Culture depth analysis for *Isochrysis galbana* during winter. Dashed black line represents the optimal temperature, while dashed red line represents the maximum growth temperature. Color description is as follows: Blue 5 cm, Orange 10 cm, Yellow 15 cm, Purple 20 cm, Green 25 cm and Cian 30 cm.

So, it can be difficult to cultivate in very warm periods or locations. Its main application is as feed for fish and mollusks. Figures 4.12, 4.13, 4.14 and 4.15 represent the results obtained with the depth analysis for the four seasons.

During spring, represented in Figure 4.12, the behavior is similar to the rest of the strains. At the beginning of the season, a shallow depth favors productivity, but as summer approaches, productivity decreases and depth needs to be increased.

This strain of microalgae is the one with the lowest maximum temperature of those studied. During the summer period (see Figure 4.13), it is observed how a low culture depth causes such high temperatures that they result in zero productivity, even being harmful to the microalgae.

During the autumn and winter (see Figures 4.14 and 4.15), the behavior is the same as for the rest of the strains studied. Shallow depths cause high temperatures that maximize biomass productivity.

Spirulina platensis

The microalgae strain *Spirulina platensis* is known worldwide for its multiple applications, being the most widespread for human consumption. Among other applications are the production of plastics and alcohols. It is a strain resistant to high temperatures, its optimum cultivation temperature being also high, which makes it difficult to reach its maximum productivity. Figures 4.16, 4.17, 4.18 and 4.19 represent the results obtained with the depth analysis for the four seasons.

This strain is the one with the highest optimal cultivation temperature. Therefore, for the spring, autumn and winter periods (represented in Figures 4.16, 4.18 and 4.19 respectively), the maximum productivity is reached with shallow depth (5 cm). On the other hand, in summer (see Figure 4.17), a shallow cultivation depth is also necessary to increase productivity, but not as low as in the rest of the seasons.
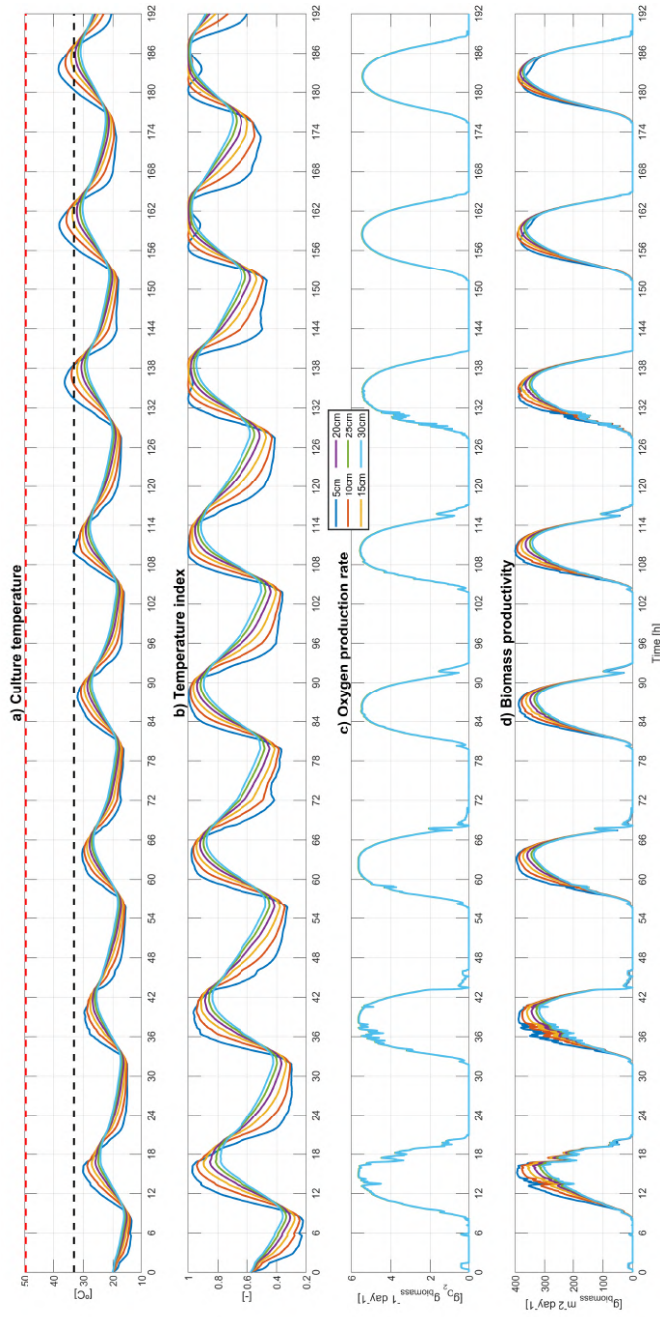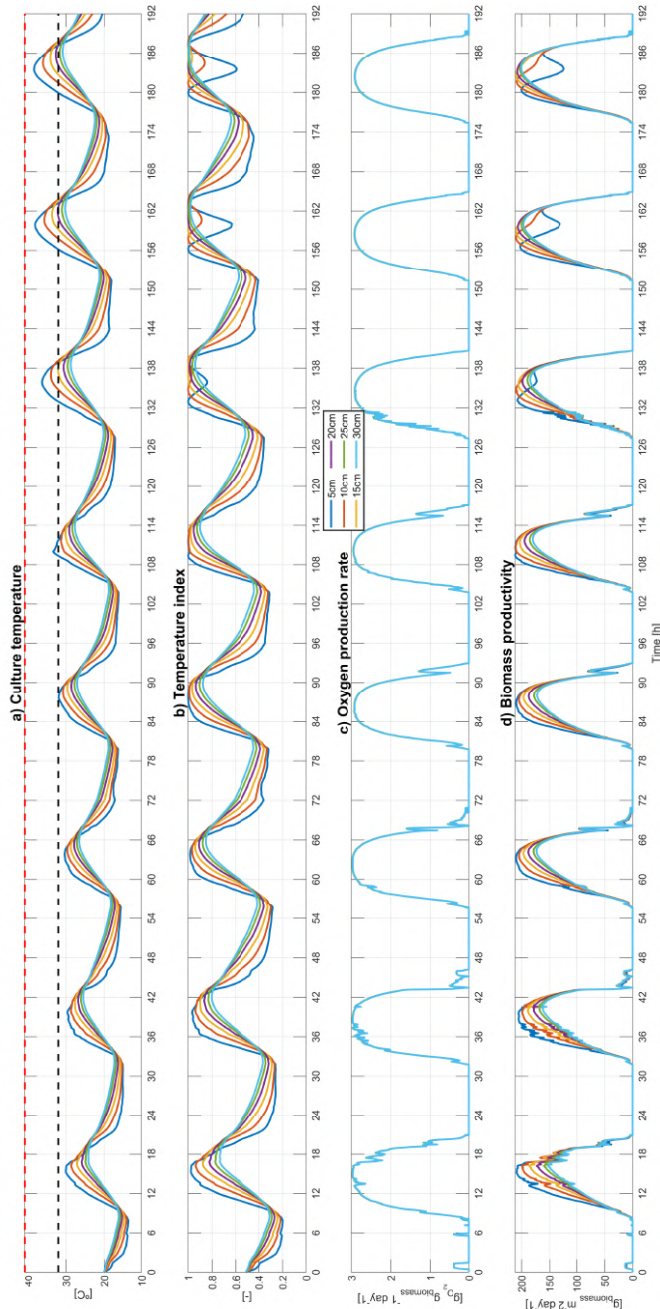
Figure 4.12: Culture depth analysis for *Nannochloropsis gaditana* during spring. Dashed black line represents the optimal temperature, while dashed red line represents the maximum growth temperature. Color description is as follows: Blue 5 cm, Orange 10 cm, Yellow 15 cm, Purple 20 cm, Green 25 cm and Cian 30 cm.
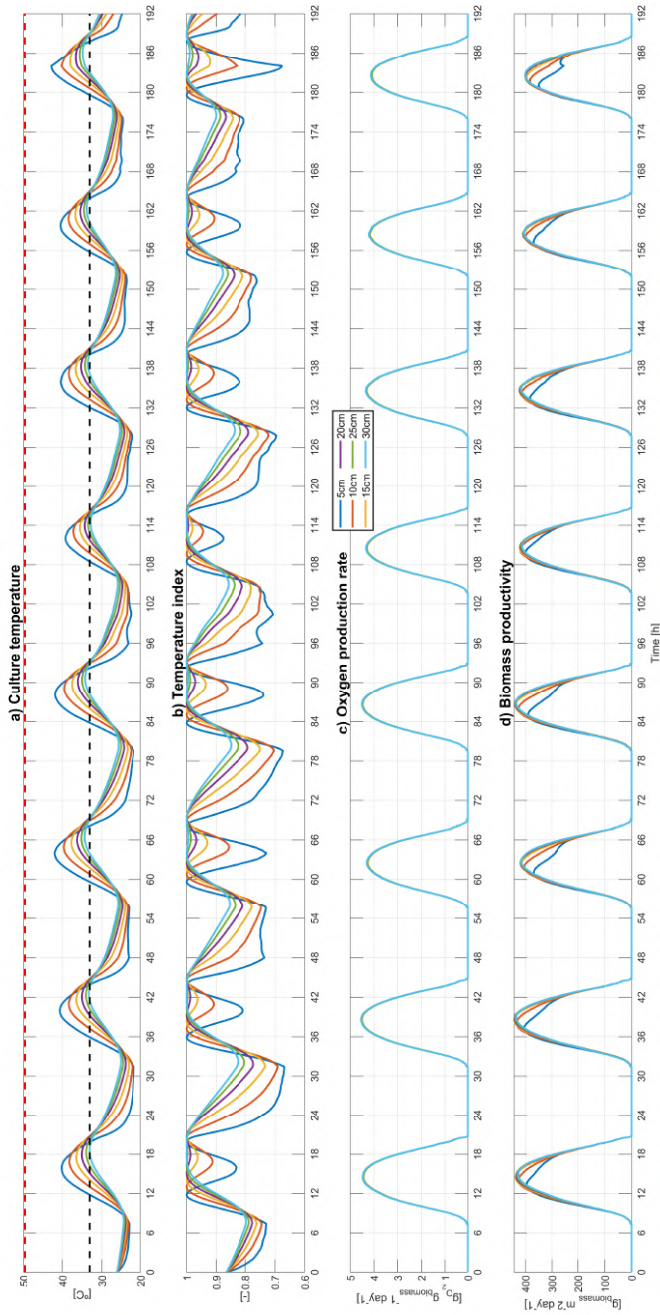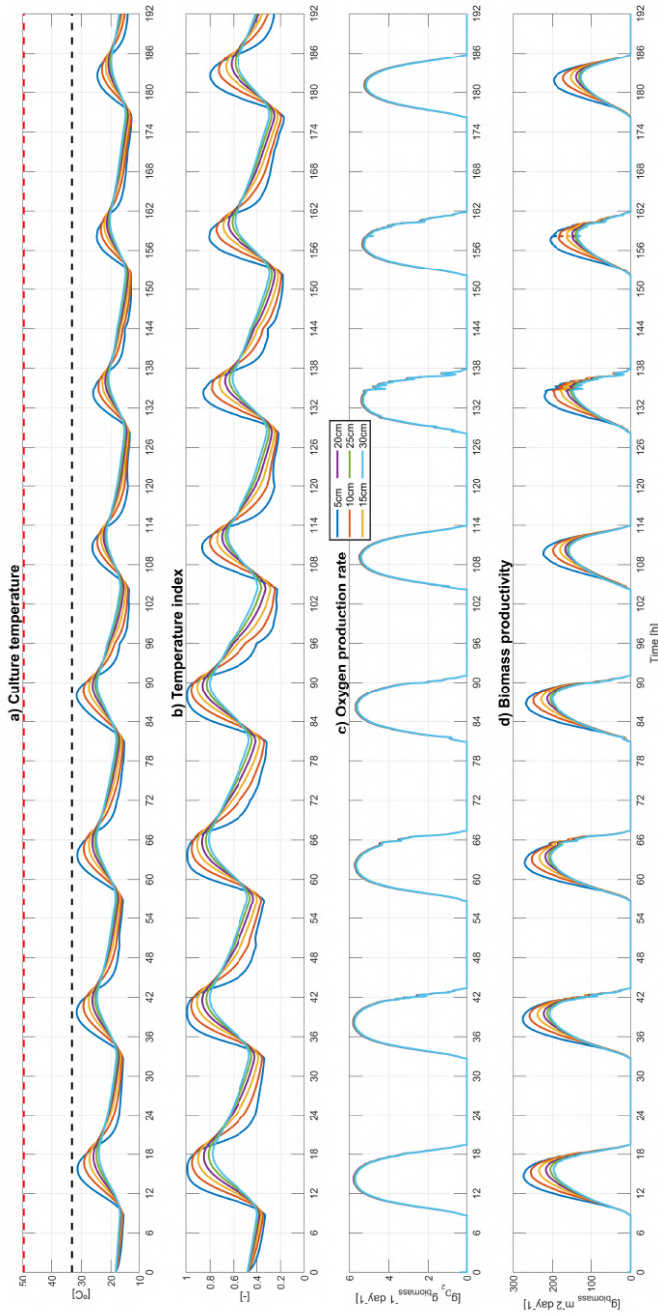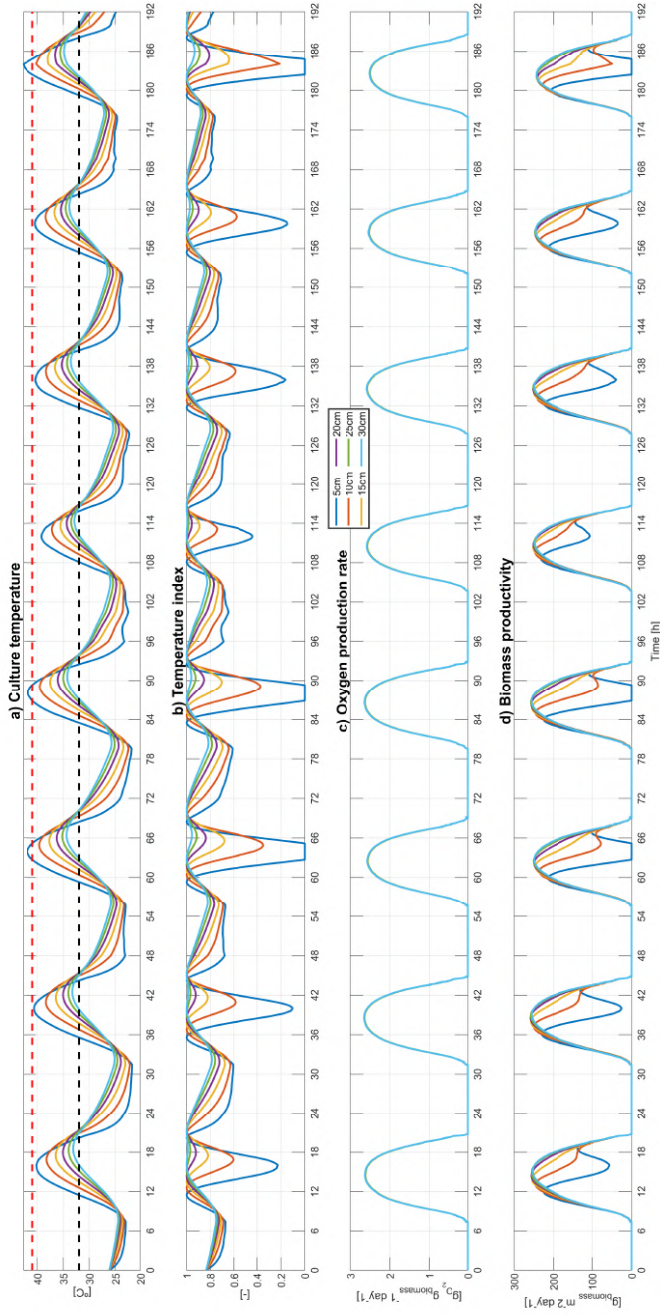
Figure 4.13: Culture depth analysis for *Nannochloropsis gaditana* during summer. Dashed black line represents the optimal temperature, while dashed red line represents the maximum growth temperature. Color description is as follows: Blue 5 cm, Orange 10 cm, Yellow 15 cm, Purple 20 cm, Green 25 cm and Cian 30 cm.
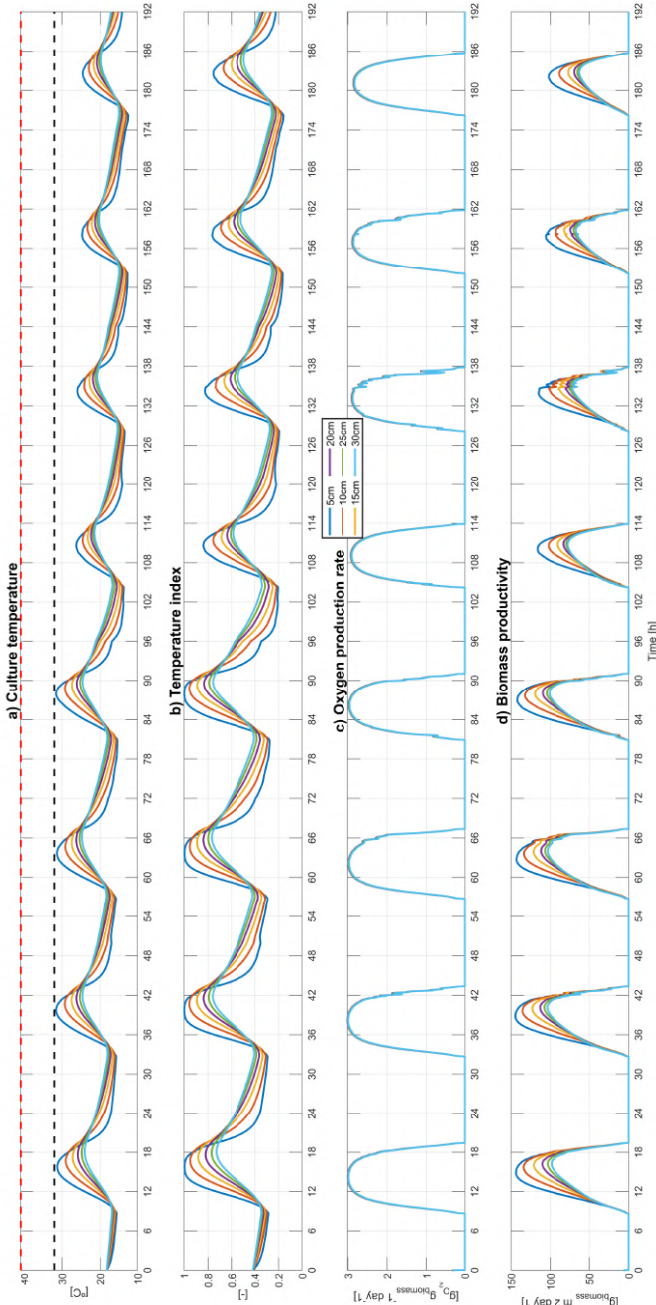
Figure 4.14: Culture depth analysis for *Nannochloropsis gaditana* during autumn. Dashed black line represents the optimal temperature, while dashed red line represents the maximum growth temperature. Color description is as follows: Blue 5 cm, Orange 10 cm, Yellow 15 cm, Purple 20 cm, Green 25 cm and Cian 30 cm.
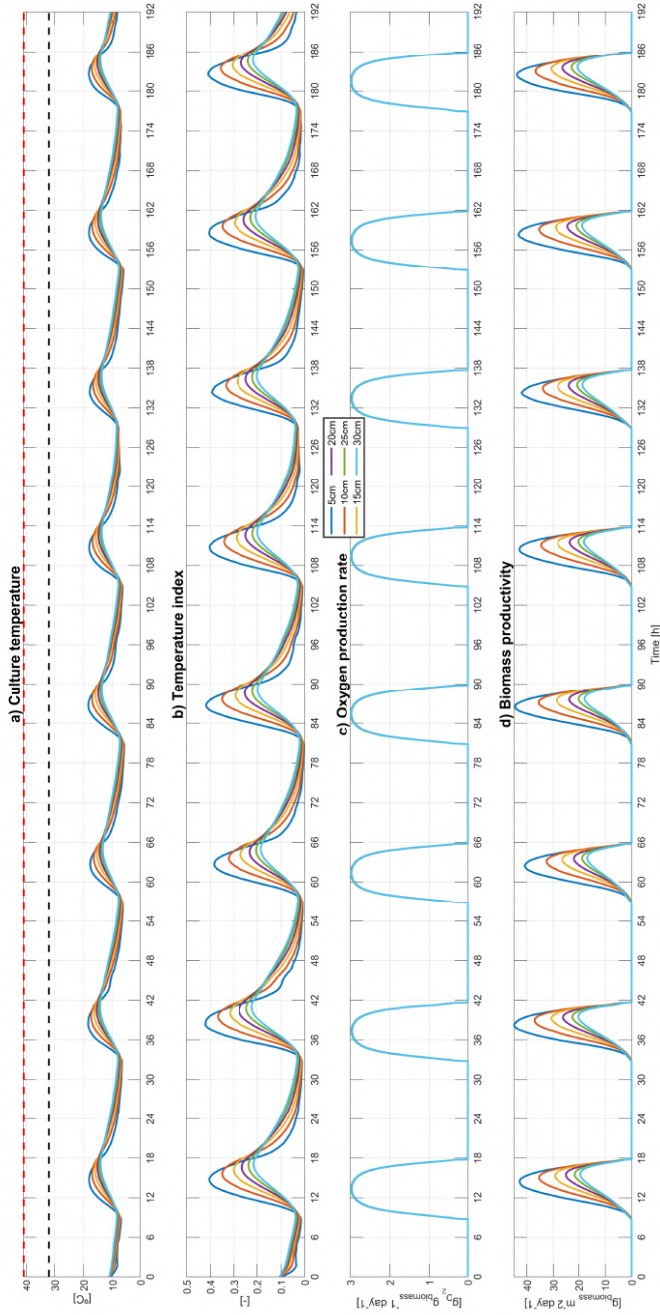
Figure 4.15: Culture depth analysis for *Nannochloropsis gaditana* during winter. Dashed black line represents the optimal temperature, while dashed red line represents the maximum growth temperature. Color description is as follows: Blue 5 cm, Orange 10 cm, Yellow 15 cm, Purple 20 cm, Green 25 cm and Cian 30 cm.
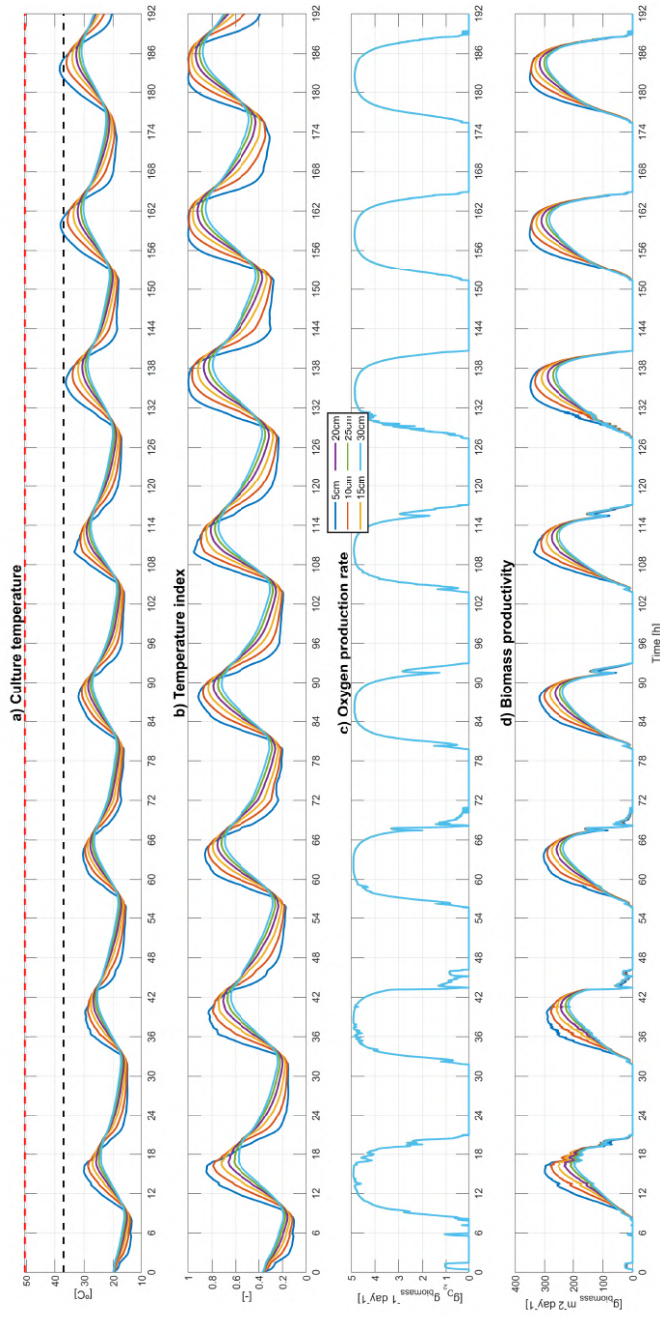
Figure 4.16: Culture depth analysis for *Spirulina platensis* during spring. Dashed black line represents the optimal temperature, while dashed red line represents the maximum growth temperature. Color description is as follows: Blue 5 cm, Orange 10 cm, Yellow 15 cm, Purple 20 cm, Green 25 cm and Cian 30 cm.
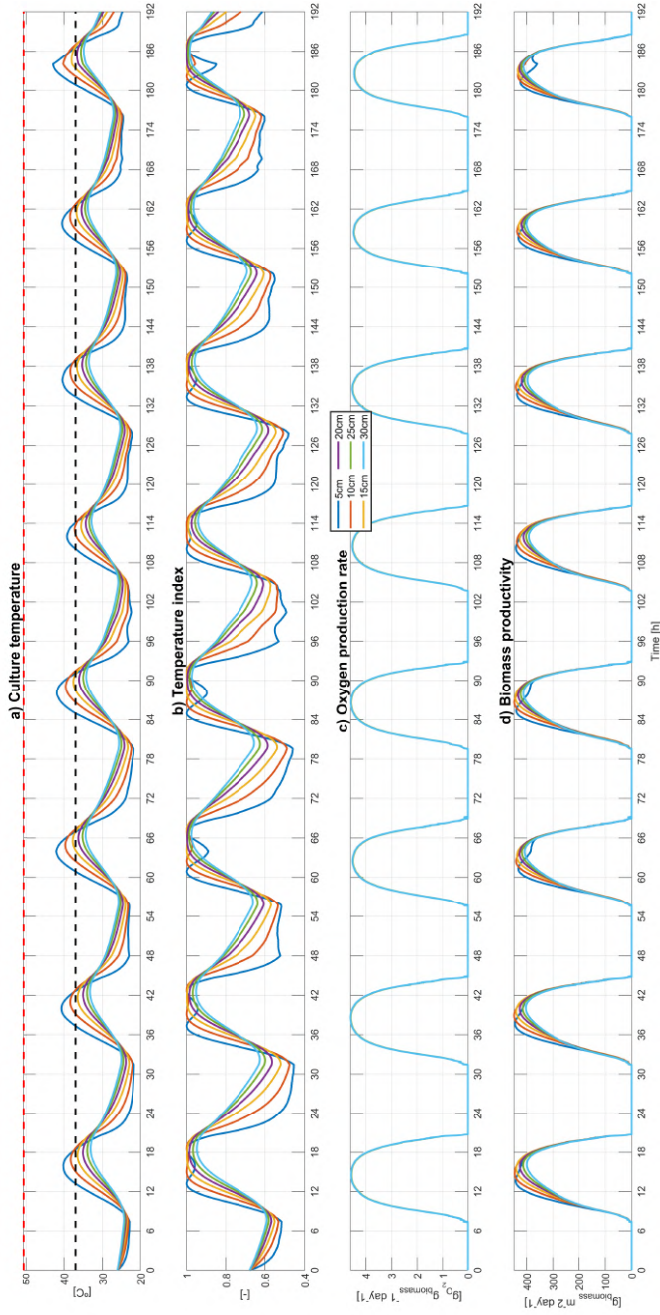
Figure 4.17: Culture depth analysis for *Spirulina platensis* during summer. Dashed black line represents the optimal temperature, while dashed red line represents the maximum growth temperature. Color description is as follows: Blue 5 cm, Orange 10 cm, Yellow 15 cm, Purple 20 cm, Green 25 cm and Cian 30 cm.
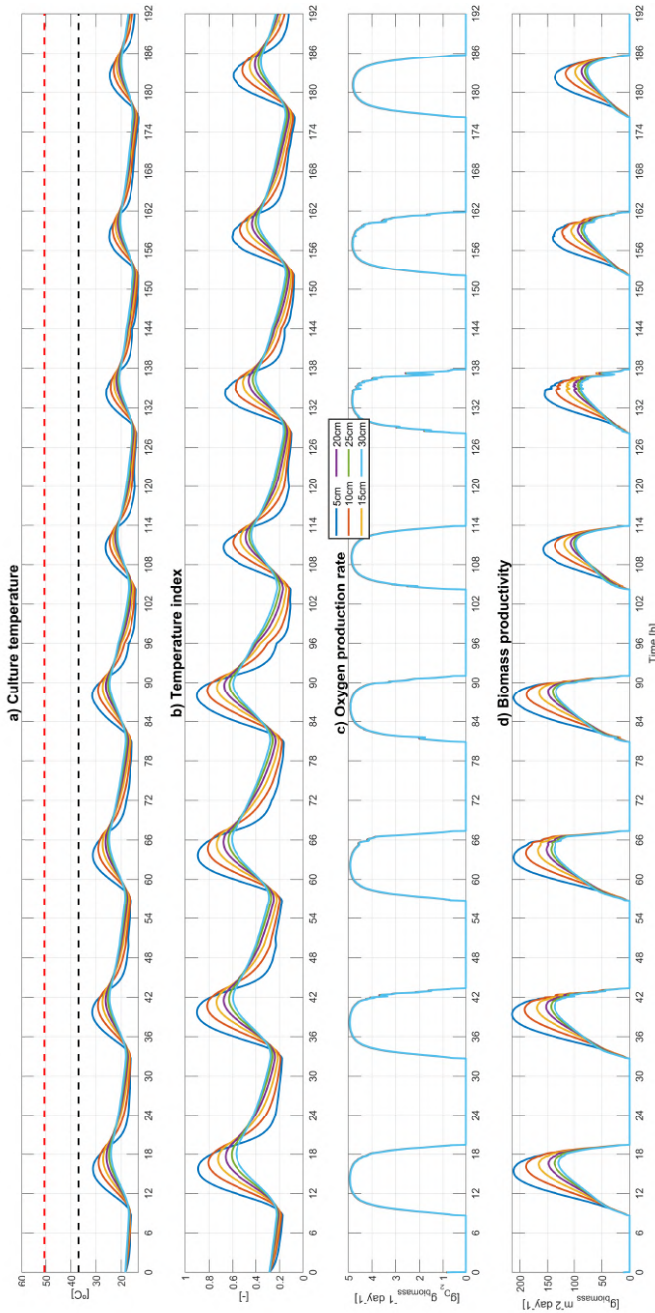
Figure 4.18: Culture depth analysis for *Spirulina platensis* during autumn. Dashed black line represents the optimal temperature, while dashed red line represents the maximum growth temperature. Color description is as follows: Blue 5 cm, Orange 10 cm, Yellow 15 cm, Purple 20 cm, Green 25 cm and Cian 30 cm.
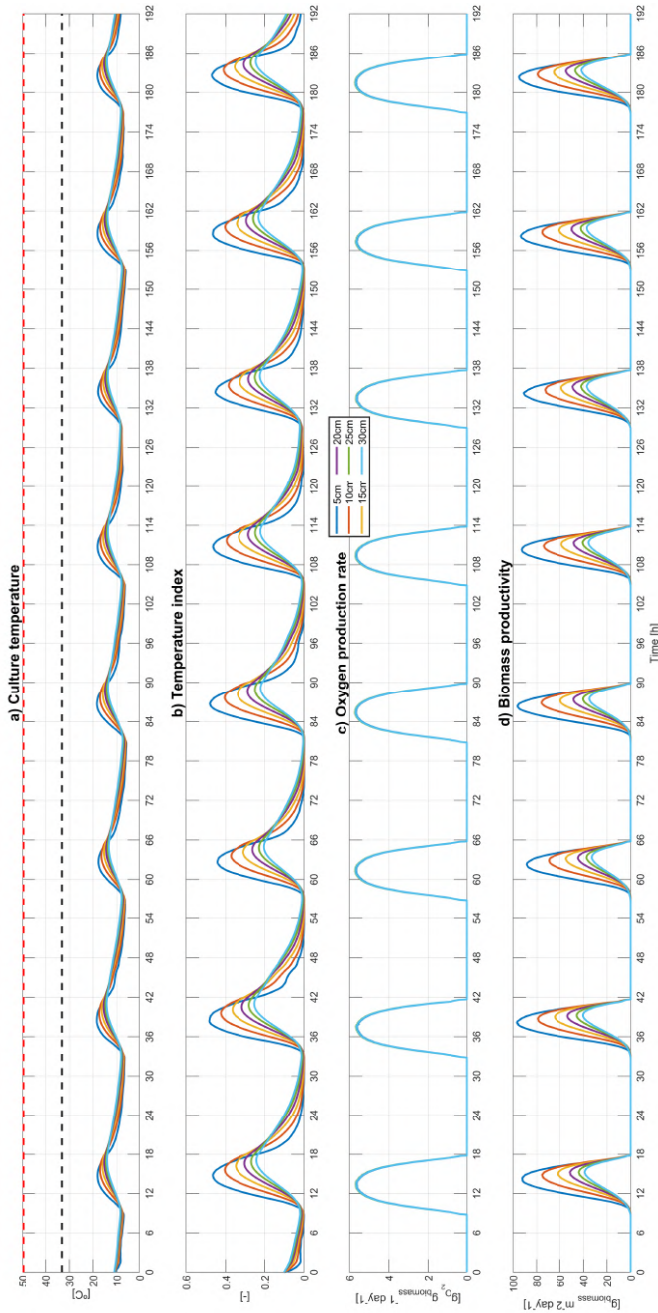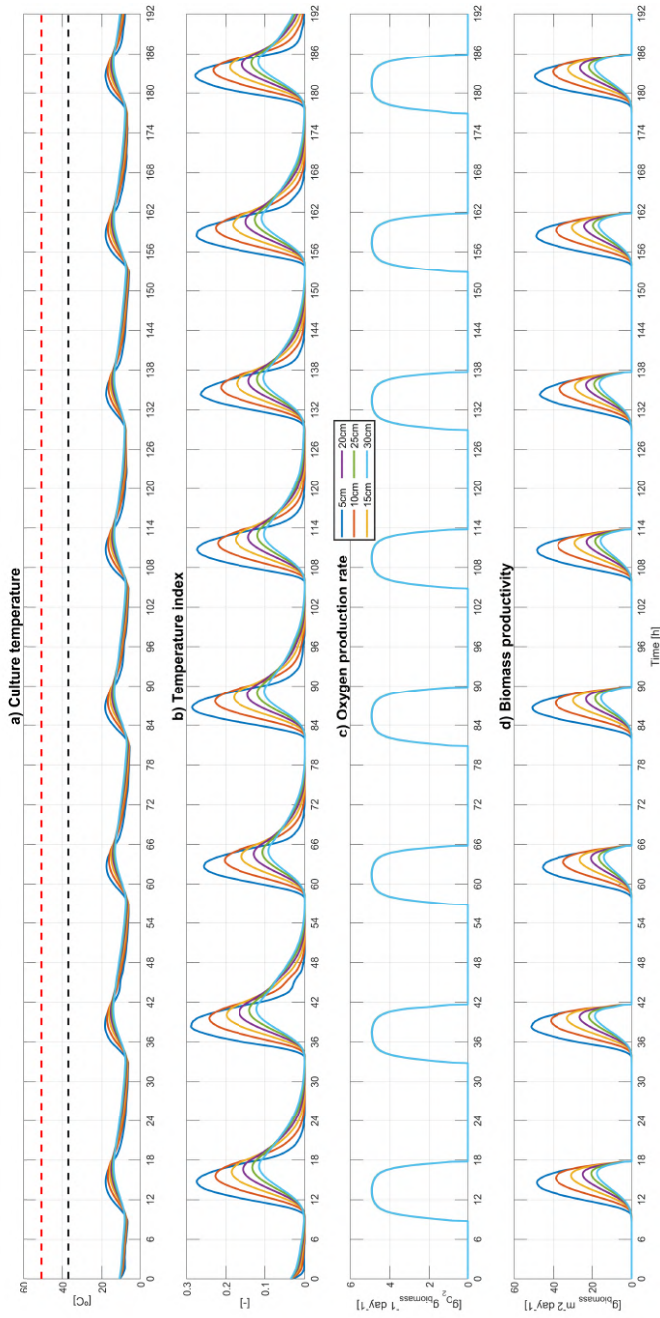
Figure 4.19: Culture depth analysis for *Spirulina platensis* during winter. Dashed black line represents the optimal temperature, while dashed red line represents the maximum growth temperature. Color description is as follows: Blue 5 cm, Orange 10 cm, Yellow 15 cm, Purple 20 cm, Green 25 cm and Cian 30 cm.

Discussion

Table 4.5 shows the average productivity values for each season and culture depth, obtained for each microalgae strain analyzed, in addition to the average temperature index during daytime, the period in which microalgae perform photosynthesis. In red colour, the maximum values associated with the culture depth are highlighted. Observing the biomass productivity data, it is noted that the highest values are obtained in summer, being the ideal time to cultivate this type of strains. On the other hand, during winter, productivity is very low, being a difficult period for its cultivation, even lowering the depth in the reactor. It is possible to appreciate a direct relationship between the temperature index and biomass productivity, since the maximum values for both variables occur almost at the same culture depths. Because the optimal temperatures for all microalgae strains have high values, the highest average productivity during spring, autumn and winter is reached with shallow depths of 5 cm. On the other hand, during the summer, the maximum productivity is reached with depths between 25 and 30 cm, due to the high temperatures that are reached in this period.

A characteristic fact that can be obtained by checking the maximum values (represented in red) is that the optimum cultivation depth is almost 5 cm for all seasons except summer. From this result, it can be intuited that the cultivation of these strains in open thin-layer reactors (where culture depths are around 2 cm) would allow a much higher productivity than their cultivation in raceway reactors, during spring, autumn and winter.

Feasibility study

From the previous analysis presented on the microalgae strains with different culture depth, a comparison of the biomass productivity has been carried out, throughout the four seasons, differentiating between the operation of the reactor with a fixed depth of 15 cm and the operation with the optimal depth for each period. The objective is to demonstrate that the use of the optimal culture depth increases biomass productivity.

Figure 4.20 represents the feasibility study for *Chlorella vulgaris* strain. Following the results of Table 4.5, culture depths of 5 cm have been chosen

	Culture depth [cm]	Average productivity [day^{-1}]				Temperature index [–]			
		Spring	Summer	Autumn	Winter	Spring	Summer	Autumn	Winter
Chlorella vulgaris	5	127.817	123.470	62.540	18.017	0.890	0.903	0.726	0.318
	10	123.432	129.484	56.289	13.873	0.862	0.930	0.666	0.257
	15	118.788	132.097	51.624	10.870	0.833	0.945	0.622	0.208
	20	115.004	132.972	48.706	8.894	0.809	0.952	0.595	0.173
	25	111.855	133.165	47.248	7.593	0.792	0.955	0.578	0.150
	30	110.090	133.156	46.397	6.796	0.779	0.957	0.568	0.134
Isochrysis galbana	5	194.174	238.829	86.185	15.799	0.805	0.841	0.649	0.244
	10	186.727	253.774	75.662	11.164	0.781	0.881	0.574	0.183
	15	178.743	262.518	67.276	7.746	0.752	0.907	0.518	0.130
	20	172.166	265.453	61.959	5.516	0.727	0.920	0.483	0.094
	25	165.871	266.990	59.702	4.064	0.709	0.928	0.461	0.070
	30	163.478	266.256	58.498	3.181	0.694	0.932	0.448	0.055
Nannochloropsis gaditana	5	71.178	53.759	34.460	12.326	0.858	0.742	0.691	0.272
	10	69.998	71.547	30.603	9.560	0.843	0.833	0.624	0.222
	15	67.544	80.979	27.615	7.594	0.814	0.886	0.574	0.183
	20	65.177	84.696	25.743	6.348	0.786	0.914	0.542	0.156
	25	62.952	86.298	24.900	5.568	0.764	0.929	0.522	0.138
	30	61.875	86.807	24.435	5.069	0.747	0.937	0.510	0.126
Spirulina platensis	5	114.994	161.123	48.574	9.546	0.763	0.908	0.552	0.183
	10	107.215	158.921	41.749	7.040	0.716	0.896	0.482	0.141
	15	100.016	155.843	36.720	5.231	0.671	0.880	0.432	0.107
	20	94.596	152.557	33.648	4.050	0.636	0.866	0.401	0.084
	25	90.105	150.287	32.272	3.270	0.611	0.855	0.382	0.069
	30	87.953	148.035	31.516	2.804	0.592	0.848	0.371	0.059

Table 4.5: Average seasonal biomass productivity and temperature index for microalgae study.

for spring, autumn and winter, while for summer a depth of 25 cm has been chosen. With this change, productivity increases by 4% on spring, 0.6% on summer, 20.4% on autumn and 65.5% on winter. Despite the fact that in summer the increase on biomass productivity is practically zero, during the autumn and winter a considerable improvement is achieved.

Figure 4.21 represents the feasibility study for *Isochrysis galbana* strain. In this case, a depth of 5 cm has also been chosen for spring, autumn and winter, while 25 cm for the summer. The improvements obtained have been 4.5% for spring, 1.5% for summer, 27% for fall and 104% for winter. In this case, the improvement on biomass productivity is reflected especially during the autumn and winter, as observed from the figure.

Figure 4.22 represents the feasibility study for *Nannochloropsis gaditana* strain. A culture depth of 5 cm has been taken for spring, autumn and winter, while a depth of 30 cm for summer. The biomass productivity increase has been of 3.6% for spring, 6.8% for summer, 24% for fall and 57.5% for winter. The optimum temperature for this strain is the lowest among those studied, so during the summer, a high depth
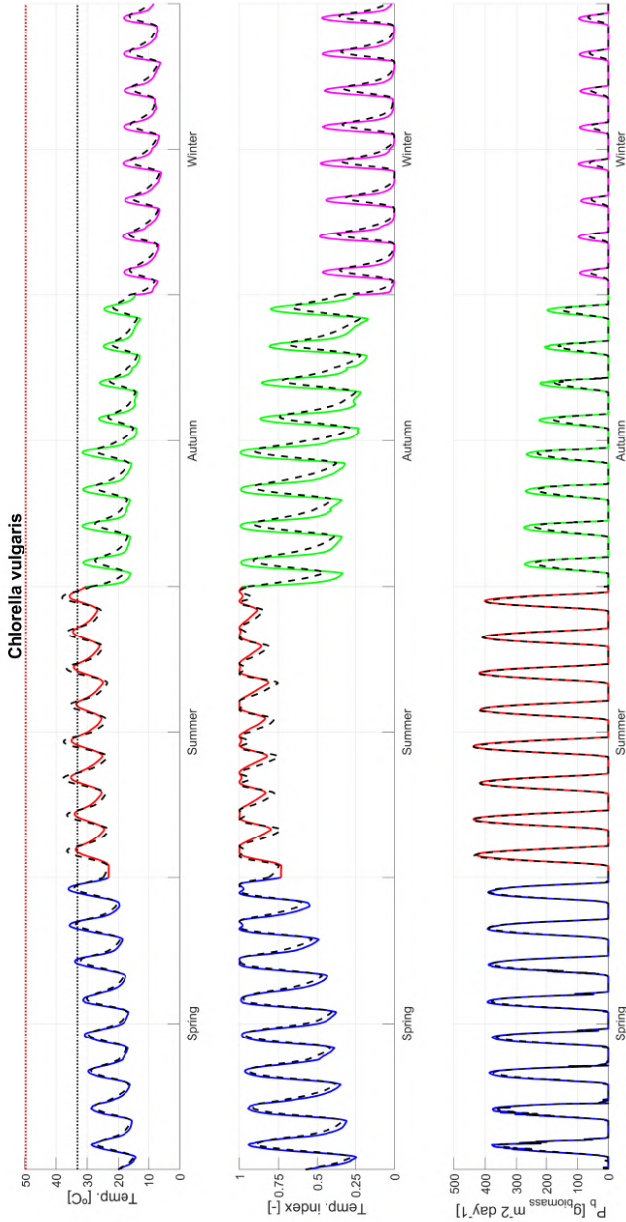
Figure 4.20: Feasibility study comparison for *Chlorella vulgaris* between changing culture depth and fixed depth during four seasons. Upper graph represents the estimated culture temperature; middle graph presents the temperature index; and bottom graph shows the biomass productivity. Dashed black lines represent the results with fixed 15 cm depth, while solid lines represent the optimized depth results. Dashed horizontal black points line states the optimum growth temperature, while dashed red points line represents the maximum growth temperature.
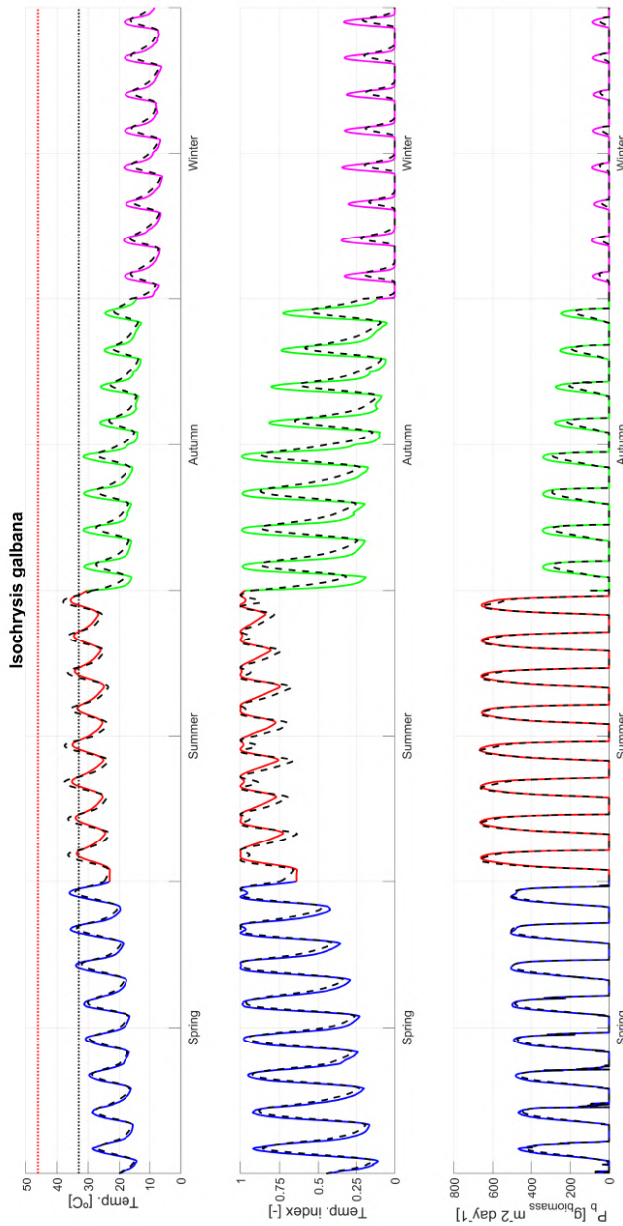
Figure 4.21: Feasibility study comparison for *Isochrysis galbana* between changing culture depth and fixed depth during four seasons. Upper graph represents the estimated culture temperature; middle graph presents the temperature index; and bottom graph shows the biomass productivity. Dashed black lines represent the results with fixed 15 cm depth, while solid lines represent the optimized depth results. Dashed horizontal black points line states the optimum growth temperature, while dashed red points line represents the maximum growth temperature.

considerably improves the temperature of the culture and its productivity.

Figure 4.23 represents the feasibility study for *Spirulina platensis* strain. For this strain, a culture depth of 5 cm has been used during all seasons, since it presents the highest optimum temperature of all the strains studied. In this case, the improvement in productivity has been 15% in spring, 2% in summer, 31% in autumn and 82% in winter. As it is a warm ambient strain, the increase in temperature during cold periods considerably improves its productivity.

As a result of this study, it can be concluded that the strains of microalgae studied need warm climates to maximize their productivity. Under this condition, the cultivation during autumn and winter is difficult. However, low culture depths have been shown to increase the culture temperature on the reactor, and consequently biomass productivity. Cultivation in open thin-layer reactors, where higher temperatures are reached, can be an interesting option during the coldest critical months (autumn and winter).

4.2 Optimization control problem

The influence of the medium temperature on the microalgae growth has been demonstrated in the previous sections. From the performed analysis, it can be seen that it is important to regulate the temperature in the reactor. However, in the literature, there is a lack of solutions for the temperature regulation problem in raceway reactors, where the tradeoff between efficiency and profitability is managed. This section presents a simple method for temperature regulation by varying the volume in the reactor throughout the daytime period [72], in a similar way as the strategies presented in [23] and [24]. The core idea is based on the influence of the atmospheric conditions and the liquid depth on culture temperature. A culture depth optimizer has been designed to determine the culture depth variation that minimizes the difference between the reactor temperature and the desired optimal culture temperature. The control of the culture depth in the reactor is carried
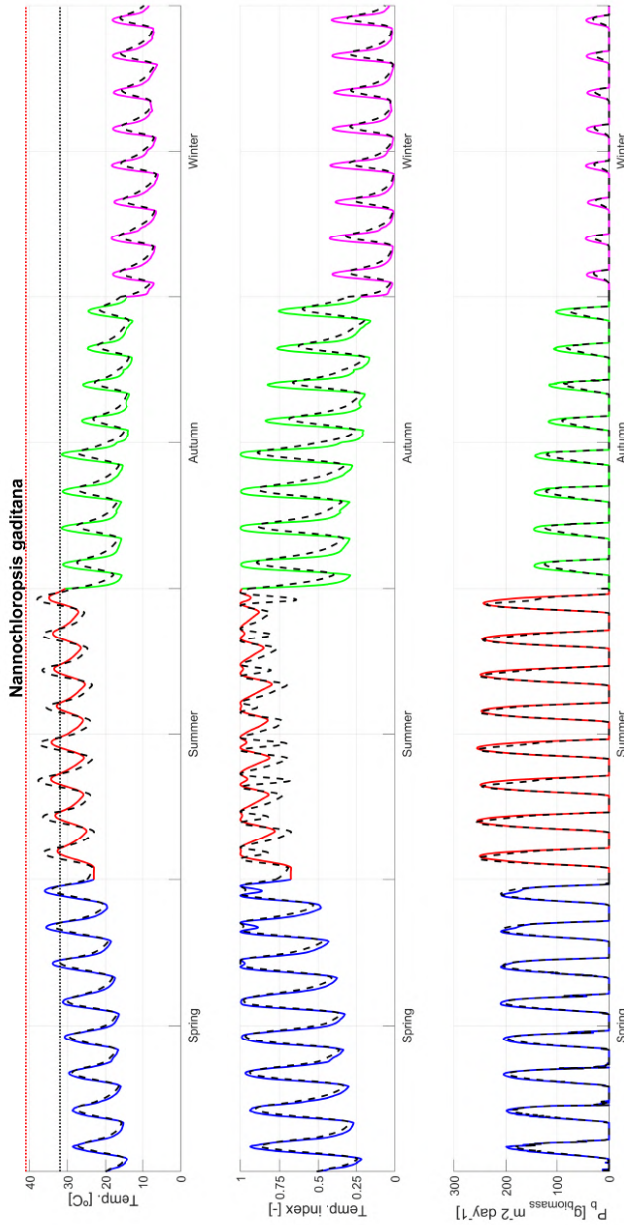
Figure 4.22: Feasibility study comparison for *Nannochloropsis gaditana* between changing culture depth and fixed depth during four seasons. Upper graph represents the estimated culture temperature; middle graph presents the temperature index; and bottom graph shows the biomass productivity. Dashed black lines represent the results with fixed 15 cm depth, while solid lines represent the optimized depth results. Dashed horizontal black points line states the optimum growth temperature, while dashed red points line represents the maximum growth temperature.
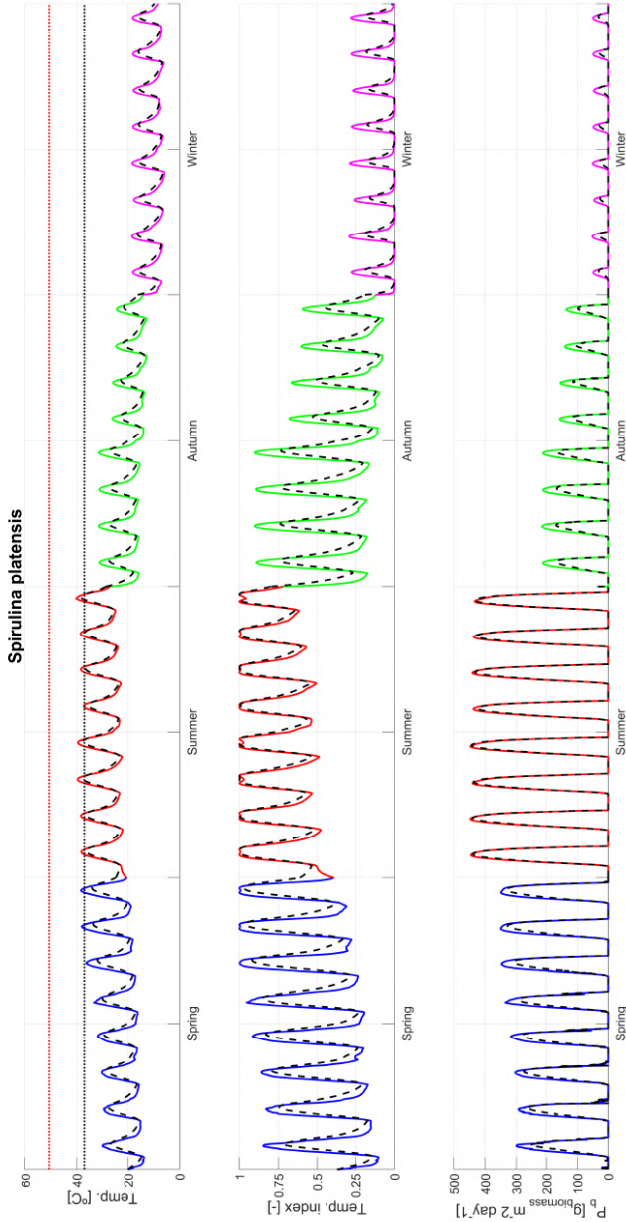
Figure 4.23: Feasibility study comparison for *Spirulina platensis* between changing culture depth and fixed depth during four seasons. Upper graph represents the estimated culture temperature; middle graph presents the temperature index; and bottom graph shows the biomass productivity. Dashed black lines represent the results with fixed 15 cm depth, while solid lines represent the optimized depth results. Dashed horizontal black points line states the optimum growth temperature, while dashed red points line represents the maximum growth temperature.

out by means of the harvesting and dilution processes, being a method
that does not require the use or installation of new devices for cooling or
heating the reactor culture. A schematic of the system is shown in Figure
4.24.
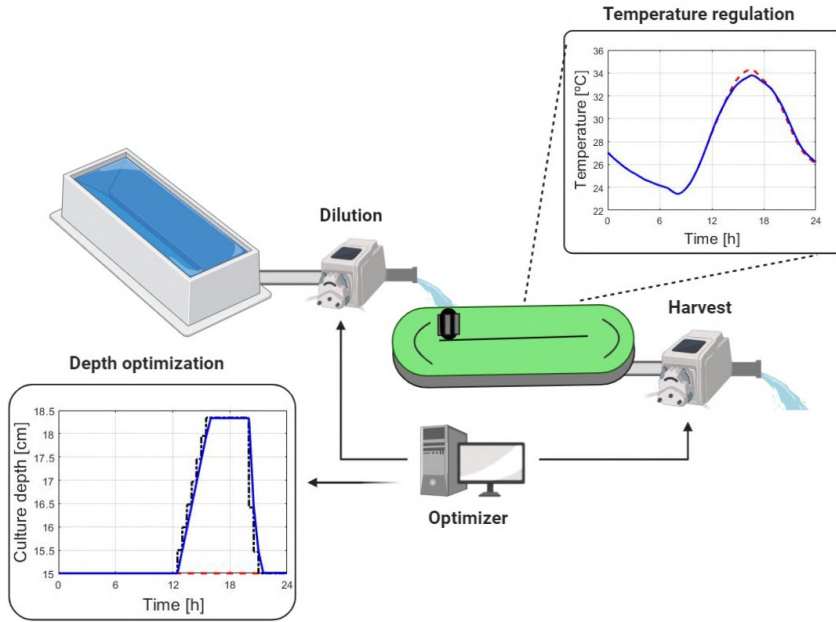
Figure 4.24: Culture depth optimization scheme.

In order to show better the temperature effect on the process
productivity, it is assumed that the pH and the dissolved oxygen
variables are perfectly controlled [61, 73, 70], and thus the corresponding
factors described by (1.6) and (1.7) are considered equal to one. In this
way, the specific growth rate model only depends on solar radiation and
temperature.

Analyzing the temperature regulation problem for microalgae
production, the aim is to keep the medium temperature T_w as close as
possible to the strain optimum growth temperature $T_{optimum}$. In this
way, the normalized temperature index given by (1.5) will be increased

and thus the biomass productivity will be maximized. Therefore, the optimization problem proposed in this work can be posed as:

$$\min_{\text{h}} J = |T_w(t) - T_{optimum}| \tag{4.1}$$

subject to:

$$\frac{dT_w(t)}{dt} = \frac{Q_{total}(t)}{h(t) \cdot A \cdot C_p \cdot \rho} \tag{4.2}$$

$$h_{min} \leq h(t) \leq h_{max} \tag{4.3}$$

$$-\Delta h_{max} \leq \Delta h(t) \leq \Delta h_{max} \tag{4.4}$$

$$\tag{4.5}$$

$$T_{min} \leq T_w(t) \leq T_{max} \tag{4.6}$$

$$\tag{4.7}$$

where Q_{total} is the sum of all heat terms described in Section 3.1. On the other hand, the culture depth should be limited to avoid overestimated harvesting or dilutions. Therefore, minimum (h_{min}) and maximum (h_{max}) culture depth values are included in the optimizer based on the dilution rate parameter (the % of volume that can be added or removed from the reactor so that the biomass concentration a the end of the day is the same as at the beginning of the day) and on the variation in reactor volume. Likewise, to avoid sudden changes in the culture depth, a maximum increment (Δh_{max}) of 1 cm on the depth has been established for each iteration of the optimizer, performed with a period of half an hour. Finally, the reactor temperature is limited between T_{min} and T_{max} values that are determined by the characteristics of the microalgae strain (see Table 4.1) in order to avoid a detrimental effect on the microalgae growth. The microalgae analyzed with the optimization approach has been *Scenedesmus almeriensis*.

The implementation of the cost function to minimize has been carried out in the Matlab programming and calculation environment, using the *fmincon* function. The objective of this function is to find the minimum of a restricted nonlinear multivariate problem from a cost function, subject to linear and nonlinear restrictions. The structure of this function is as follows:

$$\min_{\mathbf{x}} f(x) \ such \ that \ \begin{cases} c(x) \leq 0 \\ ceq(x) = 0 \\ A \cdot x \leq b \\ Aeq \cdot x = beq \\ lb \leq x \leq ub \end{cases} \qquad (4.8)$$

where x is the optimized variable (in this case, the culture depth), $f(x)$ represents the cost function, $c(x)$ are the nonlinear inequality constraints, $ceq(x)$ are the nonlinear equality constraints, A and b are linear inequality constraints, Aeq and beq are linear equality constraints, lb is the lower bound and ub is the upper bound.

The culture depth adjustment in the reactor is carried out from the removal of volume by means of a harvesting pump or the injection of freshwater with nutrients from a reservoir by means of a dilution pump. The amount of harvested and diluted volume is established by the dilution rate parameter (D), which determines the percentage of volume that can be withdrawn from the reactor and added, so that the biomass concentration at the end of the day is the same as at the beginning. In this way, the biomass concentration can be considered practically constant between days, calling this method continuous operation. The dilution rate depends on each season and month. During the summer, the period of maximum biomass productivity, this parameter can reach values of around 40%. However, in winter, due to low productivity, the dilution rate is around 15%. Due to the operating characteristics and the design of the reactor, it is not possible to execute the harvesting and dilution processes simultaneously. Due to the configuration in the pipe network, it can be counterproductive to activate harvest and dilution at

the same time. On the other hand, when these processes are simultaneous, the biomass concentration of the harvested volume decreases over the time in which the activity is carried out, due to the constant dilution of the reactor. This is a very important restriction with regard to the optimization problem, since the volume changes in the reactor are made by setting fixed values to harvest and dilution flow rates in each iteration of the optimizer, but not at the same time.

As a solution to the optimization problem, two approaches have been proposed. Initially, a one-step horizon has been established for the optimization, so that the objective function is based only in the current inputs values. Subsequently, weather forecast and future horizon optimization have been included with the aim of improving performance.

The technical characteristics of the computer where the simulation has been carried out are the following:

- Processor Intel Core i7-4700HQ CPU 2.40 GHz.

- 8 GB RAM memory.

4.2.1 One-step horizon approach

The proposed one-step horizon architecture consists of two layers, the representation of which is presented in Figure 4.25. The upper layer, where the optimizer presented by (4.1) calculates the optimal culture depth set-point according to the proposed cost function. And the bottom layer, a culture depth on/off control is carried out by means of the harvesting and dilution pumps.

With this approach, at each optimization instant, a simulation of the temperature of the culture is carried out towards the next instant, taking into account different culture depths. As a method of estimating the culture temperature, the model (3.17) has been used, so the inputs of the objective function are the net heat accumulated in the reactor (Q_{total}), the culture depth to optimize and the environmental conditions (solar radiation, ambient temperature, relative humidity and wind speed). Being a one-step optimization, the environmental variables remain constant for the next time instant.
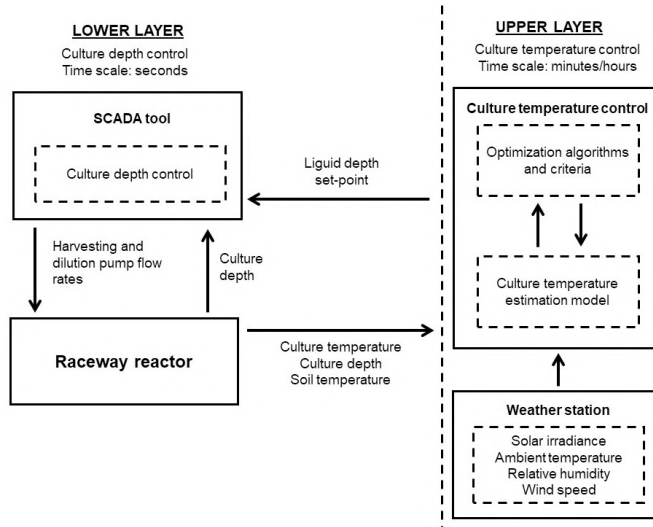
Figure 4.25: Control hierarchy for one-step optimization.

The optimization frequency is a user-chosen parameter, and represents the time that elapses between the calculation of one culture depth set-point and the next. This optimization frequency or optimization time (t_o) has been established in half an hour, taking into account the harvest and dilution flow rates and their ability to vary the volume of the reactor. Even so, it is a modifiable parameter, and can be lower or higher, adjusting to the specific situation of each scenario.

During the optimization process, the objective function estimates the reactor temperature for the entire time interval, that is, if the optimization time t_o is half an hour, the cost function estimates the temperature for a half an hour onwards. This estimation takes into account the evolution of both, the harvesting and dilution flows, as well as the progressive volume of liquid in the reactor. However, environmental conditions remain constant for this interval. Once the temperature is estimated for the entire interval t_o, the absolute error between the estimated temperature and the optimal temperature of the microalgae strain is calculated. As a result of the optimization, the culture depth set-point that minimizes the error in the culture temperature during the interval t_o is obtained.

From the culture depth set-point, the corresponding harvesting and dilution flows are calculated, taking into account the applied restrictions. The harvesting flows can be set as variables (e.g. for simulation purposes), so that the reference depth is reached before the next optimization instant, or on the contrary, they can be set as fixed flow rates, representing a more realistic scenario, which conditions the optimization process.

Using this approach, two configurations for the optimization have been designed:

One-step unconstrained optimization: to check the effect of the depth optimizer with respect to the normal operation of the reactor. Initially, the optimization function has been used without the restrictions described in this section. Computational time: 18 seconds to simulate a day.

One-step constrained optimization: to represent a more realistic scenario. The aforementioned restrictions have been incorporated, so that the comparison between normal operation and this new approach is as faithful as possible. Computational time: 61 seconds to simulate a day.

4.2.2 Future horizon approach

Starting from the initial one-step optimization approach, an upper layer has been added to the control hierarchy shown in Figure 4.25. This new layer represents weather forecast for the input variables in the optimization function. So, it is possible to improve the optimization problem and regulation of temperature in the reactor using a prediction horizon in the estimation of the culture temperature. This new hierarchy of control is represented in Figure 4.26 and presents a higher level of prediction with respect to optimization.

This new optimization approach is based on a receding horizon approach, where at each optimization instant a series of future depth set-points are calculated. Only the first step of the control strategy is implemented, then the plant state is sampled again and the calculations are repeated starting from the new current state, yielding a new control
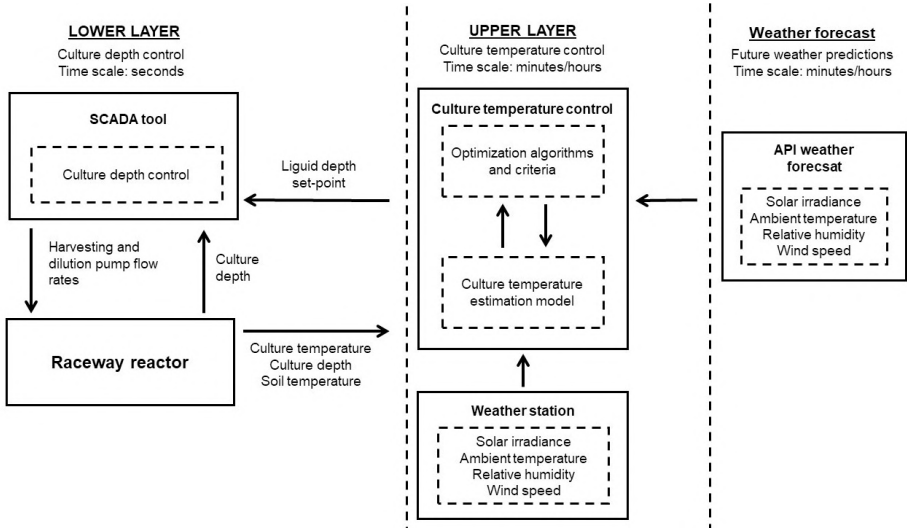
Figure 4.26: Control hierarchy for future optimization.

and new predicted state path, discarding future references calculated in the previous instant. The number of set-points corresponds to the value of the prediction horizon (N_p), being a vector which values are modified depending on the conditions present at each optimization instant.

The optimization time (t_o) is still a user-chosen parameter, but a new term is introduced, the prediction horizon N_p equivalent to the number of predictions or optimization intervals that will be carried out in advance. The value of N_p can be selected by the user and its interpretation depends on the optimization time. If the optimization time is 1 hour, the value of N_p will represent the number of hours of prediction into the future. For example, a value of N_p equal to 10 with an optimization time of 1 hour, the forecast horizon would be 10 hours. However, with an optimization time of half an hour, the forecast horizon would be 5 hours, with optimization actions every half hour. For the simulations, an optimization time (t_o) of half an hour and a prediction horizon (N_p) of 10 (5 hours) have been used. The vector of results obtained from the objective function at each optimization instant represents the liquid depth set-points for future instants, based on current environmental

conditions and weather forecast. The new cost function is presented as follows:

$$J = |\sum_{i=1}^{N} T_w(i) - T_{optimum}| \qquad (4.9)$$

The values of the results vector are not fixed, but can be modified at each optimization instant if the input conditions change, such as perturbations in the forecast. In this way, the performance of the optimization is improved to take into account, at present moment, possible future scenarios or disturbances that affect the temperature of the culture.

From this new approach, three types of configurations have been considered for optimization:

Constant weather receding horizon optimization: during the prediction horizon, constant values of the environmental variables, at the optimization time, are used. Computational time: 639 seconds to simulate two days.

Perfect forecast receding horizon optimization: during the prediction horizon, the real values of the measured environmental variables are used, which correspond to the vector positions of the future instants. This scenario is only possible to apply it in simulation. Computational time: 560 seconds to simulate two days.

Real forecast receding horizon optimization: at each optimization instant, a weather forecast API tool is used to determine weather future values of environmental condition variables.

4.3 Simulation results

Such as described above, with the proposed culture depth optimizer, it is possible to determine a set-point for the culture depth to modify the

volume in the reactor and regulate the temperature value for maximizing the growth rate of the microalgae, and subsequently, biomass productivity. Thus, in this study the aim is to compare the temperature and microalgae growth, by means of biomass productivity, using the culture depth optimizer contrasted with the normal operation of a reactor with a culture depth of 15 cm (harvesting at 9 a.m. and dilution at 11 a.m.). The simulation tests have been carried out from environmental data measured for the summer and winter periods, in order to establish the differences between two seasons where the temperature reaches its maximum and minimum values. Specifically, Figures 4.27 and 4.28 represent the data used for simulation tests, corresponding to a week in January and a week in August, respectively.
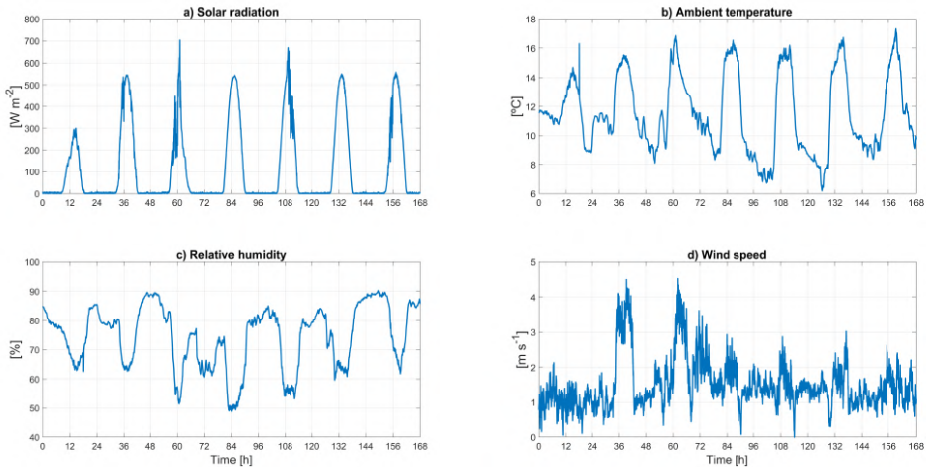
Figure 4.27: Weather variables during January.

For the different seasons, initial biomass concentration of 0.32 (g L^{-1}) during winter and 0.75 (g L^{-1}) for summer have been used, respectively. In addition, the dilution rate established for normal operation has been 17% for the winter period and 40% for the summer period. The dilution rate with the optimizer has been adapted to equal the biomass concentration at the end of the test period, so that a fair comparison can be made between both scenarios. In winter, due to the low temperature and low growth
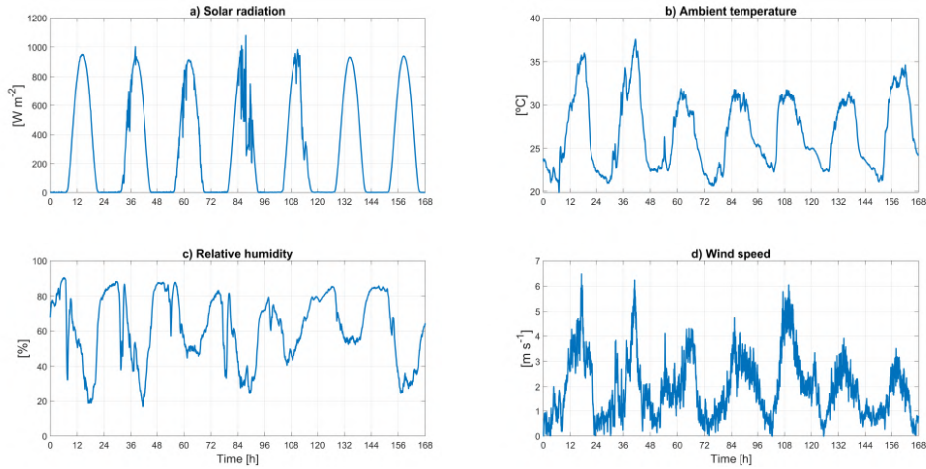
Figure 4.28: Weather variables during August.

rate of the microalgae, the biomass concentration is lower, as well as its dilution. On the other hand, summer is the period of greatest growth of the microalgae, with a higher concentration of biomass and the maximum annual dilution rate value.

The temperature of the dilution medium is a very important factor to take into account in optimization. This parameter is variable throughout the day, with a profile similar to the temperature of the culture inside the reactor. Due to the lack of measurement sensors in the physical reservoir, to estimate this dynamics, the culture temperature evolution model described in Section 3.1 has been used to simulate a 100 m^3 water reservoir. The objective is to represent a dilution medium temperature real scenario, instead of using a constant value throughout the simulation period. This method can also be used in simulation in the absence of experimental measurements.

As an indicator to differentiate the performance of the two scenarios (optimized operation and normal operation), the amount of biomass harvested in the entire time period evaluated for the two cases has been estimated. This calculation is made from the volume harvested in the reactor (each time the culture depth decreases) and the biomass

concentration at each harvest moment.

4.3.1   One-step unconstrained optimization

Two initial tests were carried out in which no dilution or harvest restrictions were taken into account for the optimized scenario. For these tests, culture depth regulation limits have been established between 5 and 30 cm, without restriction between depth set-points. Figures 4.29 and 4.30 show the results of the tests without constraints.

The normal operation of the reactor (represented in red) is carried out every day at morning, harvesting microalgae and, later, diluting the reactor. When harvesting occurs (at the same time every morning), culture is removed from the reactor until the dilution rate is achieved (when a certain culture depth is achieved). Then, fresh medium is added to replenish lost volume.
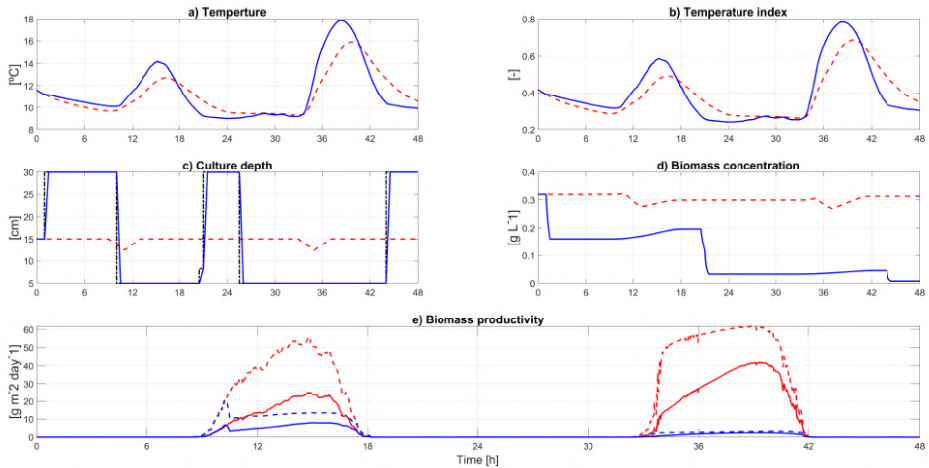
Figure 4.29: Biomass productivity comparison without constraints for two consecutive days of January. Red lines represent the results for normal reactor operation, while blue lines represent the results applying the culture depth optimizer. Dashed black lines on graph c represent the culture depth set-point from the optimizer. Dashed lines on biomass productivity (graph e) represent maximum theoretical biomass productivity.

Figure 4.29 represents the results obtained without restrictions for two consecutive days in January. The red curves represent the normal operation of a reactor with a culture depth of 15 cm. This is done to maintain the normal operating level of the reactor over time and to maintain a constant biomass concentration throughout the days. On the other hand, the blue curves represent the results obtained by regulating the culture depth in the reactor by using the proposed optimized approach, with an initial and final depth of 15 cm. Figure 4.29.a represents the culture temperature for both scenarios. Using the optimizer, the maximum temperature during the day increases on average 1.7°C, getting closer to the optimum temperature. Figure 4.29.b shows the temperature index, obtained by using 1.5. In this case, the optimized temperature index increases 15.33% with respect to the normal operation, during the daytime period. Figure 4.29.c represents the culture depth in the reactor for both cases. The black dashed line represents the depth set-point established by the optimizer. It is interesting to note how the depth decreases during the day to increase the temperature. However, during the night period, the depth increases to prevent the culture temperature from falling excessively due to the low ambient temperature. Figure 4.29.d represents the concentration of biomass. It can be seen that it drops drastically due to the lack of restriction in dilution. This fact highlights the need to constraint the dilution rate in the optimization problem. Finally, Figure 4.29.e shows the biomass productivity (obtained from 1.8) in solid lines, in addition to the maximum theoretical productivity represented in dashed lines (when the temperature index is 1). Due to the lack of dilution restrictions, the decrease in biomass concentration causes a decrease in productivity. As a result, it is established that the use of the optimizer without constraints is not feasible.

The test without constraints for the summer period (in August) is shown in Figure 4.30. As for January, two consecutive days have been analyzed. In this case, the temperature of the culture is higher than the optimal temperature for the microalgae strain. So, the optimizer must manage to reduce the temperature in the reactor. Figure 4.30.a shows the culture temperature for both scenarios, where the optimizer approach

reduces the average maximum temperature by 2.2°C compared to normal operation. The temperature index, represented by Figure 4.30.b, improves on average 50.3% during the daytime period. The profile of the culture depth (Figure 4.30.c) shows a behavior contrary to the January test. During daytime, the culture depth is increased to inject fresh medium into the reactor (which is at a lower temperature) and prevent the reactor from reaching a higher temperature than normal operation. During the night-time period, the depth decreases to cool the reactor more quickly and, when it decreases from the optimal temperature, fresh medium is injected (which in this case is at higher temperatures) to slightly raise the temperature in the reactor and avoid a drastic drop. Figure 4.30.d represents the biomass concentration, which, as in the previous test, decreases drastically to 0. Biomass productivity (Figure 4.30.e) also decreases to 0 compared to normal operation, due to over-dilution in the reactor.
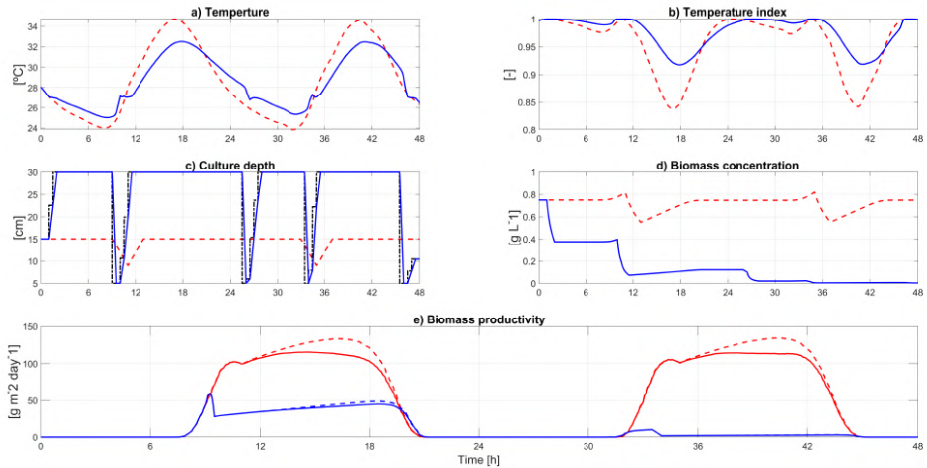
Figure 4.30: Biomass productivity comparison without constraints in one day of August. Red lines represent the results for normal reactor operation, while blue lines represent the results applying the culture depth optimizer. Dashed black lines on graph c represent the culture depth set-point from the optimizer. Dashed lines on biomass productivity (graph e) represent maximum theoretical biomass productivity.

4.3.2 One-step constrained optimization

Due to the undesired results related to the biomass concentration obtained by applying the optimizer without constraints (Figures 4.29 and 4.30), it is evident that the physical application is not feasible. Therefore, some constraints have been defined in order to represent a more realistic behavior and simulate a practical application of the optimizer for the reactor described in Section 2.2.1. Figures 4.31 and 4.32 represent the results obtained for a week in January and another week in August, using the culture depth optimizer with the constraints previously defined. The main constraint applied is the dilution rate of the medium in the reactor, which allows the biomass concentration to remain almost equal from one day to another. The dilution rate constraint is achieved by regulating the minimum and maximum limits of culture depth established for the optimizer. The optimization time t_o was set to half an hour (period in which optimization runs). Notice that this is a significant difference when compared to previous approaches found in the literature, as in [23, 24].

Figure 4.31 represents the results obtained using the optimizer with the one-step approach during a week in January. Because the dilution restrictions are very restrictive, there is not much difference in the culture temperature between both scenarios (Figure 4.31.a). In that sense, the temperature increase has been 0.63°C. The increase in the temperature index (Figure 4.31.b) was 5.6%. The variation in depth, represented in Figure 4.31.c, is very representative. At the beginning of the day, the culture depth drops to the allowed limit, throughout the daytime period, to increase the temperature. At the beginning of the night-time period, the depth returns to its initial value to avoid a further drop in temperature. Regarding the biomass concentration represented in Figure 4.31.d, contrary dynamics can be observed between both scenarios, where the concentration of the optimized approach increases during daytime (due to harvesting) and decreases at the end of the night-time period (due to dilution). Regarding biomass productivity (Figure 4.31.e), a similar result is observed, with an increase of 6.8%. Analyzing the estimated harvested biomass, making use of the optimizer, there is an increase of 5.1% with respect to the harvested biomass during
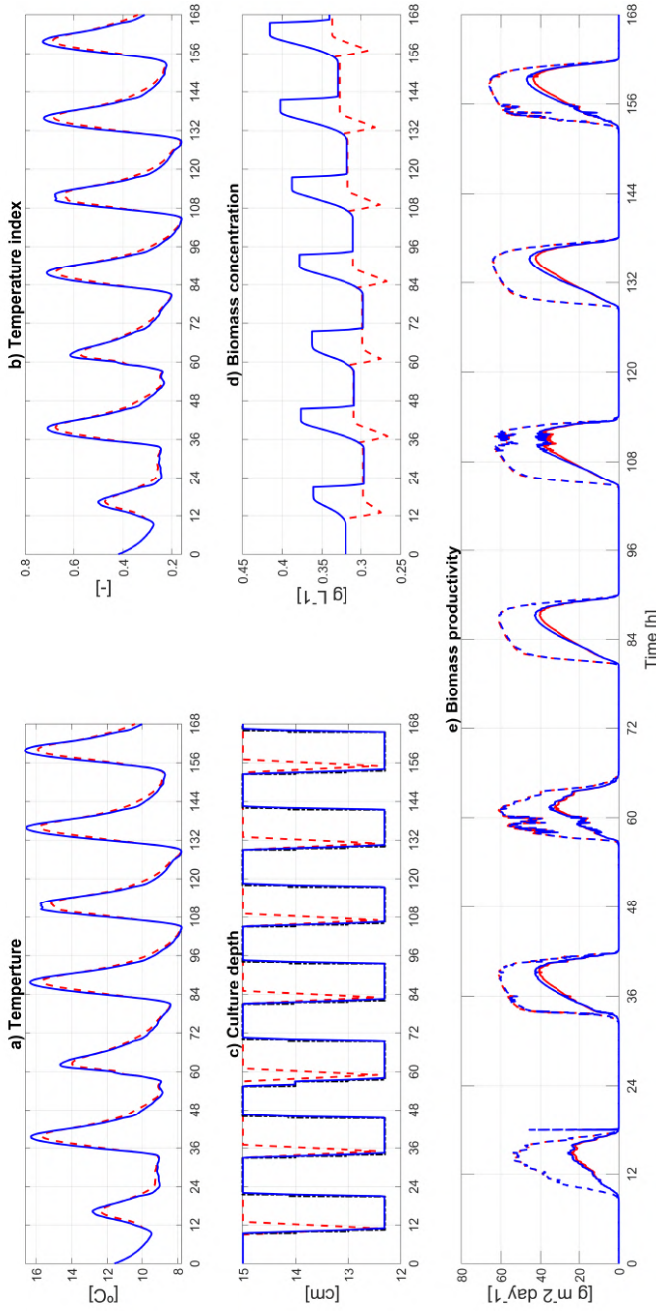
Figure 4.31: One-step constrained optimization comparison results for a week on January. Red lines represent the results for normal reactor operation, while blue lines represent the results applying the culture depth optimizer. Dashed black lines on graph c represent the culture depth set-point from the optimizer. Dashed lines on biomass productivity (graph e) represent maximum theoretical biomass productivity.

the normal operation of the reactor for the evaluated period.

Figure 4.32 represents the results obtained using the optimizer with the one-step approach during a week in August. As Figure 4.32.a shows, the difference in the culture temperature is small, only 0.5°C. Even so, this slight difference has allowed the dilution rate parameter to be increased in the optimized scenario. The improvement in the temperature index (Figure 4.32.b) was 12%. As can be seen in Figure 4.32.c, the evolution in the culture depth, at the beginning of the day, is similar to the normal operation. However, because the dilution is greater, the depth during the dilution period increases more, in addition to allowing a greater harvesting capacity. In this case, the dilution rate for the optimized scenario has been 43% of the total volume in the reactor, instead of 40% for normal operation during this period. Although the dilution rate with the optimizer is higher, the biomass concentration (Figure 4.32.d) at the end of the test has been the same as for normal operation, which denotes the improvement in biomass productivity (Figure 4.32.e), which increases 11% on average. Due to this improvement, the estimate of the harvested biomass is 6.8% more than the biomass harvested with normal operations.

4.3.3 Constant future weather horizon optimization

Based on the results obtained with the one-step optimization approach, a receding horizon approach using future predictions has been designed. The aim of this approach focuses on improving the optimization when environmental conditions change or are not favorable, being able to anticipate disturbances. As an initial configuration, an optimizer implemented within a receding horizon approach has been designed where the environmental variables remain constant at the current value throughout the prediction horizon. Figures 4.33 and 4.34 represent the results obtained using the receding horizon optimizer with constant environmental variables.

Figure 4.33 shows the January results obtained for this case. The results have been practically identical to those obtained for January using the one-step approach (Figure 4.31). This is due to the fact that the dilution rate in winter is so small that it is hardly possible to vary the
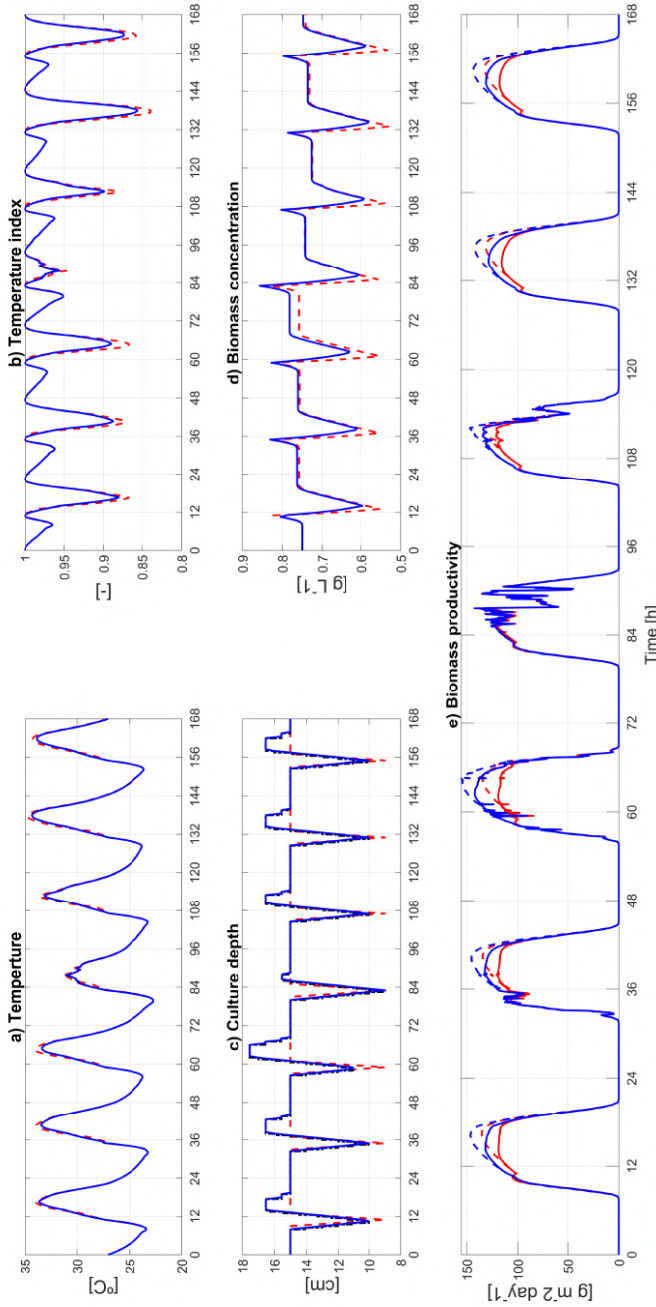
Figure 4.32: One-step constrained optimization comparison results for a week on August. Red lines represent the results for normal reactor operation, while blue lines represent the results applying the culture depth optimizer. Dashed black lines on graph c represent the culture depth set-point from the optimizer. Dashed lines on biomass productivity (graph e) represent maximum theoretical biomass productivity.
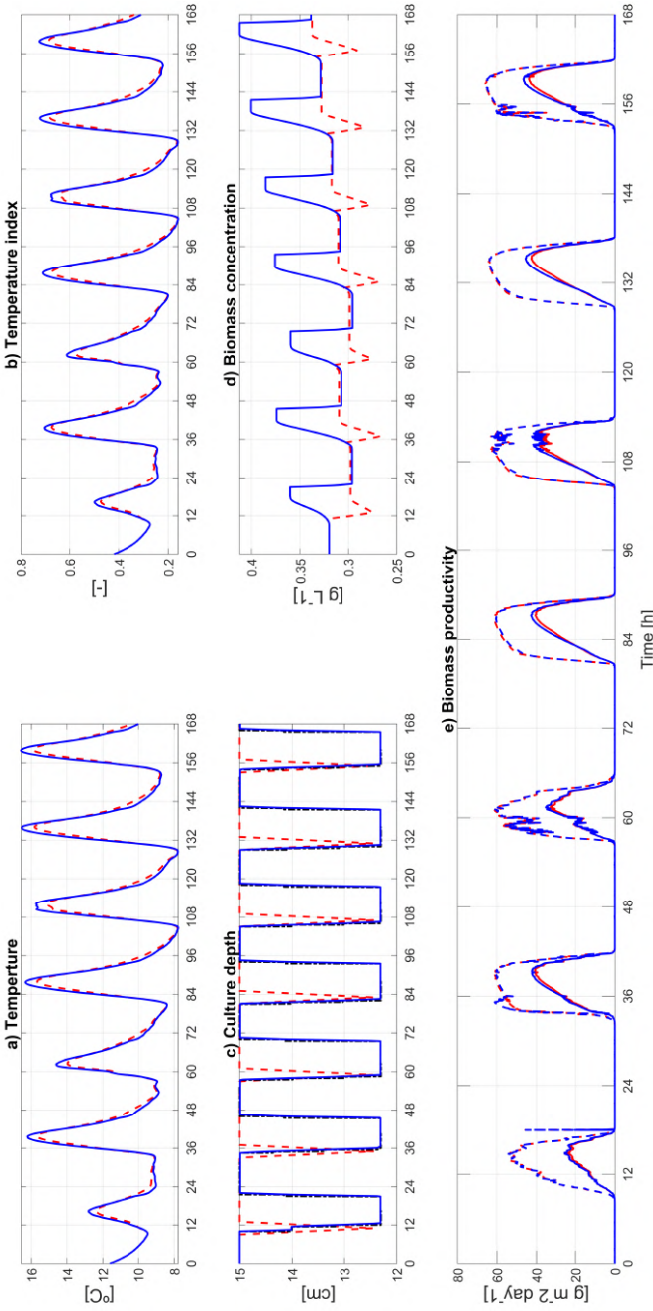
Figure 4.33: Receding horizon optimization comparison results with constant environmental variables for January. Red lines represent the results for normal reactor operation, while blue lines represent the results applying the culture depth optimizer. Dashed black lines on graph c represent the culture depth set-point from the optimizer. Dashed lines on biomass productivity (graph e) represent maximum theoretical biomass productivity.

culture depth, so a better result cannot be obtained.

However, the results obtained during the summer have been noticeably different. Figure 4.34 shows the results obtained for August using the optimizer with future predictions, keeping the environmental variables constant during the prediction horizon. The decrease in maximum culture temperature (Figure 4.34.a) during daytime period has been on average 1.3°C less than normal operation. The improvement in the temperature index, represented in Figure 4.34.b, has been 31.6% compared to normal operation. As for the culture depth, represented in Figure 4.34.c, at the beginning of the daytime it increases so that the temperature decreases during the daytime period. At the end of the day, the depth decreases to harvest biomass and return to the initial culture depth point. As in Figure 4.32, due to the improvement in temperature, the biomass productivity is higher, which allows increasing the dilution rate. In this case, the dilution rate was 55% the total volume of the reactor compared to 40% for normal operation, which considerably increases the amount of harvested biomass. The biomass concentration, represented in Figure 4.34.d, for both scenarios has a similar evolution. At the end of the evaluated period, the value is the same for both cases, despite the fact that with the optimizer, the dilution rate is higher. The improvement in biomass productivity has been 43.4%, so the microalgae growth speed is higher and it is possible to increase the dilution rate. During harvesting, an increase on biomass amount of 26.42% compared to normal operation has been estimated for the time period evaluated.

4.3.4   Perfect forecast receding horizon optimization

After verifying the operation of the optimizer with receding horizon approach considering constant environmental variables, a different configuration has been designed where the real values of the environmental variables are taken into account along the horizon during the optimization process. Being a simulation approach, in each optimization period, the experimental measured values of the environment variables are taken for the computation of the cost function. In this way, it is possible to have a perfect forecast of the weather
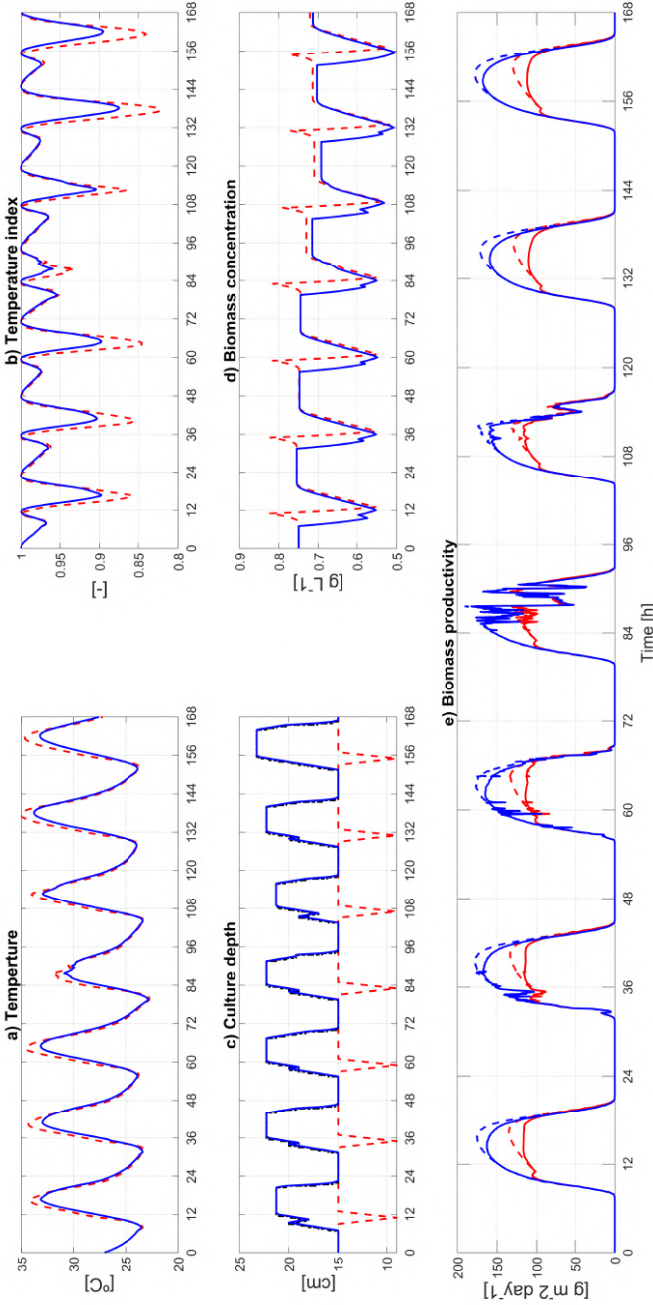
Figure 4.34: Receding horizon optimization comparison results with constant environmental variables for August. Red lines represent the results for normal reactor operation, while blue lines represent the results applying the culture depth optimizer. Dashed black lines on graph c represent the culture depth setpoint from the optimizer. Dashed lines on biomass productivity (graph e) represent maximum theoretical biomass productivity.

conditions during optimization.

Figure 4.35 represents the results obtained for January using the optimizer with perfect forecast. Like the results obtained in the previous cases for January (Figures 4.31 and 4.33), in this case, the values obtained have been practically identical. This fact is indicative that the improvement using the optimizer during the winter is very limited.

Figure 4.36 represents the results obtained for August using the optimizer with perfect forecast. The values obtained in this case have been very similar to those obtained in the previous case (Figure 4.34). Observing Figure 4.36.a, the decrease in the maximum culture temperature has been on average 1.3°C less than the normal operation case. The improvement in the temperature index (Figure 4.36.b) was 31.8%, very similar to the previous case. For the culture depth, represented in Figure 4.36.c, there is a certain difference with respect to the previous case. For the fourth and fifth days, where the solar radiation is irregular, the variation of the depth has better behavior than applying the optimizer with constant environmental conditions. The biomass concentration, represented in Figure 4.36.d, has also been similar. The improvement in biomass productivity (Figure 4.36.e) has been 45% compared to normal operation, slightly higher than the previous case. Due to this increase, the estimation for biomass harvesting has been 26.4% more than normal operations.

Discussion

Comparing the results, the considerable improvement in biomass productivity through the use of the optimizer can be observed when compared to the normal day-to-day operation in a raceway reactor. During the winter period, where temperatures are low, there is not much improvement in the use of the optimizer with its different settings. Even so, an increase of approximately 6.8% in biomass productivity and 5% in biomass obtained during harvesting has been estimated. However, as the dilution rate is small, the amount of biomass obtained with the improvement is not very significant.

On the other hand, during the summer period, when the reactor
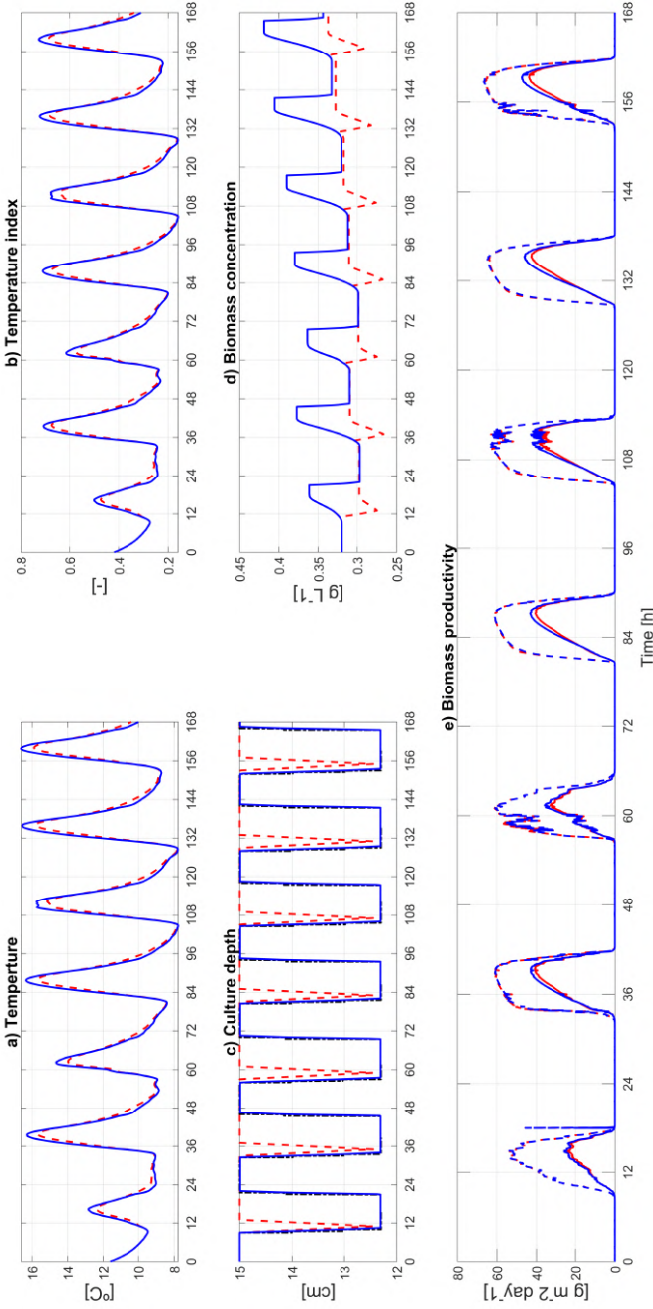
Figure 4.35: Perfect forecast receding horizon optimization comparison results for January. Red lines represent the results for normal reactor operation, while blue lines represent the results applying the culture depth optimizer. Dashed black lines on graph c represent the culture depth set-point from the optimizer. Dashed lines on biomass productivity (graph e) represent maximum theoretical biomass productivity.
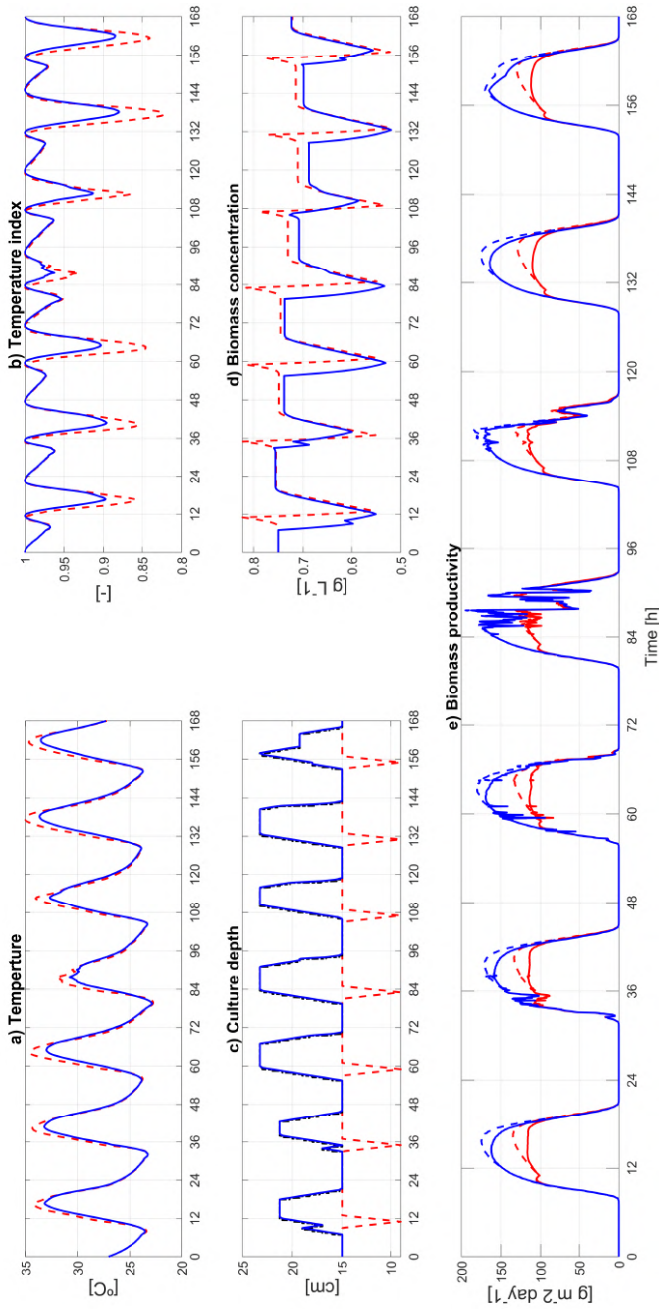
Figure 4.36: Perfect forecast receding horizon optimization comparison results for August. Red lines represent the results for normal reactor operation, while blue lines represent the results applying the culture depth optimizer. Dashed black lines on graph c represent the culture depth set-point from the optimizer. Dashed lines on biomass productivity (graph e) represent maximum theoretical biomass productivity.

performance is optimal, a significant difference can be seen between the different proposed approaches. Using the one-step optimizer, the increase in biomass productivity was 11%, obtaining 6.8% more harvested biomass. Although the percentage is similar to that obtained for winter, the dilution rate in summer is much higher, so the amount of harvested biomass considerably increases. Furthermore, by using the optimizer with predictions (both with fixed environmental variables and perfect forecast), this improvement has increased even more. Biomass productivity has risen 43.4% compared to normal operation, which translates into a 26.42% increase in harvested biomass, much above the one-step configuration.

Simulation tests have demonstrated the importance of controlling certain variables in the operation of reactors, such as the dilution rate and its duration. By applying the liquid depth optimizer, it has been possible to regulate the temperature of the culture inside the reactor. Due to this, a significant improvement has been achieved on biomass productivity and the amount of harvested biomass, compared to the classic operation that is carried out every day in raceway reactors. Both the one-step optimization approaches and the receding horizon solutions have shown that productivity can be increased. Furthermore, this improvement is achieved through an adequate management of the harvesting and dilution processes, something intrinsic in the operation of raceway reactors. So, this solution does not imply any additional costs of material or the installation of external devices, such as heat exchangers.

4.4 Experimental results

This section describes the experimental tests about temperature control carried out in the reactor described in Section 2.2.1, located at the IFAPA research center (Almería, Spain). As previously described, the implementation of the culture depth optimizer has been performed in the SCADA tool that controls the reactors. The liquid depth control is carried out through an On/Off architecture with hysteresis using the harvesting and dilution pumps. Since the research center has two

raceway reactors that operate in parallel, a comparison has been possible by applying the depth optimizer to one of them, while the other operates normally. Figures 4.37 and 4.38 represent the real results obtained applying the optimizer, in comparison with the normal operation of the other raceway reactor. The tests were carried out in September, with a dilution rate of 20% for the reactor operated normally, while for the scenario with the optimizer a dilution rate of 13% was used, equivalent to 2 cm of difference from the initial base depth of 15 cm (due to a preliminary implementation of the optimizer). For these tests, it has only been possible to evaluate the culture temperature, the culture depth and the temperature index. Currently, all the biomass that is harvested in the reactors of the IFAPA research center is collected in the same tank, so it has been impossible to quantify the biomass harvested individually.

4.4.1   One-step constrained optimization
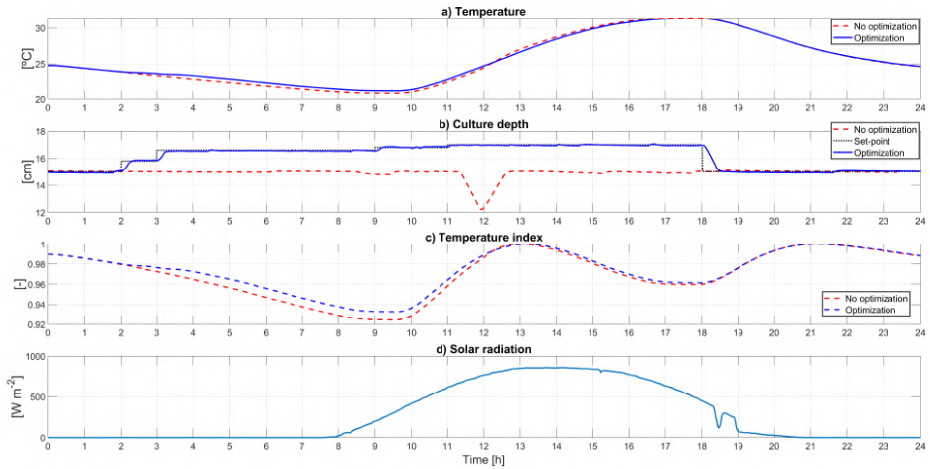
Figure 4.37: Optimization experimental results with one-step structure. The red dashed lines represent the results with normal operation, while blue lines represent the results applying the optimization.

Figure 4.37 shows the results of an experimental test applying the optimizer with the one-step architecture. Figure 4.37.a represents the

culture temperature for the two scenarios. Although the difference between the optimizer and the normal case is not very significant, it can be seen that there is a period in which it increases more rapidly until reaching the optimum temperature. Subsequently, the maximum temperature reached is slightly lower than for normal operation. This result is indicative of the correct functioning of the optimizer. Figure 4.37.b represents the culture depths in both cases. Using the optimizer, the depth increases at the beginning of the day to slightly heat the reactor and make the maximum temperature lower (due to a higher volume). Near the end of the afternoon, the culture depth drops to its initial value to harvest the established ratio. As mentioned, even though the temperature difference is small, it is possible to observe the improvement in the temperature index, represented in Figure 4.37.c, with an increase of 11.2% with respect to normal operation.

4.4.2   Real forecast future horizon optimization
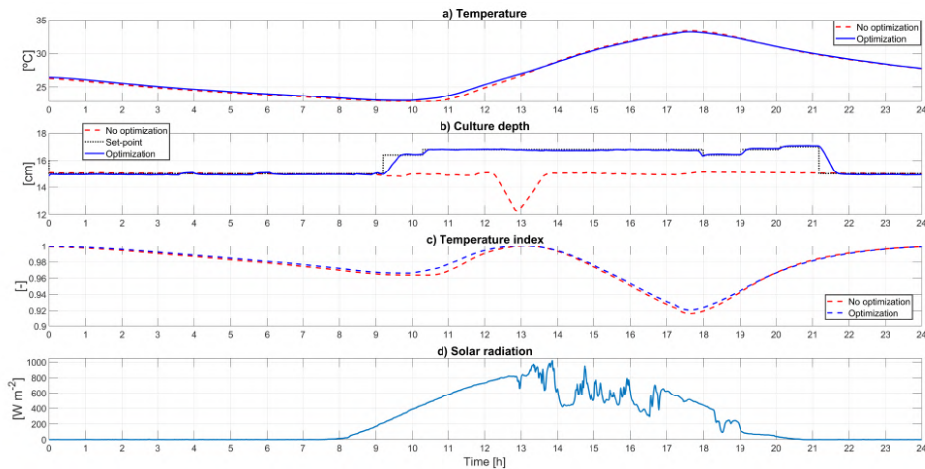
Figure 4.38: Optimization experimental results with predictions. The red dashed lines represent the results with normal operation, while blue lines represent the results applying the optimization.

Differently form the previous case, Figure 4.38 presents the

experimental results applying the optimizer with future predictions. The implementation of environmental predictions in the optimizer has been done from a weather forecast API (Application Programming Interfaces) called *weatherbit* [94]. This API is capable of predicting the weather 48 hours onwards, with a resolution time of one hour. At each execution of the optimizer, a call is made to the weather API and the obtained values are passed as inputs to the optimizer. In this case, the prediction that is made is not perfect, but it is a good approximation. Figure 4.38.a represents the temperature of the culture, which results to be very similar to that obtained in the previous case (Figure 4.37). On the other hand, there is a difference in the culture depth, represented in Figure 4.38.b. The depth increases later than in the previous case, which coincides with the rise in solar radiation. Furthermore, the harvest is carried out later, when the temperature drops below the optimum temperature. The temperature index (Figure 4.38.c) increases of 13% with respect the reactor at normal operation, slightly higher than in the previous case.

Discussion

Although the improvement in the experimental results has been small, the contribution of the optimizer has been evident. Due to the characteristics of the implementation, the dilution rate for the optimizer has been much lower than during the simulation tests, which greatly limits the performance. Even so, a slight improvement in culture temperature is noted, being a very interesting fact for future configurations for the optimizer and its implementation. Also, it is clear that the dilution rate is a very important factor, as well as the inlet temperature of the dilution medium.

4.5   Conclusions and contributions

In this chapter, an analysis of the influence of temperature and culture depth in raceway reactors on biomass productivity has been presented. This analysis is complemented with different feasibility studies carried out on different strains of microalgae, each with different temperature

characteristics. Furthermore, a simple method for temperature regulation is presented by varying the volume in a raceway reactor through optimization of the liquid depth.

Culture temperature is one of the parameters that mostly affects the growth of microalgae, being also a difficult variable to control at an industrial level. The tests carried out on a laboratory scale include heating and cooling systems that allow the temperature of the culture to be modified, so that they always maintain an optimal value. However, when the work is extrapolated to industrial scale reactors (such as raceway reactors) the difficulty of controlling the temperature of the culture becomes evident. Due to the high cost of temperature control facilities for large volumes of liquid, this type of control is not carried out in open microalgae reactors, which is why culture temperature presents a very important disturbance on biomass productivity. Therefore, temperature regulation through the optimal use of the harvesting and dilution processes is an interesting an innovative approach.

The results obtained with the application of the optimizer with constraints have been satisfactory, with a considerable increase on biomass productivity during summer with respect to the normal operation of the raceway reactor performed everyday. The culture depth optimizer opens the door to new ways of controlling temperature and improving biomass productivity. Due to its characteristics and restrictions, the regulation is carried out by means of the dilution and harvesting processes in the reactor, and it does not require any expensive devices with respect to the normal operation of the reactor, such as heat exchangers for cooling and heating.

Moreover, the dilution rate is a parameter which value depends on experimental studies carried out for every month. However, with a proper cost function, it could be a variable parameter that depends on the microalgae and environmental conditions, in such a way that it can be combined with the culture depth optimizer to also control the biomass concentration. Therefore, the culture depth optimizer application serves as a design tool for temperature control architectures without the need for additional equipment.

Daytime/Night-time pH control

In this chapter, the advantages of using event-based pH control approaches for raceway reactors and new ideas for daytime/night-time control schemes are proposed and demonstrated, both in simulation and experimentally.

The structure of this chapter is as follows: Section 5.1 details the pH control problem. The daytime and night-time models are presented in Section 5.2. The classical and event-based control approaches are described in Sections 5.3 and 5.4. Simulation results are presented in Section 5.5, while the experimental results are shown in Section 5.6. Finally, the conclusion are drawn in Section 5.7.

5.1 pH control problem

Microalgae growth depends on several variables, the main ones being solar radiation, medium temperature, pH and dissolved oxygen [20]. The incidence of solar radiation and temperature conditions are determined by the orientation and location of the reactor or by indirect control such as shown for the temperature in the previous chapter. So, usually, they are not controllable variables and act as disturbances [61]. Indeed, pH and dissolved oxygen are the controlled variables in the process, being the pH the most critical due to its influence on the photosynthesis process. Thus, the pH of the culture will be the variable considered for control purposes in this chapter.

The photosynthesis process performed by the microalgae changes the acidity of the culture medium, increasing the pH, while CO_2 injections reduce its value due to the formation of carbonic acid. An adequate pH

control is required in this type of processes, since the pH has an optimum range that maximizes biomass production, as well as influencing the health of microalgae, being lethal when it exceeds certain limits. On the other hand, CO_2 injections should not be arbitrary. If the culture conditions are inadequate for the microalgae, the CO_2 is stripped to the air instead of being consumed or stored in the water as bicarbonate buffer. Moreover, it can be harmful to the microalgae culture and generating unnecessary waste.

Manipulated variable

· Valve opening percentage [%]

INPUTS   PROCESS   OUTPUTS

Disturbances

· CO_2 flow rate [L min^{-1}]   · Solar irradiance [W m^{-2}]   · pH value [-]
                                             · Nutrient's pH value [-]
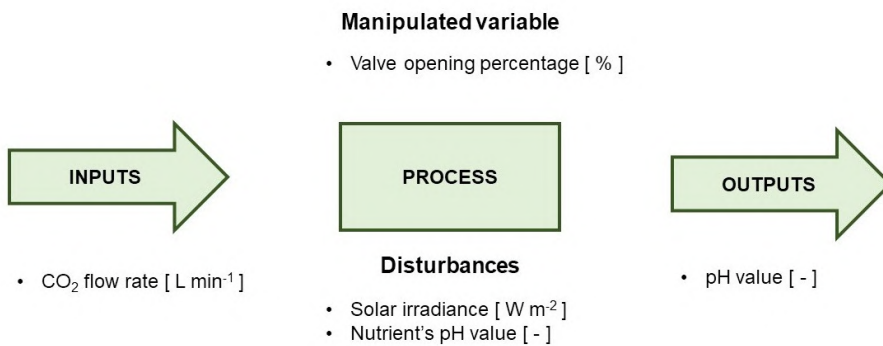
Figure 5.1: Process main variables.

Furthermore, the pH of the nutrients present in the dilution medium causes disturbances in the reactor, decreasing the pH of the culture in a heterogeneous way until an equilibrium is established. Therefore, it is essential to design a correct control architecture that allows optimal pH control by reducing CO_2 injections and losses. Moreover, better use of CO_2 leads to increase biomass production and reduces stress on microalgae. Summarizing, the main variables are presented in Figure 5.1 as follows: the process output is the culture pH, the aperture of CO_2 valve is the manipulated variable, and the solar radiation and the pH of nutrients act as the main disturbances.

Figure 5.2 shows the process scheme of the control problem. The CO_2 injections are made by means of a valve controlled from the SCADA system tool described in Section 2.2.4, where different types of control algorithms are implemented. Figure 5.3 schematically shows the measurement points
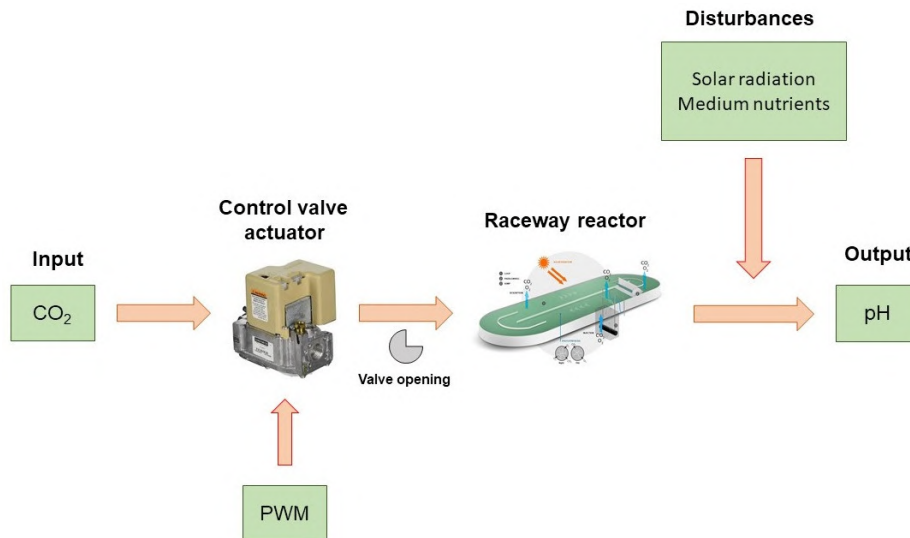
Figure 5.2: pH control problem scheme.

housed in the reactor. Each point has a pair of pH and dissolved oxygen sensors (described in Table 2.1). The pH sensor located at the end of the reactor (the measure point 1 of Figure 5.3) is taken as the output of the system. This point is considered the most unfavorable from the control point of view and is the one used for this study. Due to its position, relative to the injection point, a time delay appears in the transfer function relating CO_2 injection to pH.

Figure 5.3: Raceway reactor measure points.

Traditionally, raceway reactors are operated only during the daytime period by performing a pH control using an On/Off control architecture applied to the CO_2 injection valve. Due to this On/Off daytime control,

the pH evolves freely overnight, producing variations in pH between day and night, which can considerably affect the health of microalgae.

In addition, due to this difference between night and day, the On/Off control performs a larger injection at the beginning of the day to reduce the error, consuming large amounts of CO_2. Other control schemes can solve the effect, but the variation of pH during the night-time period still continues. The night-time pH control would avoid this problem and reduce the injection of CO_2 that occurs during daytime, especially with the On/Off control, since the pH would remain close to the set-point during the whole night. Moreover, event-based control approaches allow the establishment of a relationship between performance and control effort to maintain the pH at optimal values without performing a large number of injections, therefore reducing CO_2 consumption. All these ideas will be explored in the next sections.

5.2   pH modeling

For the design of the control architecture, two models, named as $G(s)_{daytime}$ and $G(s)_{nighttime}$, have been identified from the raceway reactor described in Section 2.2.1. They represent the pH dynamic evolution during the daytime and the night-time periods, respectively, with respect to CO_2 injections. These models are described as FOPDT transfer functions [3], where the delay or dead time represents the time it takes for a cell to reach the final part of the reactor, considered as the measurement point 1 in Figure 5.3 (that is, the time it takes to see the effect of a CO_2 injection on the output pH). It was decided to identify two models due to the differences observed in the dynamics between daytime and night-time periods. So, open-loop experiments were performed for a pH range from 7.4 to 8.2, taking into account an operating point of pH equal to 8. The resulting transfer functions (which are models expressed in the Laplace domain by the complex variable s) relating the pH to the CO_2 are the following:

$$G(s)_{daytime} = \frac{-0.0911}{7380\,s + 1}\,e^{-180\,s} \tag{5.1}$$

$$G(s)_{nighttime} = \frac{-0.1293}{10378\,s + 1}\,e^{-180\,s} \tag{5.2}$$

Figures 5.4 and 5.5 represent the validation of the daytime and night-time models contrasted with experimental measured data.
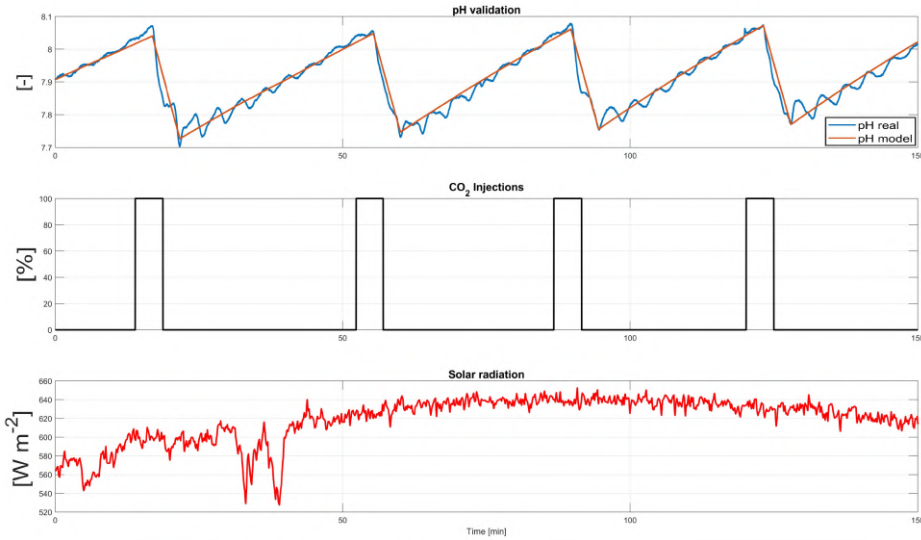
Figure 5.4: Model validation during daytime period. Upper graph represents the evolution of the real pH (blue) and the estimated one (red). Middle graph represents the valve opening, input for the model. Bottom graph represents the environmental global solar radiation disturbance.

The input variable for both models represents the opening of the CO_2 valve, being in a range from 0% to 100%, while the solar radiation acts as a disturbance during the daytime (Figure 5.4), causing the pH to rise. In theory, for obtaining a linear model (transfer function) relating CO_2 injection to pH, constant conditions of disturbances are required. Nevertheless, this is difficult to achieve in this kind of systems and tests have been done in (almost) clear day conditions and around midday, so that variations in solar irradiance and temperature are small and smooth, and thus they are considered constants during the test. The same applies

to biomass concentration, that changes in a slower time scale.

Notice that the models represent the dominant dynamics of the system. There is an oscillatory behaviour which period corresponds to the residence time of the system. However, it is not modelled here to be used for control design purposes as it would increase the control effort without a noticeable improvement in performance. An example of control application taking into account both dynamics (FOPDT plus second order oscillatory behaviour) can be found in [14].
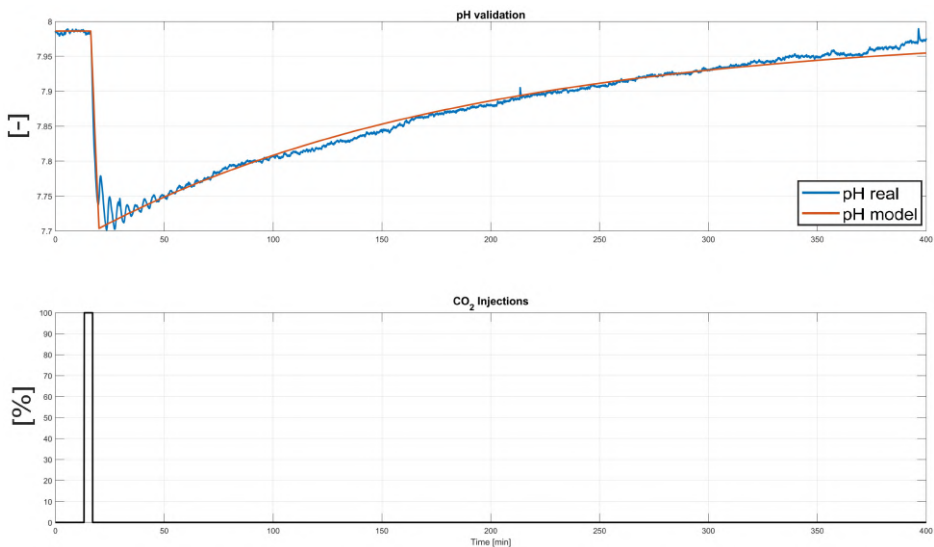
Figure 5.5: Model validation during night-time period. Upper graph represents the evolution of the real pH (blue) and the estimated one (red). Bottom graph represents the valve opening, input for the model.

During the night-time period (Figure 5.5), solar radiation is zero and the process dynamics is much slower, with a rise in pH caused by an imbalance in the concentrations of the different compounds in the medium. A phenomenon called bicarbonate buffer appears, allowing the stabilization of the culture pH inside the reactor, causing a pH drop when CO_2 is supplied and a pH increment when no CO_2 is externally provided, and that already present in the medium is consumed by the cells. This is due

to the equilibrium carbonate-bicarbonate of the different inorganic carbon forms present in water (CO_2, HCO_3 and CO_3). Due to these dynamics, the pH control during the night-time period is less critical (require less actions) than during the daytime period, but it is in any case necessary because the rise in pH can be very high (sometimes over values of 9.5).

5.3 Classical control approaches

Classical control architectures for pH control are frequently applied in the operation of raceway reactors. By default, the most common and widespread control architecture is the On/Off control. On the other hand, multiple examples of pH control approaches based on PI controllers can be found in the literature.

5.3.1 On/Off operation

The On/Off control approaches are widely used for pH control in raceway reactors as in other industrial processes, due to its simplicity. Its behaviour is a relay with hysteresis and represents the most simple feedback controller that can be used to control a process. This type of control is suitable for processes that have two states (open and close) because the controller switches the control variable between two states (On or Off), depending on the set-point error with respect to the controlled variable. However, this type of control is characterized by low accuracy and pH oscillations due to the changes in the control signal, causing a negative influence on microalgae. The On/Off control valve is opened and carbon dioxide is injected until the pH measure decreases below the set-point. Then, the control valve is closed until the pH reaches a value above the set-point, and so on. The control structure is presented in Figure 5.6 and the pH control is carried out exclusively during the daytime period, leaving it free during the night-time period.
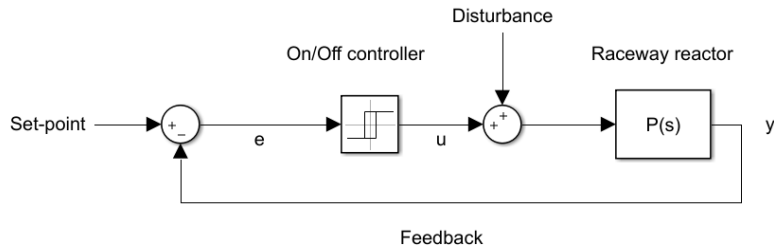
Figure 5.6: Control scheme of the On/Off control architecture. e represents the process error, u represents the control signal (valve opening) and y represents the process output (pH).

5.3.2   PI-based operation

Many examples of pH control in raceway reactors by means of PI controllers can be found in the literature with satisfactory results [37, 61, 62]. Notice that the pH presents different dynamics at the diurnal and nocturnal periods as observed in models (5.1) and (5.2). Thus, two controllers have been designed for each model depending on the period of the day, named as $C(s)_{daytime}$ and $C(s)_{nighttime}$. The control structure is presented in Figure 5.7, where the PI controller changes depending on the daytime and night-time periods.
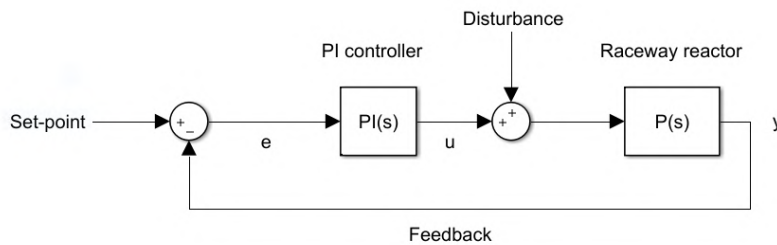
Figure 5.7: Control scheme of the PI-based control architecture. e represents the process error, u represents the control signal (valve opening) and y represents the process output (pH).

It is worth noting that the normalized dead time of the system, that is, the ratio between the dead time and the time constant, in both cases, is very small, i.e., the process is lag dominant. For this reason, among the wide variety of PID tuning rules [57], a Simple-Internal-Model-Control (SIMC) tuning rule [33] has been selected, which states that the PI parameters have to be selected as:

$$K_p = \frac{1}{k} \frac{T}{\lambda + \theta},$$

$$T_i = min\{T, 4(\lambda + \theta)\},$$

where θ is the dead time of the process, T is its time constant and λ is the desired closed-loop time constant.

This tuning rule states that a closed-loop time constant greater than or equal to the system delay should be used for robustness purposes. In this case, closed-loop time constants of 369 and 180 seconds were set for the daytime and the night-time periods, respectively according to (5.1) and (5.2). For the daytime, the value is calculated according to 0.05 times the open-loop time constant, to ensure a quick response while avoiding aggressive control actions. On the other hand, for the night-time period a 180 seconds closed-loop time constant value has been used, corresponding to the time delay. In both cases, simulations were performed to select those control parameters providing adequate results. Therefore, the following transfer functions for the PI controllers were obtained:

$$C(s)_{daytime} = -149 \cdot \left(1 + \frac{1}{2192\,s} \right) \qquad (5.3)$$

$$C(s)_{nighttime} = -224 \cdot \left(1 + \frac{1}{1440\,s} \right) \qquad (5.4)$$

Because the CO_2 valve is discontinuous, Pulse Width Modulation (PWM) transformation has been performed to control the opening range from 0% to 100%, corresponding with a flow rate from 0 to 15 (L min^{-1}).

Obviously, when tuning a PI controller, it is important to ensure the asymptotic stability of the system [32, 88, 90]. For this reason, the analysis

provided in [16] to determine the parameter stability region for which there
are no limit cycles for the two systems (5.1) and (5.2) have been performed.
Results are shown in Figures 5.8 and 5.9 and they confirm that, for both
controllers, the parameters have been selected so that the avoidance of
limit cycles and instability is ensured. Moreover, the tuning is also robust
as the parameters are far from the border of the region.
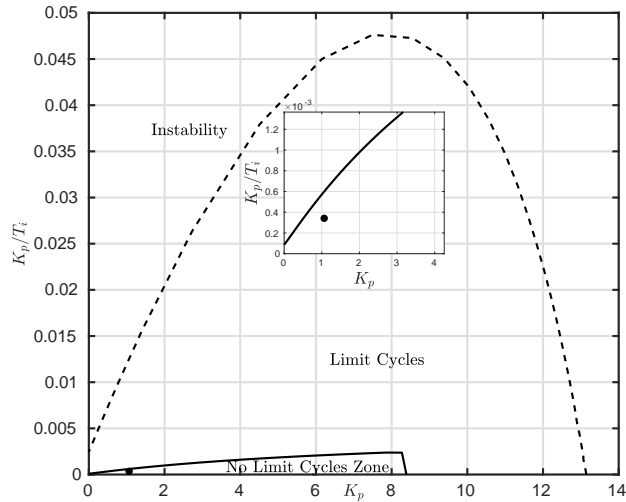
Figure 5.8: Stability region for daytime controller.

5.4   Event-based control approaches

The event-based control architecture designed for pH control in raceway
reactors is based on the Symmetric-Send-On-Delta method (SSOD). This
method is presented by Beschi *et al.* in [16] and it is a modification of the
so-called Send-On-Delta (SOD) event-based method ([49]).   Denote as
$v(t)$ the input signal to the SSOD sampled algorithm and as $v^*(t)$ the
sampled output signal, which can assume only values multiple of a
predefined threshold Δ multiplied by a gain $\beta > 0$, namely $v^*(t) = i\Delta\beta$
with $i \in \mathbb{Z}$.   The sampled signal changes its value to the upper
quantization level when the input signal $v(t)$ increases more than Δ, or
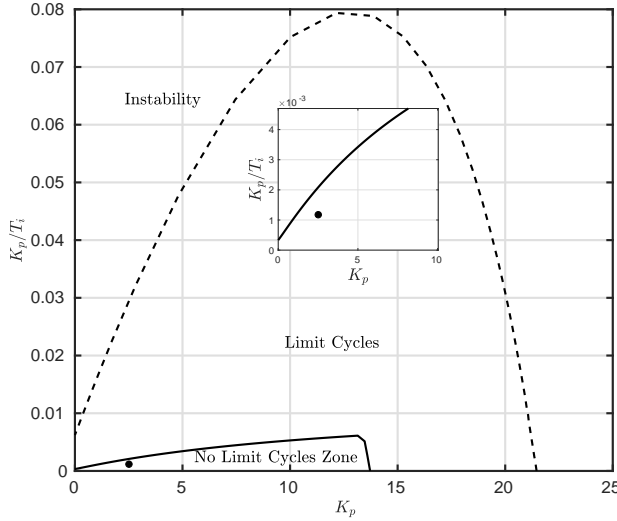
Figure 5.9: Stability region for night-time controller.

to the lower quantization level when $v(t)$ decreases more than Δ. The behaviour can be described with the following equation:

$$
v^*(t) = \begin{cases}
(i+1)\Delta\beta & \text{if } v(t) \geq (i+1)\Delta \text{ and } v^*(t^-) = i\Delta\beta \\
i\Delta\beta & \text{if } v(t) \in [(i-1)\Delta, (i+1)\Delta] \text{ and } v^*(t^-) = i\Delta\beta \\
(i-1)\Delta\beta & \text{if } v(t) \leq (i-1)\Delta \text{ and } v^*(t^-) = i\Delta\beta
\end{cases}
$$
(5.5)

The relationship between $v(t)$ and $v^*(t)$ can be considered as a generalization of a relay with hysteresis, where there are an infinite number of thresholds $(i\Delta\beta)$. This mathematical description can be interpreted as a state-machine representation, where i is the state number, $v(t) \geq (i+1)\Delta$ is the condition to jump to the upper state $i+1$ and $v(t) \leq (i+1)\Delta$ is the condition to jump to the lower state $i-1$.

The Δ parameter establishes the change amplitude in the error signal deadband, so the system error is increased or reduced in Δ intervals. In [16], it has been demonstrated that this parameter influences the system tolerance without affecting the system stability. For this reason, it has to

be properly tuned to establish a trade-off between the increments of the steady-state error and the decrements of the number of events. Due to its implementation and operation characteristics, this method can be used with wireless sensors to reduce the number of communications with the control unit.

Two different architectures are implemented with the SSOD technique based on the event-triggered data exchange position in the control loop and are shown in Figures 5.10 and 5.11.

SSOD-PI Scheme

In the SSOD-PI scheme, presented in Figure 5.10, the event-based method is applied to the system error, before the PI controller in the control loop. In this way, the last sampled error is maintained until a certain tolerance, established by the Δ parameter, is exceeded. One of the benefits of this configuration is the reduction on the communication between the sensor and the control unit, improving the life span of the batteries of wireless sensors.
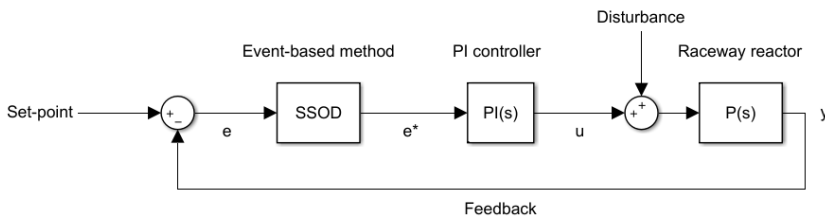
Figure 5.10: Control scheme of the SSOD-PI event-based control architecture. The SSOD block represents the error treatment performed by the Symmetric-Send-On-Delta method. e (v(t)) represents the process error, e* (v*(t)) represents the event-based sampled error, u represents the control signal (valve opening) and y represents the process output (pH).

PI-SSOD Scheme

On the other hand, in the PI-SSOD scheme, presented in Figure 5.11, the event-based method is applied to the control signal, after the PI

controller in the control loop. The last control action received is maintained until the next change that exceed the control deadband imposed by the Δ parameter. Analogous as the SSOD-PI scheme, this configuration presents a reduction of the number of changes in the control action, thus the actuator wear can be reduced.
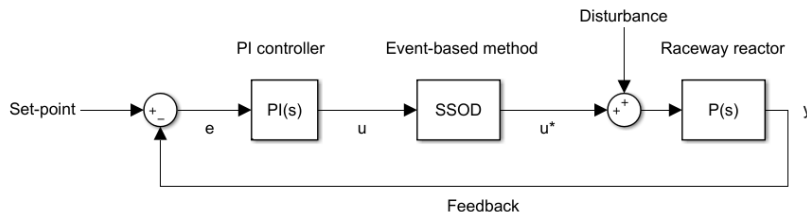
Figure 5.11: Control scheme of the PI-SSOD event-based control architecture. The SSOD block represents the error treatment performed by the Symmetric-Send-On-Delta method. e represents the process error u (v(t)) represents the control signal, u* (v*(t)) represents the event-based sampled control signal (valve opening) and y represents the process output (pH).

As can be seen in Figures 5.10 and 5.11, this event-based method is coupled with a PI controller in the control loop, that can be designed by any tuning rule. This is one of the most powerful advantages of this event-based method, being able to convert any PI controller into an event-based controller, just adding the SSOD block into the control loop, before or after the PI controller. This event-based method was applied with the PI controllers previously designed to evaluate different deadbands in the pH error.

5.5 Simulation results

This section discusses the results obtained in simulation with the application of two SSOD event-based architectures for the pH control problem with a nonlinear model [69, 70]. This simulation model for biomass production, presented in [31], takes into account fluid-dynamic,

mass transfer, and biological phenomena taking place in a microalgae raceway photobioreactors. Several experiments were performed with different solar radiation profiles during five days to observe how the event-based controller reacts to changes in the photosynthesis rate and in the pH variable. An evaluation of the pH referred to the Integral Absolute Error (IAE), to the control effort and to the CO_2 consumption associated with the injection time have been carried out.

The aim is to establish a comparison between the traditional On/Off control architecture and the SSOD event-based method. An initial comparison was made between the traditional On/Off control operating during daytime and a PI control architecture that operates both during daytime and night-time periods. Afterwards, further comparisons have been made with the SSOD event-based control architectures (SSOD-PI and PI-SSOD) from the initially designed PI controllers and applied to the combined daytime plus night-time solution. Results about the stability of SSOD-PI and PI-SSOD for FOPDT processes can be found in [16].

Usually, the pH control is performed only during the diurnal period because of its influence on the photosynthesis process. Thus, the system is working in open-loop during the night-time period to save CO_2 injections and thus saving costs and reduce CO_2 losses. However, due to the carbonate-bicarbonate balance, pH can rise above the set-point during night-time (without being critical). At the beginning of the day, as the pH starts outside the optimal value, a considerable injection is necessary to regulate it. In addition, changes in pH cause stress in the microalgae strain and decrease its performance. Therefore, in this section, the control scheme will be evaluated for the whole day in order to analyse how the (event-based) control approach can contribute to control the system also during night-time and without increasing the costs too much.

For the simulation study, the characteristics of the microalgae strain *Scenedesmus almeriensis* have been taken as a reference. This strain has an optimal pH range around 8, but during the simulations a value of 7.8 has been used, due to the initial assumption of being the value that produces maximum growth.

5.5.1 On/Off vs PI control results

The first scenario shows the simulation results considering two control architectures, a traditional On/Off controller operated during daytime (the system is in open loop during the night-time) and a combined daytime plus night-time PI control. Figure 5.12 shows a two days simulation where it can be seen how the pH oscillates around set-point (established in 7.8) during daytime for the On/Off controller (represented in red). These oscillations range from 7.73 to 7.9 while, for the PI controller (represented in black), the pH remains close to the set-point. Another remarkable fact is the variation of the pH during night-time, which, in the case of On/Off control, can reach values of 8.7. On the opposite, the night-time PI controller keeps the pH around set-point in that period.
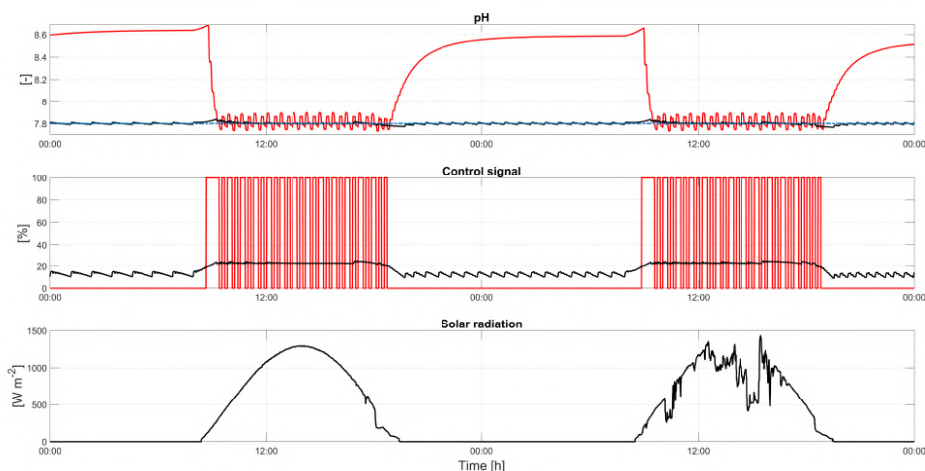
Figure 5.12: Two days comparison between traditional On/Off daytime control (red) and PI control during daytime and night-time periods (black). Blue dashed line represents pH set-point on 7.8.

Referring to the control effort, the control signal plot of Figure 5.12 represents the opening % of the injection valve for both control schemes. In this plot, it can be verified that, in the case of the On/Off controller, the valve opens completely in short periods of time, which causes a great control effort. In the case of the PI controller, the maximum opening of the

valve is around 23% during daytime period and 12.5% for the night-time period.

Indexes	On/Off Controller	PI Controller	Units
IAE	185,513.10	2972.96	–
$IAE_{daytime}$	11,590.10	1366.30	–
$IAE_{nighttime}$	173,923.00	1606.66	–
TV_u	274.00	15.99	–
IT	1856.47	1600.70	min
Gas	1.86	1.60	m^3
$IT_{daytime}$	1856.47	851.05	min
$IT_{nighttime}$	-	749.65	min

Table 5.1: Performance indexes for On/Off and Proportional-Integral (PI) control approaches

Table 5.1 shows the indexes for these two control schemes during the five days. The indexes are described as follows: IAE is the *Integral Absolute Error* (also during daytime and night-time), TV_u is the *Total Variation* in the control signal, *IT* represents the CO_2 *Injection Time* to the reactor (also during daytime and night-time) and *Gas* shows the CO_2 consumption. Starting with the IAE, it is very remarkable how the PI controller reduces this error by up to 98.40% with respect to the On/Off control, since it also operates during the night-time. Observing this error independently between the daytime and night-time periods, reductions of the order of 88.21% and 99.08% respectively for the IAE can be achieved. From the point of view of the *Total Variation* in the control signal, the PI control reduces this variation by 94.16%, due to a more accurate control during the daytime and even the night-time. This improvement in the control signal is reflected in a reduction of the control effort. The most remarkable comparison that can be made is about *Injection Time* and gas consumption. The PI controller reduces these values by 13.78% compared to the On/Off control, despite operating during the entire day and not only during the daytime period.

5.5.2 Event-based SSOD-PI control results

The second scenario presents the results of the SSOD-PI control architecture for five days. Figure 5.13 represents the SSOD-PI approach for the pH control problem with two different Δ values for daytime period ($\Delta = 0.01$ and $\Delta = 0.05$), maintaining a $\Delta = 0.05$ during the night-time period. By analysing the graphics of Figure 5.13, a comparison can be established between both Δ values, which represent the lowest and higher values studied for this SSOD configuration. Regarding pH (first plot), during night-time, both signals show similar behaviour, due to a Δ value of 0.05. On the contrary, during the daytime period, the change in the tolerance produced by the Δ parameter is appreciated. With a Δ value of 0.01 (black), it can be seen that the pH of the reactor remains around set-point with a rise peak at the beginning of the daytime period caused by the photosynthesis process (microalgae perform sunlight photosynthesis, which acidifies the culture and increases pH). On the other hand, with a Δ value of 0.05 (red), this rise peak is increased due to a lower tolerance caused by a higher Δ value. Moreover, at the end of the daytime, a drop peak is observed, which is produced by a decrement on solar radiation and the continuous gas injection caused by a greater tolerance on the event deadband.

For the control signal (second plot), during the night-time period, the response of the valve is the same in both cases. Regarding the daytime, the control signal corresponding to a Δ value of 0.05 shows a slower rise at the beginning of the daytime period and a higher average value with respect to the Δ value of 0.01. In relation to the events (third and fourth plots), a decrease in the number of events can be appreciated when the value of the Δ parameter increases, as it can be seen in Table 5.2.

The SSOD-PI performance indexes are presented in the Table 5.2, where the tests carried out with different Δ values ($\Delta = 0.01$, 0.02, 0.03, 0.04 and 0.05) are collected for five days each. Two new indexes with respect to the previous Table 5.1 are introduced: $E_{y-daytime}$ and $E_{y-nighttime}$ are the number of events during daytime and night-time periods. The IAE error increases during the daytime period as the Δ value increases, while for the night-time similar values result for all cases.

Figure 5.13: Results with the SSOD-PI controller. $\Delta = 0.01$ (black) and $\Delta = 0.05$ (red). First plot: pH output. Second plot: control signal. Third plot: daytime events. Fourth plot: night-time events. Fifth plot: solar irradiance.

Indexes	SSOD-PI Δ					Units
	0.01	**0.02**	**0.03**	**0.04**	**0.05**	
IAE	9418.45	9743.28	10,196.29	10,805.44	11,484.70	–
IAE$_{daytime}$	2089.36	2416.45	2899.45	3309.99	3974.87	–
IAE$_{nighttime}$	7329.09	7326.83	7296.84	7495.45	7509.81	–
TV$_u$	11.38	11.39	11.86	11.82	12.41	–
E$_{y-daytime}$	132	55	43	32	26	–
E$_{y-nighttime}$	91	93	95	93	96	–
IT	1537.70	1541.90	1253.50	1545.70	1542.97	min
Gas	1.54	1.54	1.54	1.55	1.54	m^3
IT$_{daytime}$	852.42	857.53	864.33	867.03	865.70	min
IT$_{nighttime}$	685.28	684.37	679.97	678.67	677.27	min

Table 5.2: Performance indexes for the Symmetric-Send-On-Delta-Proportional-Integral (SSOD-PI) control approach.

This is due to the fact that a fixed Δ value was used for the night-time period while a value range from 0.01 to 0.05 was used for daytime, thus increasing the error tolerance. Therefore, due to this increase in the error tolerance, the number of events—or communications between the sensor and the control unit—will be reduced with the increase of the Δ value, as can be seen in the table, especially during the daytime period. The *Total Variation* increases slightly in every case due to the tolerance imposed by the Δ value, which makes the control signal during the daytime period more constant but higher in the case of $\Delta = 0.05$. Regarding the *Injection Time* and gas consumption, there is no significant variation between cases, ranging from 1537.70 [min] ($\Delta = 0.01$) to 1545.70 [min] maximum ($\Delta = 0.04$), with the highest consumption during the daytime period.

5.5.3 Event-based PI-SSOD control results

The last scenario presents the results of the PI-SSOD control architecture for five days. Figure 5.14 shows the simulation performed using different Δ values ($\Delta = 0.001$ and 0.01) to compare both results. In the top plot,

the pH behaviour during the whole experiment is presented, where the pH reaches a higher value due to the photosynthesis process on daytime for the Δ value of 0.01. The photosynthesis due to solar irradiance acts as a disturbance at the same hour for every simulated day and the controller reacts later than for a Δ value of 0.001 because the event-based control method has a higher tolerance regarding the step in the control signal. On the other hand, for the Δ value of 0.001, this peak is smaller and the pH remains around the set-point. During night-time period, a Δ value of 0.006 for the PI controller was used for all the experiments, to maintain the pH oscillating close to the set-point.

In the second plot, the combined control signal applied to the actuator is shown. This signal is similar during the night-time period for both simulations, and during the start of the daytime period, it can be seen that the signal corresponding to a Δ value of 0.01 begins to act later than for the Δ value of 0.001, due to a greater deadband tolerance. The daytime and night-time events are presented in the third and fourth plots, respectively. It can be seen that, during the daytime, there are fewer events than during night-time, as it can be checked in Table 5.3, because of the small deadband in the night-time period.

Table 5.3 shows the performance indexes for all Δ cases studied ($\Delta =$ 0.001, 0.003, 0.005, 0.007 and 0.01) during a period of five days. Comparing the IAE, it can be appreciated that it increases as the Δ value increases because the increments in the control signal are greater. The error during night-time is similar in all cases, due to the same Δ value used in that period. The *Total Variation* does not show a regular increase or decrease, and it varies depending on the Δ value because the control signal is similar in all cases. The only observed difference is a later actuation during the daytime period. The daytime events are reduced as the Δ value increases and they remain similar during night-time as the IAE and the night-time events. The *Injection Time* and gas consumption do not show much variation in the analyzed cases. In the case of $\Delta = 0.01$, the reduction in the *Injection Time* due to the photosynthesis process at the beginning of the daytime is compensated with an increase at the end of the daytime due to a late actuation caused by the drop on solar irradiance, which is the period in which the pH
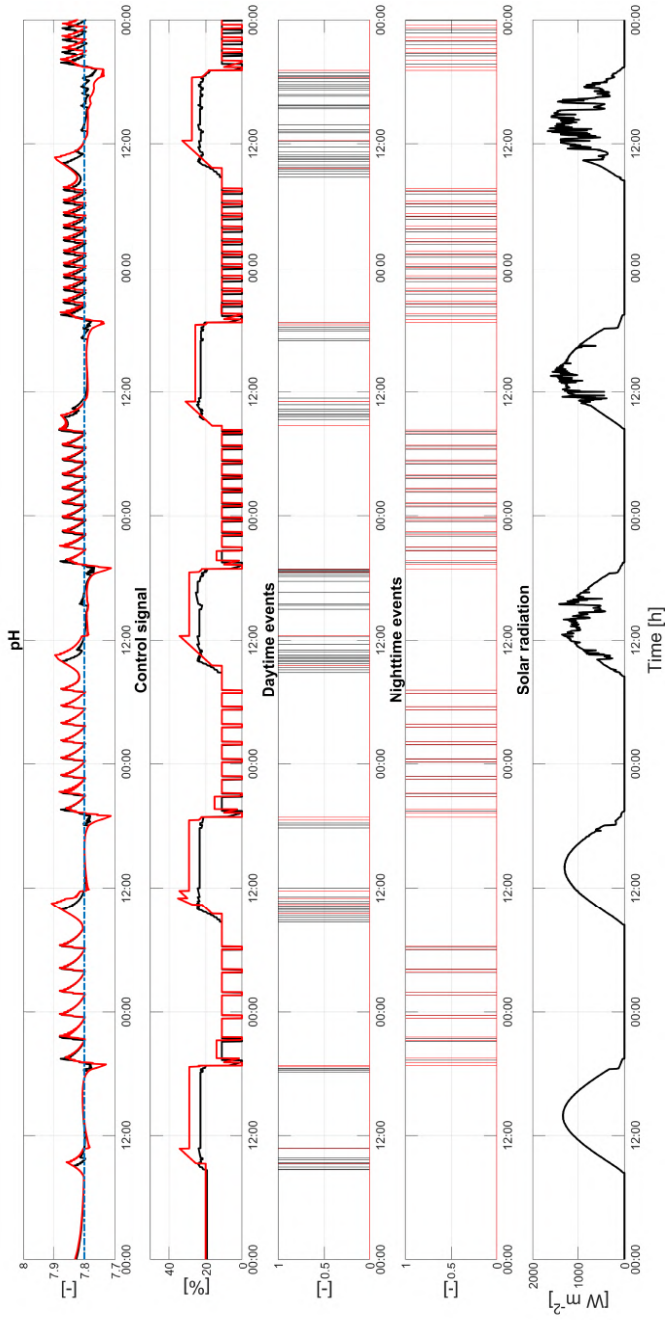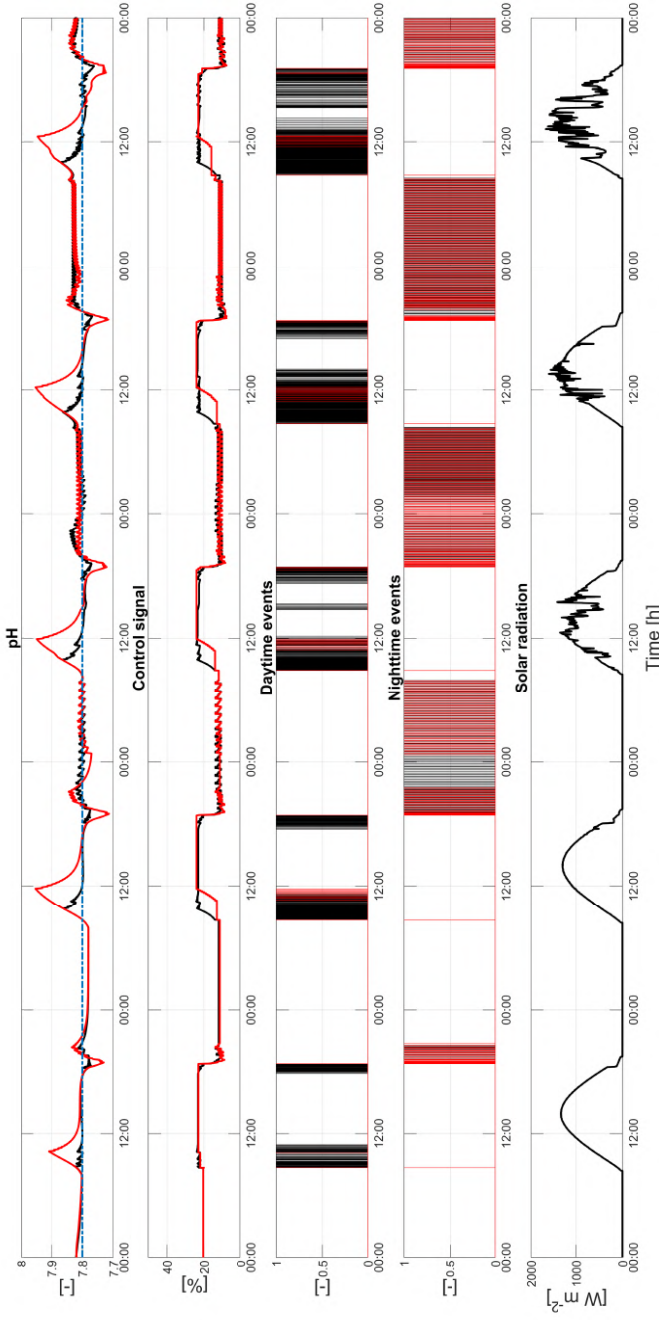
Figure 5.14: Results with the PI-SSOD controller. $\Delta = 0.001$ (black) and $\Delta = 0.01$ (red). First plot: pH output. Second plot: control signal. Third plot: daytime events. Fourth plot: night-time events. Fifth plot: solar irradiance.

remains below the set-point. Thus, gas consumption is similar to the case
of $\Delta = 0.001$, where the pH remains close to the set-point.

Indexes	PI-SSOD Δ					Units
	0.001	0.003	0.005	0.007	0.01	
IAE	6643.80	7339.80	8109.32	9260.24	12,799.96	–
IAE$_{daytime}$	2093.44	2782.69	3555.31	4462.89	7847.62	–
IAE$_{nighttime}$	4550.36	4557.11	4554.01	4797.35	4952.34	–
TV$_u$	7.73	9.43	6.31	5.85	6.09	–
E$_{y-daytime}$	1226	332	161	88	68	–
E$_{y-nighttime}$	700	1040	720	688	724	–
IT	1577.60	1585.30	1579.00	1570.30	1540.03	min
Gas	1.58	1.59	1.58	1.57	1.54	m^3
IT$_{daytime}$	849.03	856.63	851.63	845.23	818.90	min
IT$_{nighttime}$	728.57	728.67	727.37	725.07	721.13	min

Table 5.3: Performance indexes for the Proportional-Integral-Symmetric-
Send-On-Delta (PI-SSOD) control approach.

Discussion

As verified from the first scenario comparing the On/Off control with the
PI control architecture, the time-based scheme brings a series of benefits
to the pH control problem with respect to the traditional one. It provides
an improvement in the CO_2 usage even operating the reactor during both
daytime and night-time periods, while the On/Off control was used only
during the diurnal period.

On the other hand, the event-based control architectures based on the
SSOD method and coupled with a classical time-driven PI controller
(SSOD-PI and PI-SSOD) also count with the benefits that improve the
reactor control compared to the traditional On/Off control. Comparing
these event-based control architectures with respect to the PI control,
certain advantages are obtained accompanied by a series of disadvantages
related to the trade-off between tolerance and control accuracy. Looking
at Tables 5.1, 5.2 and 5.3, the first advantage for the event-based schemes

is the reduction of the CO_2 consumption, at the expense of slightly degrading the pH control performance by increasing the IAE values. This reduction in gas consumption is obviously more relevant when the plant operates for long periods of time (i.e., months). The second advantage is related to the control effort, which is reduced due to control tolerances established in both daytime and night-time periods, as can be seen, by the total variation and injection time.

Finally, the two event-based control architectures (SSOD-PI and PI-SSOD) show some differences between them regarding the event-based architectures and the Δ values suitable for its operation. One of the main differences that can be seen between the two architectures is that the Δ parameter has a greater influence on the PI-SSOD scheme since small variations of this parameter showed greater changes in IAE, as from Tables 5.2 and 5.3. The PI-SSOD scheme shows a greater reduction in the total variation of the control signal with respect to the SSOD-PI. On the contrary, the SSOD-PI scheme shows less number of events, being more suitable for use with wireless sensors. Regarding the injection time, it can be appreciated that, for the PI-SSOD architecture, it is slightly higher than for the SSOD-PI one. These differences are due to the event-based triggering method in both cases, where the Δ parameter does not work in the same way, and therefore, it must be selected regarding the needs of the process.

5.6 Experimental results

This section presents the experimental results obtained during the tests performed on the microalgae raceway reactor for the pH control problem during several days. Specifically, two-days tests will be presented for each evaluated control structure [73, 71].

The aim is to establish a comparison between the classical On/Off control operation of the reactor and a time-based controller architecture, in addition to the SSOD-PI event-based method. First, the reactor is operated with the classical On/Off control performed only during the daytime period. Second, the PI time-based control architecture is applied

to control the system during the whole day with two controllers, corresponding to the daytime and night-time periods. Afterwards, the SSOD-PI event-based method is proposed combined with the PI controllers previously designed and compared with the other control architectures applied.

It is remarkable to mention that the dynamic behavior of the physical raceway reactor is quite far from the behavior shown in the simulation part. This is due to the model used in simulation, which corresponds to a microalgae culture from a period prior to the experimental tests, and therefore, with a different configuration compared to the current one. Regarding the event-based control approach, the SSOD-PI structure has been chosen due to its application on the pH error in the system.

5.6.1   On/Off control results

The results obtained during the two days test performed with the On/Off control architecture are presented in Figure 5.15. The traditional On/Off control is characterized for a simple and fast control that does not take into account error limitations. With this type of control, the CO_2 valve opens to the maximum until the pH drops below the reference and the error decreases, but without acting against the lowering of pH below the reference that occurs.

From Figure 5.15, the effects of the On/Off control on the pH can be observed, which considerably oscillates, moving away from its optimal production value, set at a pH value of 8. In fact, this behavior causes CO_2 injections with an excessive duration, which provokes considerable drops in pH to values close to 7.5, very far from the reference. Notice that during the night-time period, due to bicarbonate buffer effect and the absence of control, the pH rises to values close to 8.2.

5.6.2   PI control results

The PI control results obtained during daytime and night-time periods are presented in Figure 5.16. The variation in pH ranges from 7.97 to 8.04, being on the optimal production zone. To maintain the pH on this range, during the night-time the PI control (input for the PWM) signal maintains

Figure 5.15: On/Off control architecture results. First graph represents the evolution of the pH (continuous green line), and the set-point (dashed red line).

approximately a 10% of the total injection flow, corresponding to a CO_2 flow rate of 0.5 (L min^{-1}); and a 20% of the total injection flow during daytime, corresponding to a CO_2 flow rate of 2 (L min^{-1}).

5.6.3   Event-based SSOD-PI control results

Figure 5.17 shows the results obtained with the SSOD-PI event-based control architecture during two days. A value of $\Delta = 0.1$ has been used in the event-based method for the tolerance deadband. The effect of the Δ value can be seen in the evolution of the pH, which varies between 7.9 and 8.1 during the night-time, with the slow dynamic characteristic of this period. On the other hand, during the daytime the pH varies between 7.9 and 8.2 because of the disturbances caused by solar radiation. The control signal during the night-time period shows a behavior similar to the On/Off control, with pulses of smaller amplitude occurring when the pH exceeds the threshold of the error band imposed by the Δ parameter. During the daytime period, the PI control signal is more active than at night-time. Regarding the CO_2 flow, it is characterized by injection pulses of varying amplitude and duration depending on the period of the day when the pH exceeds the threshold of the error zone. During night-time period, flow pulses are short and with an amplitude of 5 (L min^{-1}), while, during daytime, the flow pulses become longer with an average amplitude of 6 (L min^{-1}).

5.6.4   Performance indexes

To make a comparison between all control architectures, four performance indexes have been taken into account, which IAE, IT and Gas consumption were previously defined. The *Oxygen Production rate* or photosynthesis rate (PO_2), is an index to establish system performance, which is in relative units with respect to the On/Off control. This index represents the oxygen production per unit of biomass per day and can be calculated as the increase in the production of oxygen per unit of time. Table 5.4 shows the performance indexes described for the three control architectures calculated only based on the first day evolution, as in this day the three evaluated control approaches have the
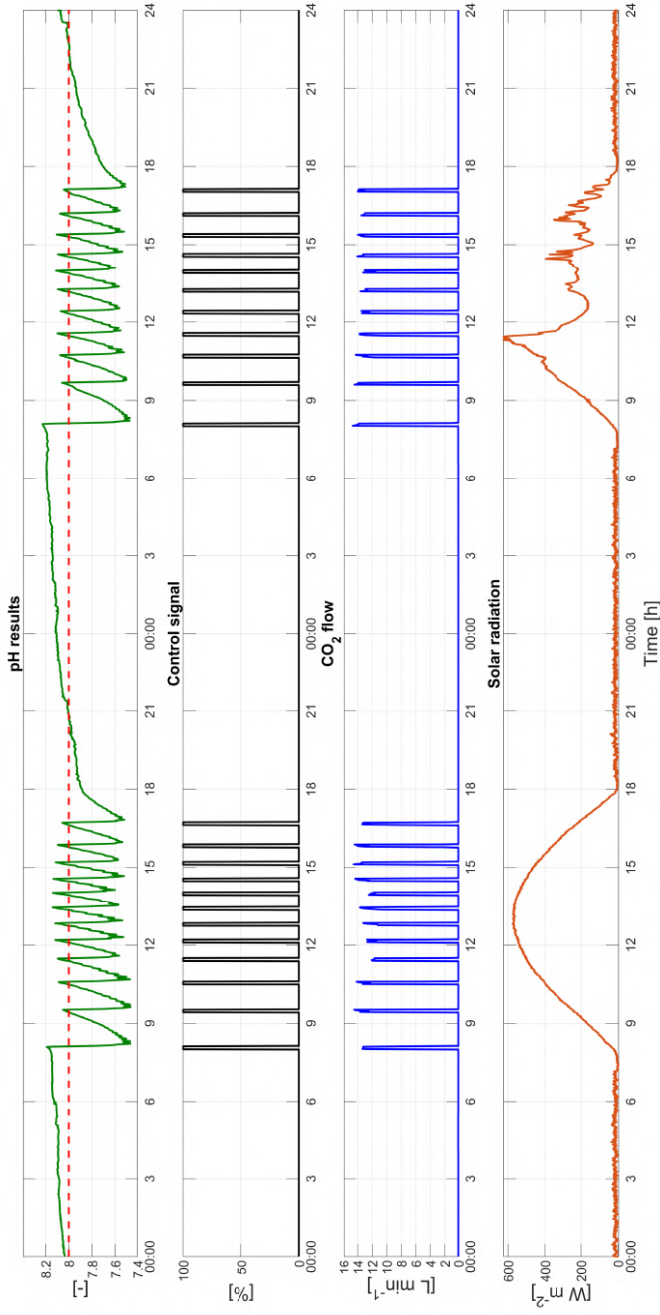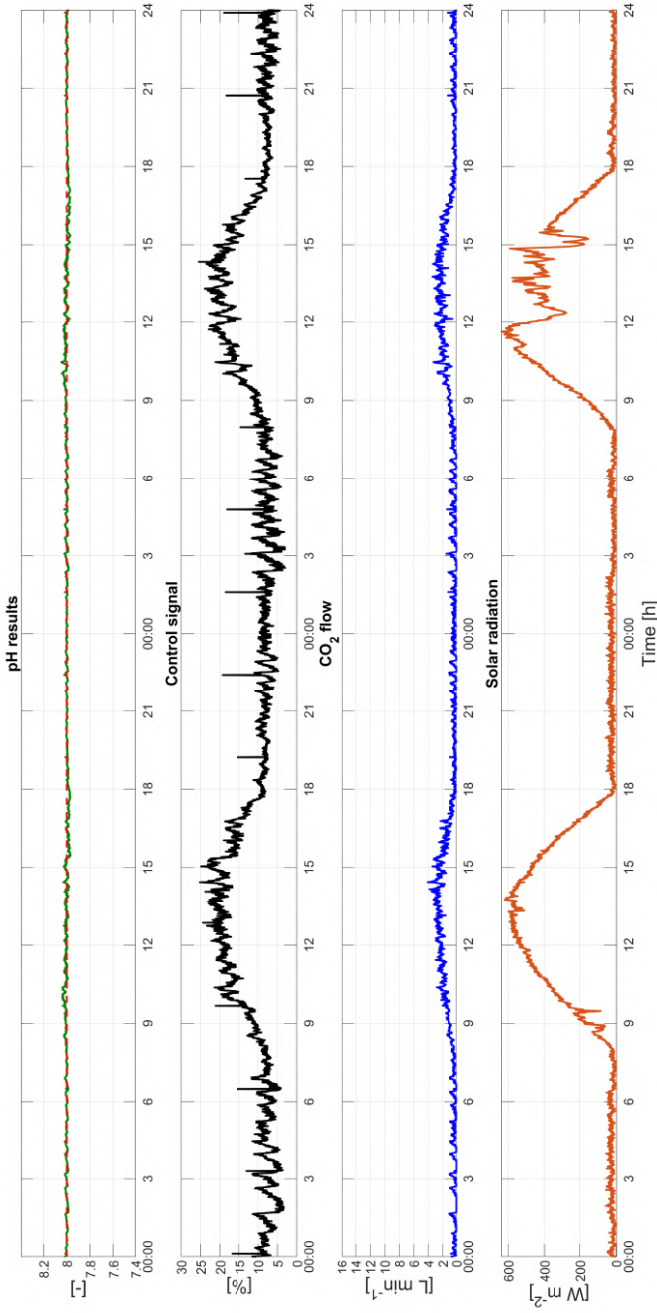
Figure 5.16: PI control architecture results. First graph represents the evolution of the pH (continuous green line), and the set-point (dashed red line).
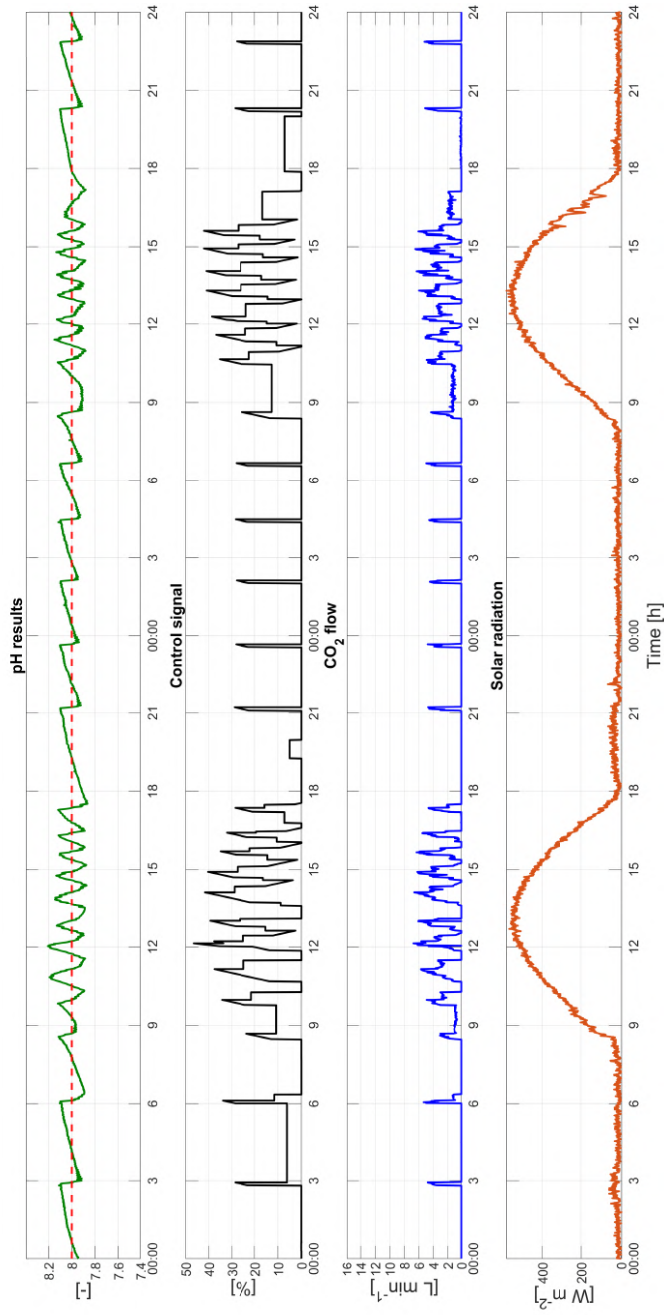
Figure 5.17: SSOD-PI event-based architecture results. First graph represents the evolution of the pH (continuous green line) and the set-point (dashed red line).

Index [1 day]	On/Off control	PI control	SSOD-PI control	Units
IAE	12793	683.5	4940	–
IT	82.3	1440	723.7	min
Gas	993.2	1302.1	1172.4	L
$\text{Gas}_{daytime}$	993.2	1132.7	1046.5	L
$\text{Gas}_{nighttime}$	0	169.4	125.9	L
PO_2	1	2.3	1.7	–

Table 5.4: Performance indexes computed for the first day due to equal conditions comparing the three control architectures presented on the results part. IAE represent the Integrated-Absolute-Error, IT represents the Injection Time, Gas represents the CO_2 total gas consumption, in addition to the consumption during the daytime and night-time periods. PO_2 represents system performance.

same operating conditions (similar levels of solar radiation, ambient temperature and biomass concentration). During the second day, both the On/Off controller and the PI controller suffer from disturbances coming from variations in the solar radiation. So, Table 5.5 shows the performance indexes for the complete two-days test performed for the control architectures under different weather conditions and in the case of PO_2, this table shows the mean Oxygen Production rate for the two days. Notice that environmental conditions cannot be fixed in experimental tests (only in simulation this is possible as it was done in the previous section [70]).

Discussion

The differences between the On/Off control and the PI control are evident by looking at Figures 5.15 and 5.16, in addition to the indexes in Tables 5.4 and 5.5. Regarding the pH, the PI control reduces the variation, keeping it in an optimum range, but at the expense of injecting during the whole day. The total gas consumption is slightly higher in the PI control compared to the traditional control, but it is understandable considering that the control is carried out even during the night-time period, with better results in pH, reflected in the IAE parameter, which

Index [2 days]	On/Off control	PI control	SSOD-PI control	Units
IAE	28282	1372	9402	–
IT	157.7	2880	1405	min
Gas	1933.3	2540.4	2446.9	L
$\text{Gas}_{daytime}$	1933.3	2179.9	2182.7	L
$\text{Gas}_{nighttime}$	0	360.5	264.2	L
$\overline{\text{PO}_2}$	1	1.9	1.7	–

Table 5.5: Performance indexes computed for the two-days tests. IAE represent the Integrated-Absolute-Error, IT represents the Injection Time, Gas represents the CO_2 total gas consumption, in addition to the consumption during the daytime and night-time periods. PO_2 represents system performance.

is reduced approximately a 95% with respect to the On/Off control. The increase in gas consumption is not high and can be translated into greater biomass production, as can be seen by the PO_2 index, which increases approximately a 50% with respect to the On/Off control. The pH is maintained at an optimal level and without variation, thanks to a higher pH stability, which could generate stress on the microalgae and reduce its performance, situation that happens with the On/Off control.

On the other hand, the SSOD-PI event-based control presents a behavior in pH very similar to that shown by the On/Off control architecture, but with a controlled amplitude, varying around the reference. Thus, the IAE error is reduced by 61% (Table 5.4 on equal conditions), at the expense of slightly higher consumption, as in the case of the PI control. Also, the Oxygen Production rate of Tables 5.4 and 5.5 are higher, with an increase of 40% with respect to the On/Off control. Comparing this architecture with the PI control, both show a similar consumption (as can be seen in Tables 5.4 and 5.5), being lower the one related to the event-based control. Injections performed during the night-time are punctual and scarce, instead of the continuous injection of CO_2 caused by the PI control architecture. Moreover, Tables 5.4 and 5.5 denote that the IAE error is greater for the event-based control with respect to the PI control, due to the oscillation of the pH caused by the

tolerance in the error, determined by the Δ parameter. As for the performance of the system observed in the Oxygen Production rate (PO_2), the PI control improves the production by approximately 20% with respect to the event-based control, at the cost of higher gas consumption.

Regarding the CO_2 consumption of each period of the day, represented in Tables 5.4 and 5.5, it can be seen that the consumption during the daytime period is practically the same for the PI and the event-based control architectures. The PI control is the one that reduces the most the error and increases the Oxygen Production rate, but also with a more variable control signal. On the other hand, the consumption during the night-time period shows a reduction of CO_2 in the case of the event-based control, with fewer injections, as can be seen with the control signal in Figures 5.16 and 5.17. This fact yields interesting control architecture, such as the combination of the PI control during the daytime period and the use of the event-based control during the night-time period. As stated earlier, the night-time period is not as critical as the daytime and tolerance in the error bands could be controlled by the Δ parameter, an intrinsic feature of the SSOD method.

5.7 Conclusions and contributions

Summarizing, this chapter describes the problem regarding the pH control carried out in the raceway reactors and the importance of a correct management in the use of resources, such as the consumption of CO_2. In addition, different control approaches based on two identified models are presented for the evolution of pH in the reactor during daytime and night-time periods. One of the most characteristic innovations of these approaches is the control carried out during the whole day, since the classical operation of pH in raceway reactors is carried out exclusively during the daytime period.

The development of these new control approaches (time-based and event-based) is aimed at improving pH control in raceway reactors while reducing CO_2 consumption, in addition to improving biomass

productivity due to less fluctuation of pH and cultivation around optimal values. The tests carried out, both in simulation and experimentally, have highlighted the difference that precise control and correct management of CO_2 supposes compared to its normal operation.

The results regarding the pH error show that the PI control reduces the error to a large degree with respect to the On/Off control architecture, keeping the pH very close to the reference, that is at the optimum production value during 24 hours. To achieve this, the PI control slightly increases the CO_2 consumption but considerably improves system performance. On the other side, the SSOD-PI event-based control architecture increases the IAE error with respect to the PI control, but reducing the CO_2 consumption during the night-time period, improving control effort and gas utilization.

As conclusion, a control structure that combines the PI control for the daytime period and the event-based control for the night-time period is an interesting architecture to consider due to the advantages that both types of control provide individually.

Conclusions and future works

This thesis has presented modeling and control approaches related to the biomass production process carried out in raceway reactors, with the aim of improving the operation of existing systems.

A detailed description of the specific microalgae growth rate model coupled with nutrients availability influence on microalgae and bacteria growth has been stated in Chapter 3. Moreover, an estimation model for culture temperature on raceway reactors has also been developed and explained. Temperature has proven to be one of the parameters that most affects the growth of microalgae and bacteria in open reactors on an industrial scale. It is a variable difficult to control, and it represents a serious challenge for microalgae cultivation. From the developed temperature model, it is possible to estimate the temperature of a culture inside a raceway reactor, based only on environmental conditions. Therefore, this model can be used as a design tool to determine the viability of cultivating different strains of microalgae at various locations. On the other hand, the combined model of biomass production and wastewater treatment, together with the calibration method based on genetic algorithms, open the door to the design of models that faithfully reflect these processes in a single reactor. The main objective of these models is the improvement or design of complete models that represent the balances and intrinsic processes of microalgae during biomass production process.

According to the model developed for culture temperature in raceway reactors, Chapter 4 has focused on analyzing the influence of temperature and liquid depth on the microalgae culture. Thus, a liquid depth optimizer has been designed to modify the volume of liquid in the reactor, and thus regulating its temperature. This optimization approach is carried out from the harvesting and dilution processes applied every day during the operation of the reactor for microalgae biomass harvesting. It should be noted that this method does not imply an additional cost in the facilities, but rather takes advantage of existing

mechanisms to improve biomass productivity. The results obtained from this approach denote a considerable improvement in the amount of biomass harvested, especially in summer, the period of maximum production due to favorable environmental conditions. Moreover, the importance of certain parameters that affect optimization should be highlighted, such as the dilution rate and the inlet temperature of the dilution medium, which must be taken into account to achieve proper optimization.

The pH control is one of the most common processes in the cultivation of microalgae, both at the laboratory level and at an industrial scale. However, this control is usually carried out using On/Off architectures, which are widespread in this field. This type of control generates considerable oscillations in the pH value, in addition to being carried out exclusively during the daytime period. Different control approaches have been presented in Chapter 5. PI controllers combined with event-based methods have shown great potential in improving pH control and reducing CO_2 consumption, compared to classical control architectures. Furthermore, innovative pH control throughout the whole day (daytime and night-time periods) has been introduced, with satisfactory results compared to the control carried out exclusively during the daytime period.

During the development of the contents shown in this thesis, a series of ideas have arisen regarding improvements that could be applied. These ideas could not be carried out due to lack of time or resources, and thus are established as future objectives to be developed. The proposed future works are the following:

- In most test presented, biomass productivity is used as a performance index to compare different approaches. In addition to this parameter, an economic or energetic analysis should be carried out to improve the comparison. Therefore, a future work will be to perform an economic and energetic analysis, with up to date values, in order to establish comparisons between the different architectures of pH control or in the culture depth control for temperature regulation.

- For the calibration of the parameters for the combined biomass production and wastewater treatment model, shown in Chapter 3, a cost function has been used that represents the RMSE between the measured and estimated variables. This result is preliminary and the cost function can be improved to include different weights in the errors for the variables analyzed, since their range of variation is diverse. In addition, data collection can be improved to try to achieve a less dispersed data set.

- The culture depth optimization process is based on a cost function that computes the error between the estimated temperature and the measured temperature in the raceway reactor. This cost function can be improved by using a factor that takes into account the biomass productivity as a function of temperature, biomass concentration and culture depth. In this way, the established control action ensures the maximization of biomass productivity. Taking online measurements of biomass concentration is a complex task to achieve. This can be done using turbidimeters that measure the turbidity of the water from refraction, but the readings are often not very accurate. Thus, another future work will be the development of biomass estimators.

- Regarding the culture depth optimizer, more tests remain to be done over extended periods of time comparing between the proposed optimization architectures (one step and receding horizon).

- The dilution rate applied in the different test carried out is a value that is taken depending on the biomass concentration and month. These values are taken from tables and historical data, however, it is a parameter that depends on the biomass concentration and the growth rate, in addition to the atmospheric conditions. Therefore, a new objective is to implement a function that calculates the dilution rate online to optimally harvest the raceway reactor each day. This implementation can be combined with the culture depth optimizer to adjust the maximum and minimum limits in the operation of the raceway reactor.

Bibliography

[1] F. G. Acién, J. M. Fernández, J. J. Magán, and E. Molina. Production cost of a real microalgae production plant and strategies to reduce it. *Biotechnology Advances*, 30:1344 – 1353, 2012. doi: 10.1016/j. biotechadv.2012.02.005. (Cited on page 13).

[2] F. G. Acién, J. M. Fernández, and E. Molina. Photobioreactors for the production of microalgae. *Reviews in Environmental Science and Bio-Technology*, 12:131–151, 2013. doi: 10.1007/s11157-012-9307-6. (Cited on page 75).

[3] K. J. Åström and T. Hägglund. *Advanced PID Control*. ISA-The Instrumentation, Systems and Automation Society, 2006. ISBN 978-1-55617-942-6. (Cited on page 146).

[4] A. Bahadar and M. Bilal Khan. Progress in energy from microalgae. a review. *Renewable and Sustainable Energy Reviews*, 27:128–148, 2013. doi: 10.1016/j.rser.2013.06.029. (Cited on page 13).

[5] T. T. Bannister. Quantitative description of steady state, nutrient-saturated algal growth, including adaptation. *Limnology and Oceanography*, 24(1):76 – 96, 1979. doi: 10.4319/lo.1979.24.1.0076. (Cited on page 9).

[6] M. Barceló-Villalobos, J. L. Guzmán, F. G. Acién, I. Martín, and J. A. Sánchez. Análisis del coeficiente de transferencia de materia en reactores raceways. *XXXVIII Jornadas de Automática*, pages 534 – 538, 2017. doi: 10.3390/app11030998. (Cited on pages xxi and 15).

[7] M. Barceló-Villalobos, J. L. Guzmán, I. Martín-Cara, J. A. Sánchez-Molina, and F. G. Acién. Analysis of mass transfer capacity in raceway reactors. *Algal Research*, 35:91 – 97, 2018. doi: 10.1016/j.algal.2018. 08.017. (Cited on page 83).

[8] M. Barceló-Villalobos, C. Gómez-Serrano, A. Sánchez-Zurano, L. Alameda-García, S. Esteve-Maldonado, J. Peña, and F. G. Acién. Variations of culture parameters in a pilot-scale thin-layer reactor and their influence on the performance of *Scenedesmus almeriensis* culture. *Bioresource Technology Reports*, 6:190 – 197, 2019. doi: 10.1016/j.biteb.2019.03.007. (Cited on pages 8, 18, 30 and 80).

[9] Q. Béchet, A. Shilton, J. K. Park, R. J. Craggs, and B. Guieysse. Universal temperature model for shallow algal ponds provides improved accuracy. *Environmental Science and Technology*, 45:3702–3709, 2011. doi: 10.1021/es1040706. (Cited on pages 17, 33 and 34).

[10] Q. Béchet, A. Shilton, and B. Guieysse. Modeling the effects of light and temperature on algae growth: State of the art and critical assessment for productivity prediction during outdoor cultivation. *Biotechnology Advances*, 31(8):1648 – 1663, 2013. doi: 10.1016/j.biotechadv.2013.08.014. (Cited on pages 12 and 18).

[11] Q. Béchet, A. Shilton, and B. Guieysse. Maximizing productivity and reducing environmental impacts of full-scale algal production through optimization of open pond depth and hydraulic retention time. *Environmental Science & Technology*, 50(7):4102 – 4110, 2016. doi: 10.1021/acs.est.5b05412. (Cited on pages 12 and 17).

[12] Q. Béchet, M. Laviale, N. Arsapin, H. Bonnefond, and O. Bernard. Modeling the impact of high temperatures on microalgal viability and photosynthetic activity. *Biotechnology for Biofuels*, 10:136, 2017. doi: 10.1186/s13068-017-0823-z. (Cited on page 18).

[13] Q. Béchet, B. Sialve, J. P. Steyer, A. Shilton, and B. Guieysse. Comparative assessment of evaporation models in algal ponds. *Algal Research*, 35:283 – 291, 2018. doi: 10.1016/j.algal.2018.08.022. (Cited on page 18).

[14] M. Berenguel, F. Rodríguez, F. G. Acién, and J. L. García. Model predictive control of pH in tubular photobioreactors. *Journal of Process Control*, 14(4):377–387, 2004. doi: 10.1016/j.jprocont.2003.07.001. (Cited on page 148).

[15] O. Bernard and B. Rémond. Validation of a simple model accounting for light and temperature effect on microalgal growth. *Bioresource Technology*, 123:520 – 527, 2012. doi: 10.1016/j.biortech.2012.07.022. (Cited on pages 11, 17, 19, 74, 75 and 80).

[16] M. Beschi, S. Dormido, J. Sánchez, and A. Visioli. Characterization of Symmetric-Send-On-Delta PI controllers. *Journal of Process Control*, 22:1930–1945, 2012. doi: 10.1016/j.jprocont.2012.09.005. (Cited on pages 152, 153 and 156).

[17] F. Camacho, F. García, J. M. Fernández, Y. Chisti, and E. Molina. A mechanistic model of photosynthesis in microalgae. *Biotechnology and Bioengineering*, 81(4):459 – 473, 2003. doi: 10.1002/bit.10492. (Cited on pages 8, 9 and 19).

[18] F. Casagli, G. Zuccaro, O. Bernard, J. P. Steyer, and E. Ficara. Alba: a comprehensive growth model to optimize algae-bacteria wastewater treatment in raceway ponds. *Water Research*, 116734, 2020. doi: 10.1016/j.watres.2020.116734. (Cited on page 20).

[19] Closed photobioreactor figure:. *https://commons.wikimedia.org/wiki/File:Photobioreactor_PBR_4000_G_IGV_Biotech.jpg*. (Cited on page 14).

[20] T. A. Costache, F. G. Acién, M. M. Morales, J. M. Fernández-Sevilla, I. Stamatin, and E. Molina. Comprehensive model of microalgae photosynthesis rate as a function of culture conditions in photobioreactors. *Applied Microbiology and Biotechnology*, 97:7627–7637, 2013. doi: 10.1007/s00253-013-5035-2. (Cited on pages 12, 17 and 143).

[21] P. Darvehei, P. A. Bahri, and N. R. Moheimani. Modeling the effect of temperature on microalgal growth under outdoor conditions. *Computer Aided Chemical Engineering*, 43:55 – 60, 2018. doi: 10.1016/B978-0-444-64235-6.50012-7. (Cited on page 18).

[22] I. de Godos, J. L. Mendoza, F. G. Acién, E. Molina, C. J. Banks, S. Heaven, and F. Rogalla. Evaluation of carbon dioxide mass transfer

in raceway reactors for microalgae culture using flue gases. *Bioresource Technology*, 153:307 – 314, 2014. doi: 10.1016/j.biortech.2013.11.087. (Cited on page 83).

[23] R. De-Luca, Q. Béchet, F. Bezzo, and O. Bernard. Optimal operation of algal ponds accounting for future meteorology. *IFAC - PapersOnLine*, 49(7):1062 – 1067, 2016. doi: 10.1016/j.jprocont.2017. 03.010. (Cited on pages 19, 111 and 127).

[24] R. De-Luca, F. Bezzo, Q. Béchet, and O. Bernard. Exploting meteorological forecast for the optimal operation of algal ponds. *Journal of Process Control*, 55:55 – 65, 2017. doi: 10.1016/j.jprocont. 2017.03.010. (Cited on pages 19, 111 and 127).

[25] R. De-Luca, M. Trabuio, M. Barolo, and F. Bezzo. Microalgae growth optimization in open ponds with uncertain weather data. *Computers and Chemical Engineering*, 117:410 – 419, 2018. doi: 10.1016/j.compchemeng.2018.07.005. (Cited on pages 12 and 19).

[26] E. A. Del Rio-Chanona, N. R. Ahmed, J. Wagner, Y. Lu, D. Zhang, and K. Jing. Comparison of physics-based and data-driven modelling techniques for dynamic optimisation of fed-batch bioprocesses. *Biotechnology and Bioengineering*, 116(11):2971–2982, 2019. doi: 10.1002/bit.27131. (Cited on page 17).

[27] V. Dolganyuk, D. Belova, O. Babich, A. Prosekov, S. Ivanova, D. Katserov, N. Patyukov, and S. Sukhikh. Microalgae: A promising source of valuable bioproducts. *Biomolecules*, 10:1 – 24, 2020. doi: 10.3390/biom10081153. (Cited on page 13).

[28] J. A. Duffie and W. A. Beckman. *Solar Engineering of Thermal Processes, 2nd ed. Wiley-Interscience*, 1991. (Cited on pages 34 and 36).

[29] I. Fernández, J. Peña, J. L. Guzmán, M. Berenguel, and F. G. Acién. Modelling and control issues of pH in tubular photobioreactors. *IFAC proceedings Volumes*, 43(6):186–191, 2010. doi: 10.3182/ 20100707-3-BE-2012.0046. (Cited on pages 17 and 21).

[30] I. Fernández, F. G. Acién, J. M. Fernández, J. L. Guzmán, J. J. Magán, and M. Berenguel. Dynamic model of microalgal production in tubular photobioreactors. *Bioresource Technology*, 126:172 – 181, 2012. doi: 10.1016/j.biortech.2012.08.087. (Cited on pages 30 and 34).

[31] I. Fernández, F. G. Acién, J. L. Guzmán, M. Berenguel, and J. L. Mendoza. Dynamic model of an industrial raceway reactor for microalgae production. *Algal Research*, 17(2):67 – 78, 2016. doi: 10.1016/j.algal.2016.04.021. (Cited on pages 17, 74 and 155).

[32] R. Gao and Z. Gao. Pitch control for wind turbine systems using optimization, estimation and compensation. *Renewable Energy*, 91:501–515, 2016. doi: 10.1016/j.renene.2016.01.057. (Cited on page 151).

[33] C. Grimholt and S. Skogestad. Optimal PI-Control and verification of the SIMC tuning rule. *IFAC Proceedings Volumes. 2nd IFAC Conference on Advances in PID Control*, 45(3):11–22, 2012. doi: 10.3182/20120328-3-IT-3014.00003. (Cited on page 151).

[34] J. L. Guzmán, F. G. Acién, and M. Berenguel. Modelling and control of microalgae production in industrial photobioreactors. *Revista Iberoamericana de Automática e Informática Industrial*, 18(1):1 – 18, 2021. doi: 10.4995/riai.2020.13604. URL `https://polipapers.upv.es/index.php/RIAI/article/view/13604/12866`. (Cited on pages 19 and 34).

[35] N. Hempel, I. Petrick, and F. Behrendt. Biomass productivity and productivity of fatty acids and amino acids of microalgae strains as key characteristics of suitability for biodiesel production. *Journal of Applied Phycology*, 24:1407–1418, 2012. doi: 10.1007/s10811-012-9795-3. (Cited on page 12).

[36] C. Houck, J. Joines, and M. Kay. A genetic algorithm for function optimization: A matlab implementation. *NCSUIE-TR-95-09. North Carolina State University, Raleigh, NC, USA*, 22, 1998. (Cited on page 41).

[37] A. Hoyo, J. L. Guzmán, J. C. Moreno, and M. Berenguel. Control robusto con QFT del pH en un fotobiorreactor raceway (Robust pH control with QFT in a raceway photobioreactor). *In XXXVIII Jornadas de Automática*, pages 6–8, September 2017. (Cited on pages 21 and 150).

[38] A. Hoyo, J. L. Guzmán, J. C. Moreno, and M. Berenguel. Linear predictive control for the pH in raceway photobioreactors. *In XL Jornadas de Automática*, 11:414–420, September 2019. doi: 10.17979/ spudc.9788497497169.414. (Cited on page 21).

[39] M. Huesemann, B. Crowe, P. Waller, A. Chavis, S. Hobbs, S. Edmundson, and M. Wigmosta. A validated model to predict microalgae growth in outdoor pond cultures subjected to fluctuating light intensities and water temperatures. *Algal Research*, 13:195 – 206, 2016. doi: 10.1016/j.algal.2015.11.008. (Cited on pages 17 and 19).

[40] K. Hwan Ryu, J. Lee, S. Heo, and J. Lee. Improved microalgae production by using a heat supplied open raceway pond. *Industrial & Engineering Chemistry Research*, 58(21):9099 – 9108, 2019. doi: 10.1021/acs.iecr.9b00986. (Cited on page 19).

[41] D. Ippoliti, C. Gómez, M. M. Morales-Amaral, R. Pistocchi, J. Fernández-Sevilla, and F. G. Acién. Modeling of photosynthesis and respiration rate for isochrysis galbana (t-iso) and its influence on the production of this strain. *Bioresource Technology*, 203:71 – 79, 2016. doi: 10.1016/j.biortech.2015.12.050. (Cited on page 75).

[42] S. C. James and V. Boriah. Modeling algae growth in an open-channel raceway. *Journal of Computational Biology*, 17:895–906, 2010. doi: 10.1089/cmb.2009.0078. (Cited on page 17).

[43] A. Karemore, Y. Yuan, W. Porubsky, and R. Chance. Biomass and pigment production for *Arthrospira platensis* via semi-continuous cultivation in photobioreactors: Temperature effects. *Biotechnology and Bioengineering*, 117(10):1–13, 2020. doi: 10.1002/bit.27480. (Cited on page 17).

[44] T. Lafarga. Cultured microalgae and compounds derived thereof for food applications: Strain selection and cultivation, drying, and processing strategies. *Food Reviews International*, 36:559 – 583, 2020. doi: 10.1080/87559129.2019.1655572. (Cited on page 13).

[45] P. Lavens and P. Sorgeloos. Manual on the production and use of live food for aquaculture. *FAO Fisheries Technical Paper, Rome*, 361: 295p, 1996. (Cited on page 6).

[46] M. Marsullo, A. Mian, A. V. Ensinas, G. Manente, A. Lazzaretto, and F. Marechal. Dynamic modeling of the microalgae cultivation phase for energy production in open raceway ponds and flat panel photobioreactors. *Frontiers in Energy Research*, 3:41–59, 2015. doi: 10.3389/fenrg.2015.00041. (Cited on page 18).

[47] J. L. Mendoza, M. R. Granados, I. de Godos, F. G. Acién, E. Molina, C. J. Banks, and S. Heaven. Fluid-dynamic characterization of real-scale raceway reactors for microalgae production. *Biomass and Bioenergy*, 54:267–275, 2013. doi: 10.1016/j.biombioe.2013.03.01. (Cited on page 83).

[48] J. L. Mendoza, M. R. Granados, I. de Godos, F. G. Acién, E. Molina, S. Heaven, and C. J. Banks. Oxygen transfer and evolution in microalgal culture in open raceways. *Bioresource Technology*, 137:188 – 195, 2013. doi: 10.1016/j.biortech.2013.03.127. (Cited on page 83).

[49] M. Miskowicz. Send-On-Delta: an event-based data reporting strategy. *Sensors*, 6:49–63, 2006. doi: 10.3390/s6010049. (Cited on page 152).

[50] E. Molina, J. A. Sánchez, F. García, J. L. García, and D. López. n-3 pufa productivity in chemostat cultures of microalgae. *Applied Microbiology and Biotechnology*, 38:599 – 605, 1993. doi: 10.1007/BF00182796. (Cited on page 9).

[51] E. Molina, F. García, J. A. Sánchez, J. M. Fernández, F. G. Acién, and A. Contreras. A mathematical model of microalgal growth in light-limited chemostat culture. *Chemical Technology and Biotechnology*,

61(2):167 – 173, 1994. doi: 10.1002/jctb.280610212. (Cited on pages 9 and 76).

[52] E. Molina, J. M. Fernández, J. A. Sánchez, and F. Garcáa. A study on simultaneous photolimitation and photoinhibition in dense microalgal cultures taking into account incident and averaged irradiances. *Journal of Biotechnology*, 45(1):59–69, 1996. doi: 10. 1016/0168-1656(95)00144-1. (Cited on page 9).

[53] J. Monod. Recherches sur la croissance des cultures bacteriennes. *Herman & cie.*, Paris, 1942. (Cited on page 9).

[54] J. L. Monteith and M. H. Unsworth. Principles of Environmental Physics. *Third Ed. AP, Amsterdam*, 2008. (Cited on page 37).

[55] S. A. Naghibi, E. Salehi, M. Khajavian, V. Vatanpour, and M. Sillanpää. Multivariate data-based optimization of membrane adsorption process for wastewater treatment: Multi-layer perceptron adaptive neural network versus adaptive neural fuzzy inference system. *Chemosphere*, 129268, 2020. doi: 10.1016/j.chemosphere. 2020.129268. (Cited on page 20).

[56] J. O. Nalley, D. R. O'Donnell, and E. Litchman. Temperature effects on growth rates and fatty acid content in freshwater algae and cyanobacteria. *Algal Research*, 35:500 – 507, 2018. doi: 10.1016/j. algal.2018.09.018. (Cited on page 18).

[57] A. O'Dwyer. *Handbook of PI and PID Controller Tuning Rules*. Imperial College Press: London, UK, 2009. (Cited on page 151).

[58] W. J. Oswald and C. G. Golueke. Biological transformation of solar energy. *Applied Microbiology and Biotechnology*, 2:223–262, 1960. doi: 10.1016/S0065-2164(08)70127-8. (Cited on page 13).

[59] A. Pawlowski, I. Fernández, J. L. Guzmán, M. Berenguel, F. G. Acién, and J. E. Normey-Rico. Event-based predictive control of pH in tubular photobioreactors. *Computers and Chemical Engineering*, 65:28–39, 2014. doi: 10.1016/j.compchemeng.2014.03.001. (Cited on page 21).

[60] A. Pawlowski, J. L. Mendoza, J. L. Guzmán, M. Berenguel, F. G. Acién, and S. Dormido. Effective utilization of flue gases in raceway reactors with event-based pH control for microalgae culture. *Bioresource Technology*, 170:1–9, 2014. doi: 10.1016/j.biortech.2014. 07.088. (Cited on page 21).

[61] A. Pawlowski, J. L. Mendoza, J. L. Guzmán, M. Berenguel, F. G. Acién, and S. Dormido. Selective pH and dissolved oxygen control strategy for a raceway rector within an event-based approach. *Control Engineering Practice*, 44:209–218, 2015. doi: 10.1016/j.conengprac. 2015.08.004. (Cited on pages 17, 21, 114, 143 and 150).

[62] A. Pawlowski, J. L. Guzmán, M. Berenguel, F. G. Acién, and S. Dormido. Application of predictive feedforward compensator to microalgae production in a raceway reactor: A simulation study. *Energies*, 11:123–140, 2018. doi: 10.3390/en11010123. (Cited on pages 21 and 150).

[63] A. Pawlowski, J. L. Guzmán, M. Berenguel, and F. G. Acién. Control system for pH in raceway photobioreactors based on Wiener models. *IFAC-PapersOnLine*, 52(1):928–933, 2019. doi: 10.1016/j.ifacol.2019. 06.181. (Cited on page 21).

[64] D. Pooya, P. A. Bahri, and N. R. Moheimani. Modeling the effect of temperature on microalgal growth under outdoor conditions. *Computer Aided Chemical Engineering*, 43:55 – 60, 2018. doi: 10.1016/B978-0-444-64235-6.50012-7. (Cited on pages 11 and 19).

[65] C. Posten. Design principles of photo-bioreactors for cultivation of microalgae. *Engineering in Life Sciences*, 9:165 – 177, 1997. doi: 10.1002/elsc.200900003. (Cited on page 13).

[66] R. Praveen-Eluripati. An improved model for estimating evaporation over lakes and ponds. *Thesis submitted to the Graduate Faculty of the University of New Orleans*, `https://scholarworks.uno.edu/cgi/viewcontent.cgi?article=1567&context=td`, 2007. (Cited on page 36).

[67] M. Ras, J. P. Steyer, and O. Bernard. Temperature effect on microalgae: A crucial factor for outdoor production. *Reviews in Environmental Science and Bio/Technology*, 12(2):153 – 164, 2013. doi: 10.1007/s11157-013-9310-6. (Cited on pages 17 and 18).

[68] E. Rodríguez, F. G. Acién, J. L. Guzmán, M. Berenguel, and A. Visioli. Modelo de temperatura para reactores abiertos de microalgas. *In XL Jornadas de Automática, Ferrol, Spain*, pages 582 – 588, 2019. doi: 10.17979/spudc.9788497497169.582. (Cited on page 33).

[69] E. Rodríguez, M. Beschi, J. L. Guzmán, M. Berenguel, and A. Visioli. Application of a symmetric-send-on-delta event-based controller for a microalgal raceway reactor. *In the 18th European Control Conference, ECC 2019, Naples, Italy*, pages 1 – 6, 2019. doi: 10.23919/ECC.2019. 8795912. (Cited on page 155).

[70] E. Rodríguez, M. Beschi, J. L. Guzmán, M. Berenguel, and A. Visioli. Daytime/Nighttime event-based PI control for the pH of a microalgae raceway reactor. *Processes*, 7(5):247–263, 2019. doi: 10.3390/ pr7050247. (Cited on pages 114, 155 and 171).

[71] E. Rodríguez, J. L. Guzmán, M. Berenguel, F. G. Acién, and A. Visioli. Diurnal and nocturnal ph control in microalgae raceway reactors. *In the 2nd IWA Conference on Algal Technologies for Wastewater Treatment and Resource Recovery, Valladolid, Spain*, pages 1 – 2, 2019. (Cited on page 165).

[72] E. Rodríguez, J. L. Guzmán, F. G. Acién, M. Berenguel, and A. Visioli. Indirect regulation of temperature in raceway reactors by optimal management of culture depth. *Biotechnology and Bioengineering*, pages 1 – 13, 2020. doi: 10.1002/bit.27642. (Cited on page 111).

[73] E. Rodríguez, J. L. Guzmán, M. Berenguel, F. G. Acién, and A. Visioli. Diurnal and nocturnal pH control in microalgae raceway reactors by combining classical and event-based control approaches.

Water Science & Technology, 82(6):1155 − 1165, 2020. doi: 10.2166/ wst.2020.260. (Cited on pages 114 and 165).

[74] E. Rodríguez, F. G. Acién, J. L. Guzmán, M. Berenguel, and A. Visioli. A new model to analyze the temperature effect on the microalgae performance at large scale raceway reactors. *Biotechnology & Bioengineering (In press)*, 2021. doi: 10.1002/bit.27617. (Cited on page 33).

[75] E. Rodríguez, A. Sánchez, F. G. Acién, and J. L. Guzmán. Feasibility seasonal study for culture depth influence on temperature for different microalgae strains. *Biotechnology and Bioengineering (Submitted)*, 2021. (Cited on page 86).

[76] A. Sánchez, J. A. Garrido, C. Gómez, M. Morales, F. G. Acié, J. M. Fernández, and E. Molina. Year-long assessment of a pilot-scale thin-layer reactor for microalgae wastewater treatment. variation in the microalgae-bacteria consortium and the impact of environmental conditions. *Algal Research*, 50:101983, 2020. doi: 10.1016/j.algal. 2020.101983. (Cited on page 20).

[77] A. Sánchez, C. Gómez, F. G. Acién, J. M. Fernández, and E. Molina. A novel photo-respirometry method to characterize consortia in microalgae-related wastewater treatment processes. *Algal Research*, 47:101858, 2020. doi: 10.1016/j.algal.2020.101858. (Cited on pages 20 and 51).

[78] A. Sánchez, C. Gómez, F. G. Acién, J. M. Fernández, and E. Molina. Modeling of photosynthesis and respiration rate for microalgae–bacteria consortia. *Biotechnology & Bioengineering*, bit.27625, 2020. doi: 10.1002/bit.27625. (Cited on pages 20, 49 and 51).

[79] A. Sánchez, E. Rodríguez, J. L. Guzmán, F. G. Acién, J. M. Fernández, and E. Molina. Abaco: A new model of microalgae-bacteria consortia for biological treatment of wastewaters. *Applied Sciences*, 11(3):998 − 1022, 2021. doi: 10.3390/app11030998. (Cited on page 49).

[80] E. Sartori. A critical review on equations employed for the calculation of the evaporation rate from free water surfaces. *Solar Energy*, 68:77–89, 2000. doi: 10.1016/S0038-092X(99)00054-7. (Cited on page 36).

[81] S. P. Singh and P. Singh. Effect of temperature and light on the growth of algae species: A review. *Renewable and Sustainable Energy Reviews*, 50:431 – 444, 2015. doi: 10.1016/j.rser.2015.05.024. (Cited on pages 17 and 18).

[82] R. Slade and A. Bauen. Micro-algae cultivation for biofuels: Cost, energy balance, environmental impacts and future prospects. *Biomass and Bioenergy*, 53:29 – 38, 2013. doi: 10.1016/j.biombioe.2012.12.019. (Cited on page 13).

[83] P. M. Slegers, M. B. Lösing, R. H. Wijffels, G. van Straten, and A. B. van Boxtel. Scenario evaluation of open pond microalgae production. *Algal Research*, 2:358–368, 2013. doi: 10.1016/j.algal.2013.05.001. (Cited on pages 18, 33 and 34).

[84] A. Solimeno. Numerical modelling of microalgae systems for wastewater treatment. *Thesis submitted to Universitat Politècnica de Catalunya (UPC), Cataluña, Spain*, 2017. (Cited on page 58).

[85] A. Solimeno, R. Samsó, E. Uggeti, B. Sialve, J. P. Steyer, A. Gabarró, and J. García. New mechanistic model to simulate microalgae growth. *Algal Research*, 12:350 – 358, 2015. doi: 10.1016/j.algal.2015.09.008. (Cited on pages 8, 19, 74 and 75).

[86] A. Solimeno, L. Parker, T. Lundquist, and J. García. Integral microalgae-bacteria model (bio_algae): Application to wastewater high rate algal ponds. *Science of The Total Environment*, 601 - 602:646 – 657, 2017. doi: 10.1016/j.scitotenv.2017.05.215. (Cited on pages 20 and 58).

[87] H. Tamiya. Mass culture of algae. *Annual Review of Plant Physiology*, 8:309 – 334, 1957. doi: 10.1146/annurev.pp.08.060157.001521. (Cited on page 9).

[88] N. Tan, I. Kaya, C. Yeroglu, and D. Atherton. Computation of stabilizing PI and PID controllers using the stability boundary locus. *Energy Conversion and Management*, 47:3045–3058, 2006. doi: 10.1016/j.enconman.2006.03.022. (Cited on page 151).

[89] O. Tetens. Über einige meteorologische begriffe. *Z. Geophys*, 6:207–309, 1930. (Cited on page 37).

[90] O. Turksoy, S. Ayasun, Y. Hames, and S. Sonmez. Gain-phase margins-based delay-dependent stability analysis of pitch control system of large wind turbines. *Transactions of the Institute of Measurement and Control*, 41(13):3626–3636, 2019. doi: 10.1177/0142331219834605. (Cited on page 151).

[91] E. van Esbroeck. Temperature control of microalgae cultivation under variable conditions. *Netherlands*, 2018. (Cited on page 19).

[92] J. P. Van Oorschot. Conversion of light energy in algal cultures. *Limnology and Oceanography*, 55:225 – 277, 1955. (Cited on page 9).

[93] P. Waller, R. Randy, K. Murat, and L. Peiwen. The algae raceway integrated design for optimal temperature management. *Biomass and Bioenergy*, 46:702 – 709, 2012. doi: 10.1016/j.biombioe.2012.06.025. (Cited on page 19).

[94] Weatherbit API forecast:. *https://www.weatherbit.io/*. (Cited on page 140).

[95] J. Weissman and R. Goebel. Design and analysis of pond system for the purpose of producing fuels. *Solar Energy Research Institute, SERI/STR-231-2840, US Department of Energy*, 1987. doi: 10.2172/6546458. (Cited on page 13).

DICHIARAZIONE DI CONFORMITÀ DELLE TESI
PER IL CONSEGUIMENTO DEL TITOLO DI DOTTORE DI RICERCA
(DICHIARAZIONE SOSTITUTIVA DI ATTO NOTORIO E DI CERTIFICAZIONE
(artt. 46-47 del D.P.R. 445 del 28.12.00 e relative modifiche)

Il/La sottoscritto/a…ENRIQUE RODRIGUEZ MIRANDA… Nato/a il…24/12/1992…………….

a ………ALMERÍA………………. Provincia/Stato ……ALMERÍA (SPAGNA)……..

Dottorato di ricerca in ………INGEGNERIA MECCANICA E INDUSTRIALE………………….

……………………………………………………………..…………………………………………

a conoscenza del fatto che in caso di dichiarazioni mendaci, oltre alle sanzioni previste dal Codice Penale e dalle Leggi speciali per l'ipotesi di falsità in atti ed uso di atti falsi, decade dai benefici conseguenti al provvedimento emanato sulla base di tali dichiarazioni,

DICHIARA

sotto la propria responsabilità, ai fini dell'ammissione all'esame finale per il conseguimento del titolo di Dottore di ricerca,

di essere a conoscenza che,

in conformità al Regolamento dell'Università degli Studi di Brescia per l'ammissione all'esame finale ed il rilascio del titolo per il conseguimento del titolo di Dottore di Ricerca, è tenuto a depositare all'U.O.C. Dottorati e Scuole di Specializzazione:

- n. 1 copia in formato cartaceo della propria tesi di dottorato e **l'esposizione riassuntiva (*abstract)* in italiano, se la redazione della tesi è stata autorizzata in lingua straniera;**

- n. 2 copie della tesi su DVD o CD-ROM per il deposito presso le Biblioteche Nazionali di Roma e di Firenze;

DICHIARA inoltre

- che il contenuto e l'organizzazione della tesi sono opera originale e non compromettono in alcun modo i diritti di terzi,

- **che sarà consultabile** immediatamente dopo il conseguimento del titolo di Dottore di ricerca, in quanto non è il risultato di attività rientranti nella normativa sulla proprietà industriale, non è stata prodotta nell'ambito di progetti finanziati da soggetti pubblici o privati con vincoli alla divulgazione dei risultati, e non è oggetto di eventuali registrazioni di tipo brevettale o di tutela.

- che l'Università è in ogni caso esente da qualsiasi responsabilità di qualsivoglia natura, civile, amministrativa o penale e sarà tenuta indenne da qualsiasi richiesta o rivendicazione da parte di terzi;

- che la tesi in formato elettronico (DVD o CD-ROM) è completa in ogni sua parte ed è del tutto identica a quella depositata in formato cartaceo all'U.O.C. Dottorati e Scuole di Specializzazione dell'Università degli Studi di Brescia e inviata ai Commissari. Di conseguenza va esclusa qualsiasi responsabilità dell'Ateneo per quanto riguarda eventuali errori, imprecisioni od omissioni nei contenuti della tesi.

Dichiara inoltre di essere consapevole che saranno effettuati dei controlli a campione. Eventuali discordanze od omissioni potranno comportare l'esclusione dal dottorato di ricerca;

Luogo e data…ALMERIA, 31/01/2021…..   Firma del dichiarante …ENRIQUE RODRIGUEZ MIRANDA…………